FULL-SCALE SHAKE TABLE CYCLIC SIMPLE SHEAR TESTING OF LIQUEFIABLE SOIL

A Thesis

presented to

the Faculty of California Polytechnic State University,

San Luis Obispo

In Partial Fulfillment

of the Requirements for the Degree

Master of Science in Civil Engineering

by

Jasper Stanford Jacobs

March 2016

COMMITTEE MEMBERSHIP

TITLE:	Full-Scale Shake Table Cyclic Simple Shear Testing of Liquefiable Soil
AUTHOR:	Jasper Stanford Jacobs
DATE SUBMITTED:	March 2016
COMMITTEE CHAIR:	Robb Moss, Ph.D., PE Associate Professor of Civil Engineering
COMMITTEE MEMBER:	Gregg Fiegel, Ph.D., PE, GE Professor of Civil Engineering
COMMITTEE MEMBER:	Nephi Derbidge, PE Lecturer of Civil Engineering

ABSTRACT

Full-Scale Shake Table Cyclic Simple Shear Testing of Liquefiable Soil

Jasper Stanford Jacobs

This research consists of full-scale shake table tests to investigate liquefaction of sandy soils. Consideration of the potential and consequences of liquefaction is critical to the performance of any structure built in locations of high seismicity underlain by saturated granular materials as it is the leading cause of damage associated with ground failure. In certain cases the financial losses associated with liquefaction can significantly impact the financial future of an entire region.

Most liquefaction triggering studies are performed in the field where liquefaction has been previously observed, or in tabletop laboratory testing. The study detailed herein is a controlled laboratory test performed at full scale to allow for the measurement of field-scale index testing before and after cyclic loading. Testing was performed at the Parson's geotechnical and Earthquake Laboratory at Cal Poly San Luis Obispo on the 1-dimensional shake table with a mounted flexible walled testing apparatus. The testing apparatus, originally constructed for soil-structure interaction experiments utilizing soft clay was retrofitted for the purpose of studying liquefaction.

This research works towards comparing large-scale simple-shear liquefaction testing to small-scale simple-shear liquefaction testing of a #2/16 Monterey sand specimen. The bucket top was modified in order to apply a vertical load to the soil skeleton to replicate overburden soil conditions. Access ports were fitted into the bucket top for instrument cable access and to allow cone penetration testing before and after cyclic loading. A

shear-wave generator was created to propagate shear waves into the sample for embedded accelerometers to measure small strain stiffness of the sample. Pore-pressure transducers were embedded in the soil sample to capture excess pore water pressure produced during liquefaction. Displacement transducers were attached to the bucket in order to measure shear strains during cyclic testing and to measure post-liquefaction volumetric deformations.

The results of this investigation provide an empirical basis to the behavior of excess pore water production, void re-distribution, shear wave velocity, shear strain and cone penetrometer tip resistance of #2/16 Monterey sand before, during, and after liquefaction in a controlled laboratory environment at full-scale.

ACKNOWLEDGMENTS

My experience as a graduate student at Cal Poly, San Luis Obispo, has been a truly formative experience having positively affected both my future as an engineer and the quality of my personal life. The opportunity to study, research, and teach has been a challenge every step of the way; without the challenge there would be no sense of accomplishment. I would like to thank my advisory committee members, Dr. Gregg Fiegel, Professor Nephi Derbidge, and Dr. Robb Moss for helping me along the way.

Dr Fiegel's commitment to providing a superior educational experience is evident in his thoughtful feedback and never-ending quest for improvement. It has been a mainstay throughout my experience at Cal Poly.

Professor Derbidge's expertise in geotechnical testing has been an invaluable resource, but his calm demeanor and patience were the most valuable characteristics to help me through the instrumentation phase of my research.

I would like to thank my advisor, Dr. Robb Moss, whose greatest strength is the ability to relate to his students. He has taught me far more lessons than the ones confined by the implications of his job title.

Lastly, I would like to thank my wonderful Girlfriend, Aubrey, who is far smarter than I, but loves me nonetheless.

Thank you all for your dedication.

TABLE OF CONTENTS

APPENDICES

LIST OF TABLES

Table Page

LIST OF FIGURES

LIST OF EQUATIONS

CHAPTER 1 LITERATURE REVIEW

1.1 Introduction

Earthquakes are a daily occurrence: many of which are either too small to cause damage or even be felt, others occur in locations of geographic isolation where there is no concern for damage. It also happens that many major population centers around the globe are located within close proximity of active faults. When earthquakes of sufficient magnitude occur in proximity to structures in which ground failure has not been considered as part of the design process, the results can be disastrous. As the single most destructive form of ground failure, liquefaction should always be considered when structures are built in the vicinity of predominantly granular materials in areas of high seismicity. Soils ranging from gravels to non-plastic silts can experience liquefaction if they are saturated and experience prolonged shaking. The soil skeleton's tendency to densify is restricted by the presence of water within the soil-skeleton's pore space, which experiences pressures in excess of hydro-static values until a critical level is reached. This critical level varies, but is generally considered to be equal to the vertical effective stress. As excess pore-water pressures accumulate, pressure on the soil skeleton decreases simultaneously until soil particles are no longer carrying the weight of soil above and become temporarily suspended. At this point the soil has liquefied and the solid soil skeleton has transformed into a viscous fluid. Liquefaction is considered an un-drained failure in soil mechanics because of its dependency on the generation of excess pore-water pressures. The following literature review presents the evaluation of

liquefaction triggering based on field and laboratory testing, as well as field performance case histories.

1.2 In-situ testing correlations to liquefaction triggering

The 1964 magnitude 7.6 earthquake in Niigata, Japan represents the first seismic event to be included in liquefaction load and resistance databases. Another earthquake occurring in the same year, the 1964 Good Friday magnitude 9.2 Earthquake, near Anchorage, Alaska also resulted in large amounts of liquefaction related damage, but was not evaluated thoroughly enough to be included in liquefaction databases.

Figure 1: Port Damage due to Liquefaction as a Result of the 1995 Kobe Earthquake (from Harder)

Researchers have come to a consensus on the correct procedure to approach liquefaction related engineering problems, from triggering to mitigation, represented as a flow-chart in Figure 2. The discussion of liquefaction triggering is this paper's focus of

discussion. Assessment of liquefaction triggering has been vigorously studied, and can be predicted using a variety of methods. Liquefaction triggering curves have been developed using soil resitance information procured from Standard Penetration Testing (SPT), Cone Penetration Testing (CPT), Shear Wave Velocity (V_s), and Becker Penetrometer Testing (BPT) (listed in descending order of popularity). Becker penetrometer testing is generally used only in the presence of gravels, and is therefore omitted from discussion hereafter. SPT and CPT based liquefaction triggering curves bear striking similarities due to the fact that factors that contribute to SPT blow counts and CPT tip resistance are the same factors that contribute to a soil's resistance to liquefaction. These factors include density with respect to the critical state (the density at which a soil experiences shear deformation without a change in volume), soil structure, cementation, ageing, and state of stress. Although V_s liquefaction triggering curves appear to be very similar to CPT and SPT triggering curves, they are fundamentally very different because V_s measurements are based on much smaller strain behavior than SPT and CPT measurements and the occurrence of liquefaction. The current level of information available to engineers regarding liquefaction triggering is sufficient for engineers to reasonably determine the susceptibility of liquefaction on any given site with tools that are common and available in most geographic regions. Recently, statistical methods have been employed to help determine liquefaction triggering potential as opposed to the previously mentioned deterministic tools. The triggering potential of liquefaction is the most fully developed aspect of liquefaction engineering, leaving the engineer empowered to decide if the consideration of liquefaction is important in the development of a particular engineering project.

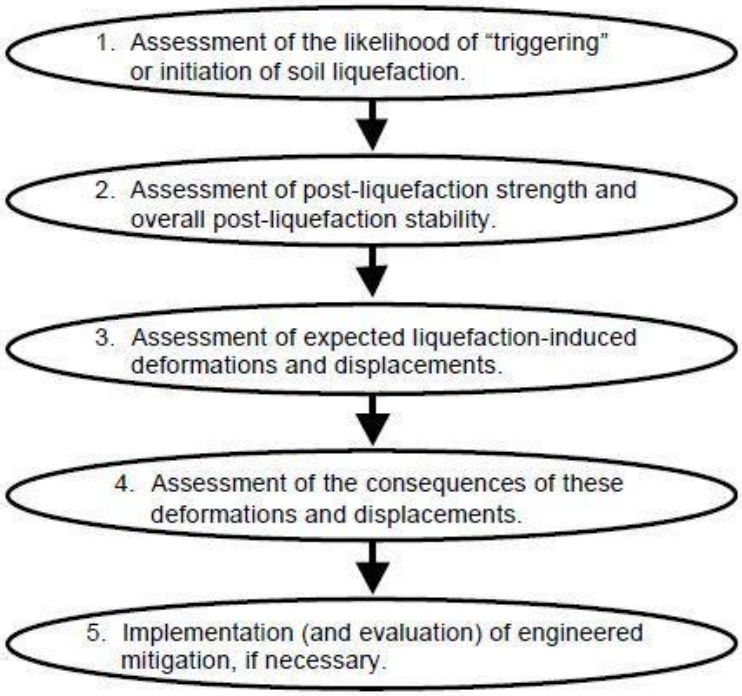

Figure 2: Key elements of Soil Liquefaction Engineering (from Seed et al., 2003)

Seed and Idriss (1971) were the first to compare the occurrence and non-occurrence of liquefaction in an effort to predict liquefaction based off of Standard Penetration Test (SPT) blow counts (resistance) and cyclic stress ratio (CSR) (Load) (Figure 3). The cyclic stress ratio is the ratio of shear stress to vertical effective stress imposed at the depth under consideration. The occurrence of liquefaction is confirmed by visual observation at the ground surface including sand boils, ground cracking, structural settlement, bearing capacity failure and uplift of buried pipes and tanks that became buoyant in the presence of liquefied sand. SPT blow counts are recorded after the occurrence of liquefaction and corrected for hammer energy (equipment type), effective overburden stress, borehole diameter, rod length, and whether or not samplers contain liners. CSR is estimated considering the peak ground acceleration (a_{max}), duration of shaking, effective and total vertical stress conditions at the critical layer considered for

liquefaction, and r_d, the reduction in shear stress for soils below the ground surface. The simplified equation first proposed by Seed and Idriss (1971) is:

$$CSR = \frac{\tau_{AV}}{\sigma_{O'}} = 0.65 \cdot \frac{a_{max}}{g} \cdot \frac{\sigma_o}{\sigma_{o'}} \cdot r_d \quad \text{..... (1)}$$

Plotting SPT blow count versus CSR and marking points corresponding to whether or not liquefaction occurred allowed for the creation of a deterministic liquefaction triggering curve. The CSR corresponding to liquefaction for a given blow count as determined by the liquefaction triggering curve is known as the Cyclic Resistance Ratio (CRR).

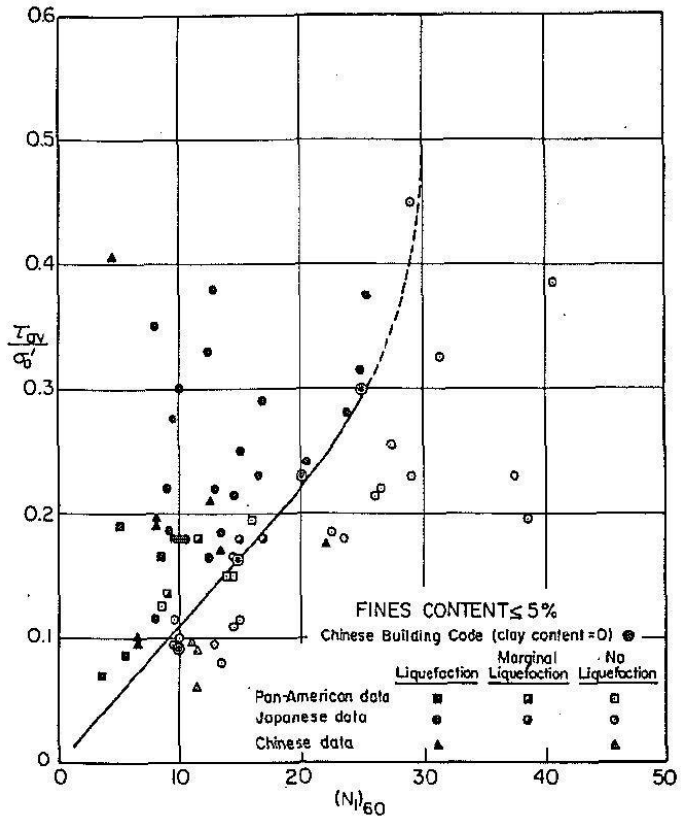

Figure 3: Relationship between Stress Ratios Causing Liquefaction and N1-values for Clean Sands for M=7.5 Earthquakes (from Seed and Idriss, 1971)

Development of CPT liquefaction triggering methods was delayed with respect to SPT methods. Part of the additional time required to develop CPT methods includes the development and calibration of the equipment itself. Modern electrical cones with the geometries we are accustomed to today were not introduced until 1974, the first of which were produced by Fugro. Robertson and Campanella (1985) produced seminal CPT based liquefaction triggering curves (Figure 4) by comparing correlated CPT values to SPT liquefaction triggering data with CPT triggering curves developed as a function of relative density and CSR.

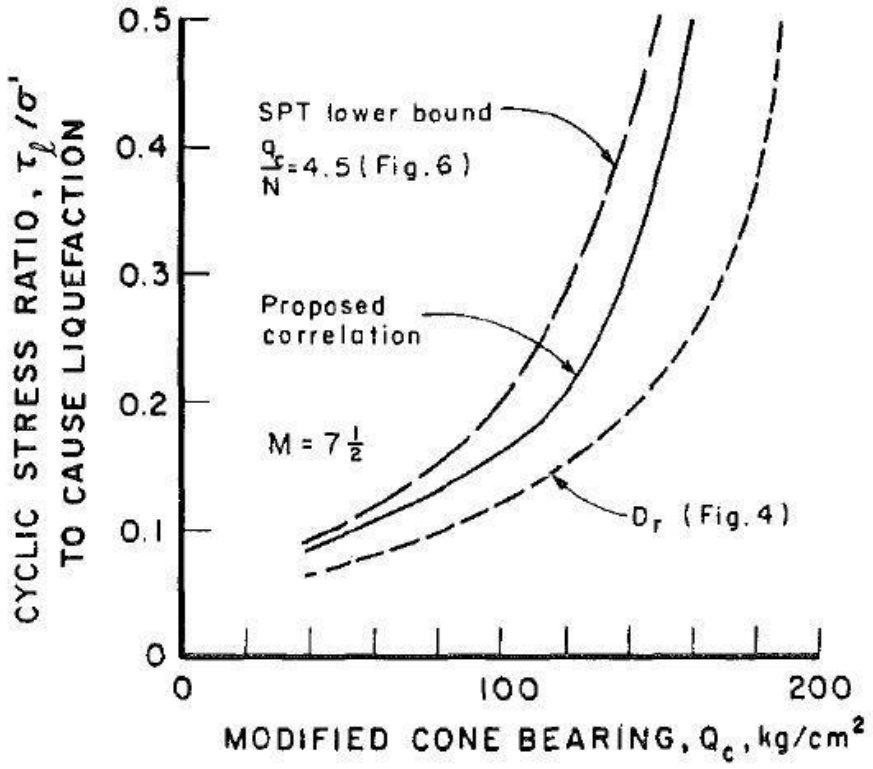

Figure 4: Summary of Correlations Between Liquefaction Resistance and Modified Cone Penetration Resistance in Sands (from Robertson and Campanella, 1985)

The liquefaction triggering curve proposed by Robertson and Campanella in 1985 was adjusted (Figure 5) by Robertson and Wride (1998) and in conjunction with the 1996

NCEER working group to be in better agreement with SPT triggering curves by Seed et al. (1985) at low SPT blow counts.

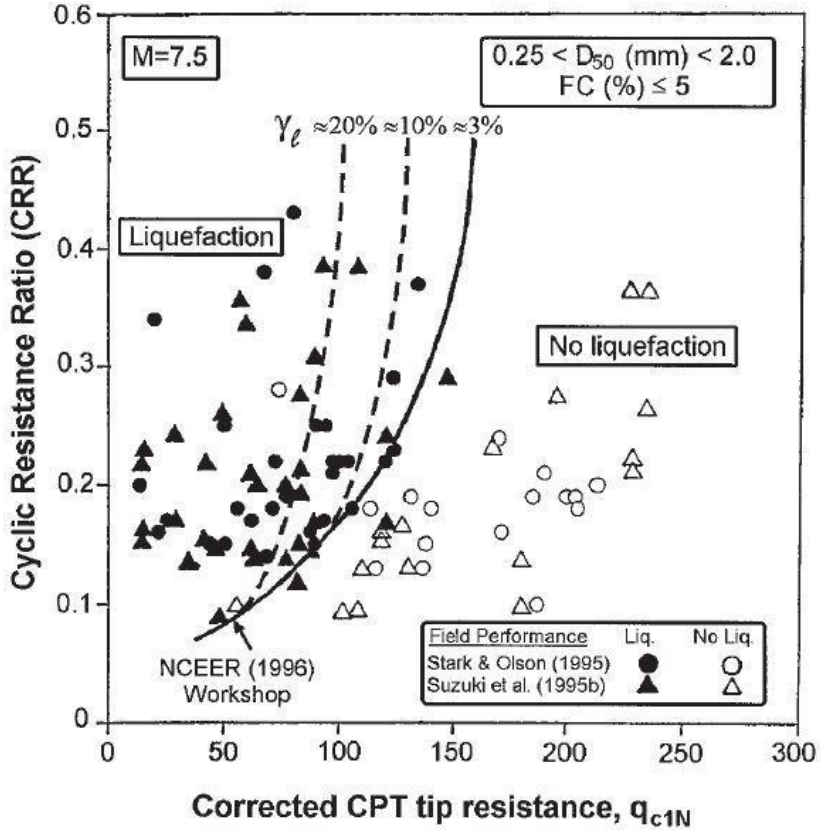

Figure 5: CPT base liquefaction triggering curves (from Robertson and Wride, 1998)

Andrus and Stokoe (2000) put forth a supplementary V_s based procedure for liquefaction triggering evaluation to supplement SPT and CPT based methods. The V_s method follows a similar procedure as methods by Seed et al. as well as Robertson and Wride. As part of the data normalization process, V_s is corrected to a reference effective overburden stress much like CPT and SPT values are normalized. Andrus and Stokoe (2000) suggested a maximum corrected V_s value of 210 m/s, roughly correlating with a SPT blow count of 30 – a value at which sandy soils are not considered to be liquefiable. Liquefaction curves constructed by Andrus and Stokoe (Figure 6) therefore do not extend beyond V_s values of 210 m/s.

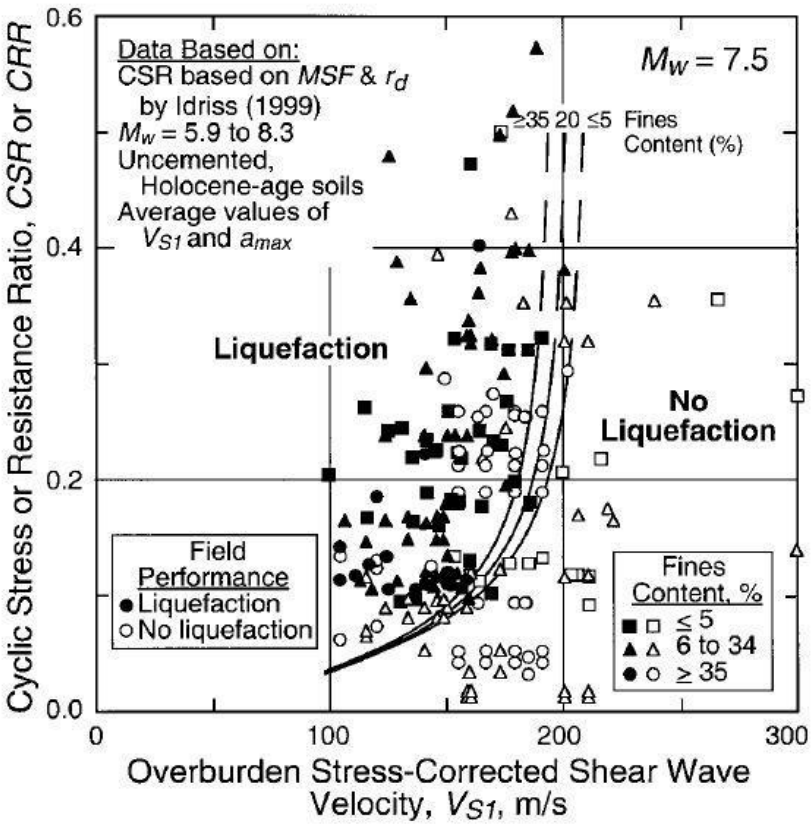

Figure 6: V_s Curves Recommended at Various Fines (from Andrus and Stokoe, 2000)

Each of the three liquefaction triggering evaluation methods discussed above have their own strengths and weaknesses. SPT methods produce physical samples which can be used to classify the soil and the SPT database is the most thoroughly populated of all test methods, but test results are not highly repeatable and data is discontinuous with depth. The CPT method can be performed quickly and produces continuous, highly repeatable data, but no samples are retrieved and soil characteristics must be inferred from empirical relationships. V_s testing can be performed on sites where CPT and SPT penetration is difficult or not possible to perform, but V_s recordings are small-strain measurements despite liquefaction being a large-strain phenomenon, samples are not recovered, and thin liquefiable layers can go un-detected due to aliasing. All three methods share the problem of having poorly populated data in the region where stiff

soils have been exposed to stronger shaking. The lack of data in this region leads to more uncertainty in assessing liquefaction susceptibility than in any other region of the liquefaction triggering curve, and is therefore the most critical. To perform a truly thorough liquefaction triggering analysis it can be advantageous to employ all testing methods and compare the results.

The liquefaction triggering curves presented herein represent only a small fraction of the available liquefaction triggering models. As of 2001, the SPT, CPT, and V_s triggering curves by Seed et al. (1985), Robertson and Wride (1998),and Andrus and Stokoe (2000) respectively were considered to be state of practice for the simplified deterministic procedures by the National Council for Earthquake Engineering Research (NCEER) working group (Youd et al., 2001).

It is evident that a great amount of epistemic uncertainty is invoked by attempting to distill the soil resistance and earthquake loading information into two single numbers. The alternative, which involves recovering an undisturbed soil sample and performing lab testing in a controlled environment, is far more difficult. Sands are easily disturbed due to the potential for un-drained loading to occur during sampling, causing significant sample disturbance. Estimating earthquake properties from ground motion recordings, and collecting soil data from the aforementioned in-situ testing approaches in an effort to build large sets so that the occurrence and non-occurrence of liquefaction can be compared is the most realistic method in an effort to develop a better understanding of the factors that control liquefaction. Although significant progress has been made assessing the loads and resistances involved in liquefaction triggering, in-situ testing does not provide a complete picture of the liquefaction triggering process.

1.3 Laboratory triggering evaluation

Boulanger and Seed (1995) performed small-scale simple-shear cyclic loading tests on saturated sand on a then-recently developed 2D bi-directional simple-shear apparatus (Figure 7). The stress, strain, and pore-water pressure response to cyclic loading showed dramatic differences for soils at varying relative density (D_r), controlled by means of tamping during deposition. In addition, tests have been performed with an added static shear stress at varying orientations in relation to the applied cyclic stresses to study its affect on the liquefaction triggering process. Static driving shear stresses are present where sloping ground surfaces and structures applying uneven vertical stress distributions exist, and are a very important issue to consider when performing liquefaction studies. Thanks to versatility in loading conditions available when performing small-scale simple-shear testing (Figure 8), laboratory liquefaction triggering data complements in-situ testing quite well.

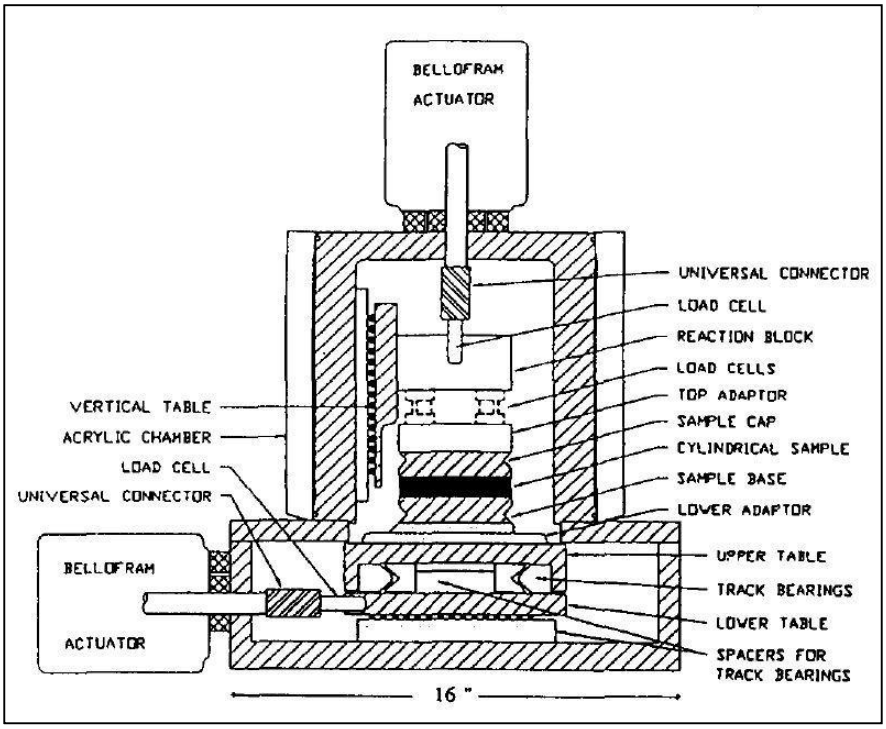

Figure 7: Schematic of UCB-2D Simple Shear Apparatus (from Boulanger and Seed, 1995)

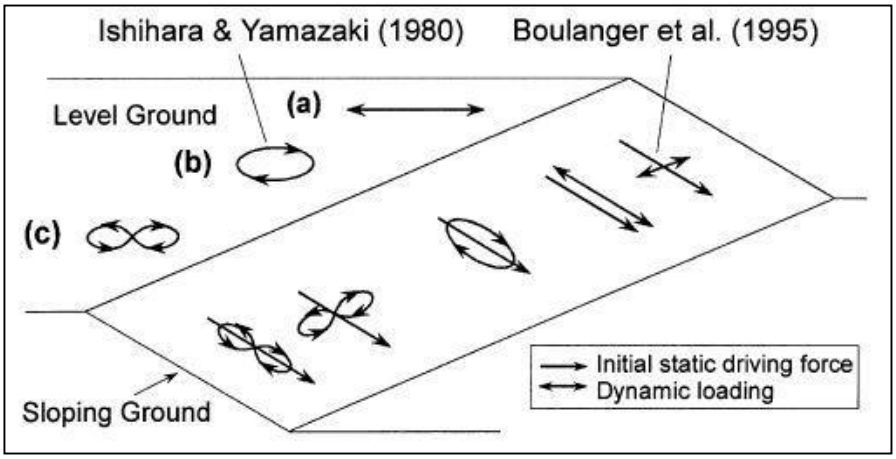

Figure 8: Schematic Illustration of Idealized Multi-Directional Loading (from Kammerer et al., 2005)

Boulanger and seed performed three types of tests using the 2D device: no static driving shear stresses were applied during cyclic loading (simulating flat ground stress conditions), static shear stresses were applied parallel to the direction of cyclic loading (simulating cyclic loading in the dip orientation of a slope) and static shear stresses were applied transverse to the direction of cyclic loading (simulating cyclic loading in the strike orientation of a slope). Excess pore-water pressure ratios approaching unity control the liquefaction process and are accompanied by shear strains approaching 3% during testing without the application of static driving shear stresses. Tests with static driving stresses applied parallel and perpendicular to the applied cyclic loading both indicated that liquefaction and accompanying shear strains greater than 3% are possible with excess pore water pressure ratios at roughly 60-65 percent of unity.

Wu (2003) continued the work of Boulanger and Seed, performing additional cyclic simple shear tests with and without the application of static shear stresses. Wu constructed soil samples artificially using a wet pluviation method. An investigation of various deposition techniques indicated that the minimum attainable relative densities for moist tamping, dry pluviation, and wet pluviation are -20%, 18%, and 33%, respectively.

Wet pluviation was chosen because the resulting soil fabric is most similar to soils that are deposited naturally, and the relative density is controllable to within 1%.

The different liquefaction behaviors of soils prepared at relative densities of 50 and 75% by Wu (Figures 9 and 10 respectively) exemplified the ability for soils to experience "brittle" and "ductile" forms of liquefaction. A suite of charts includes excess pore-water pressures, shear strains, shear stresses and effective vertical stresses plotted throughout a given test. Figure 9 shows very clearly that liquefaction can be seen as a two-stage process when a soil with a low relative density is tested. During cyclic loading, excess pore-water pressures are generated without significant shear strain accumulation until the excess pore water pressure ratio approaches 80%, corresponding with double-amplitude shear strains near 2-3%. Once liquefaction has been triggered, shear strains continue to accumulate with each passing cycle as excess pore-water pressures fluctuate due to the change in the volume of void space as individual soil particles become mobile. Observation of hysteresis loops generated from cyclic simple-shear tests indicates the soils soften and subsequently stiffen as it contracts and dilates throughout each loading cycle. As the soil dilates at the end of each cycle excess pore water pressures are reduced, effective stress increases, and the soil mobilizes enough shear strength to resist the applied shear stress. The majority of fluctuation of pore-water pressures during this phase is due to the change in the volume of the soil's void space after the soil has liquefied and shear strains accumulate.

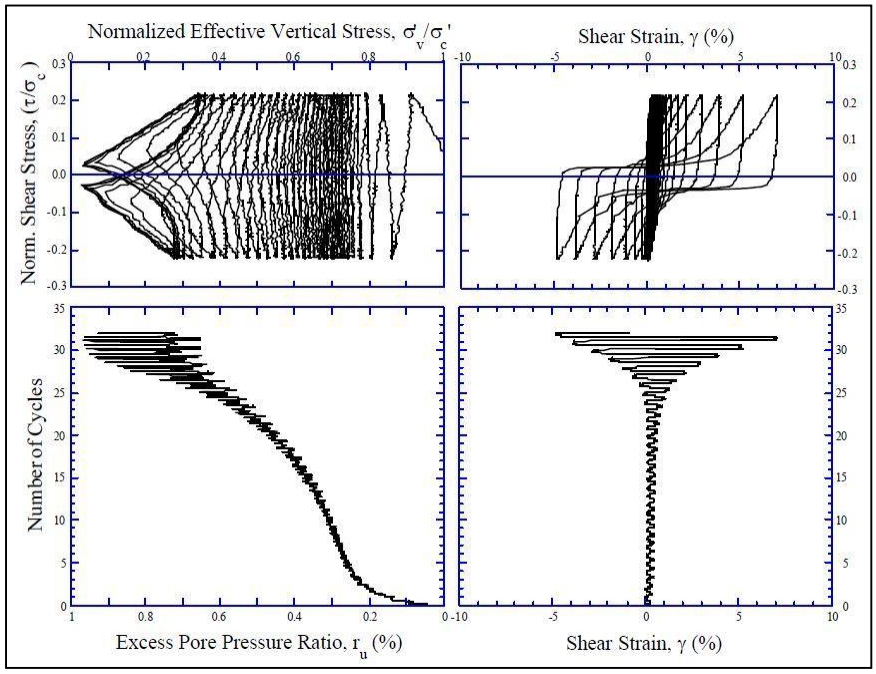

Figure 9: Undrained Cyclic Simple Shear Test on Monterey #30/0 Sand Dr=50%, σv,i=85 kPa, CSR=0.22, α=0 (from Wu, 2003)

Liquefaction of a soil prepared at higher relative densities (Figure 10) exemplifies the wide variety of soil behavior possible during liquefaction when compared to the looser specimen in Figure 9. The denser soil sample is less prone to densification and must have a much higher CSR applied in order to experience liquefaction. The point of incipient liquefaction is less pronounced, because the soil does not suddenly contract when enough pore-water pressure is generated allowing for rapid accumulation of shear strain. Both samples are considered to have liquefied when a 3% shear strain is reached, and the transition from pore-water pressure generation to fluctuation between limiting values as the soil densifies and dilates is shared for both tests. Because there is no static shear stress applied to the sample during testing, accumulation of shear strains is symmetric in both directions.

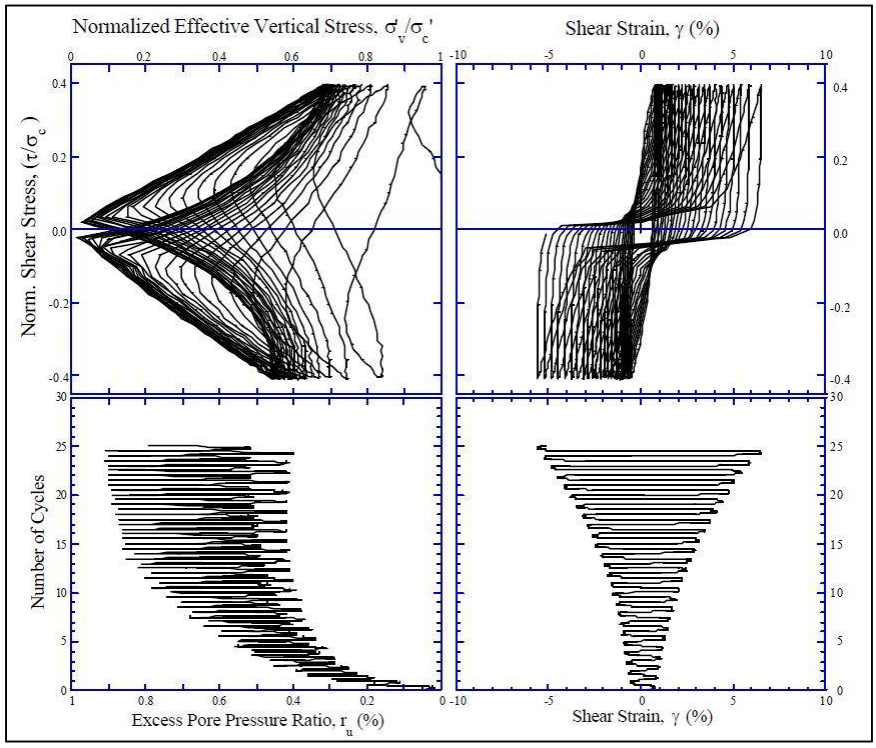

Figure 10: Undrained Cyclic Simple Shear Test on Monterey #30/0 Sand Dr=75%, σv,i=85 kPa, CSR=0.4, α=0 (from Wu, 2003)

Wu also performed cyclic simple shear tests with a static driving shear stress aligned in the direction of cyclic loading where alpha is the ratio of static applied shear stress to initial vertical effective stress.

$$\alpha = \frac{\tau_s}{\sigma_v'} \quad \text{.....(2)}$$

Results of the simple cyclic shear test with combined static shear loading (Figure 11) shares similarities with the tests that do not include a static shear stress excluding the fact that shear strains are not symmetric and progressively accumulate in the direction of the static shear stress.

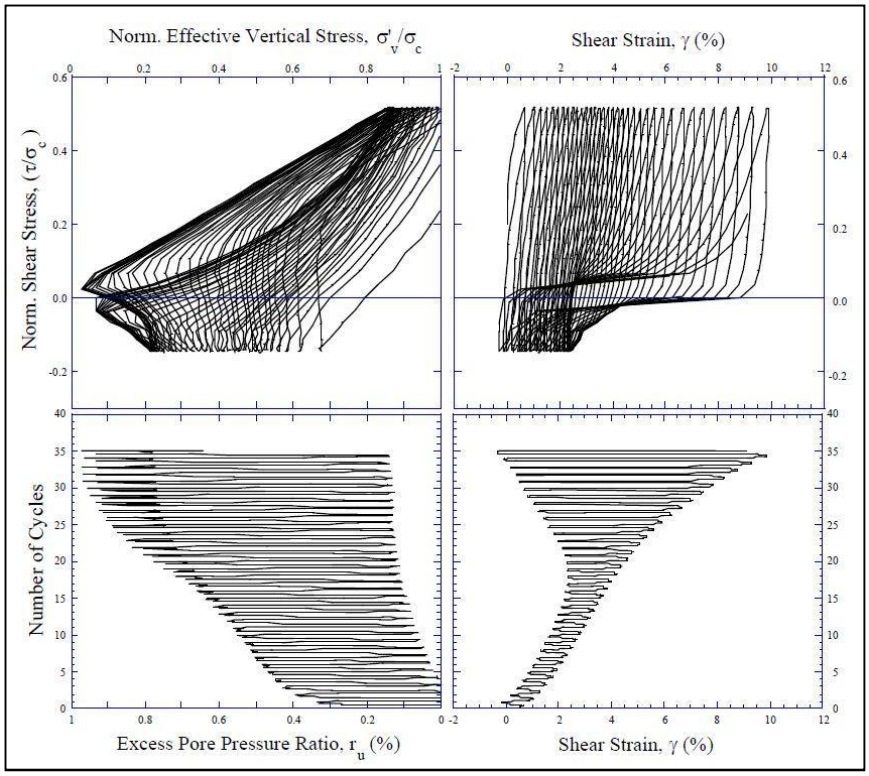

Figure 11: Undrained Cyclic Simple Shear Test on Monterey #30/0 Sand Dr=55%, σv,i=85 kPa, CSR=0.33, α=0.18 (from Wu, 2003)

Kammerer et al. (2005) also investigated the effect of static driving shear stress, but specifically investigated the effect of shear stress reversal on liquefaction triggering by varying α. Kammerer et al. used the same wet pluviation method utilized by Wu (2003), and showed that soils that do not experience shear stress reversal are much less likely to liquefy during cyclic loading (Figure 12). Two different samples tested with the same cyclic load but different static driving shear stress (and therefore different α) realized dramatically different excess pore-water pressure and shear strain generation. The soil that did not experience stress reversal in the dip direction did not generate significant excess pore-water pressures to liquefy, and therefore did not experience the shear strains associated with liquefaction. Cyclic stress in the strike direction was sufficiently low for both tests, and no excess pore-water pressure were generated due to loading in

the strike direction, however the soil that experienced liquefaction generated strains in both the strike and dip direction during cyclic loading.

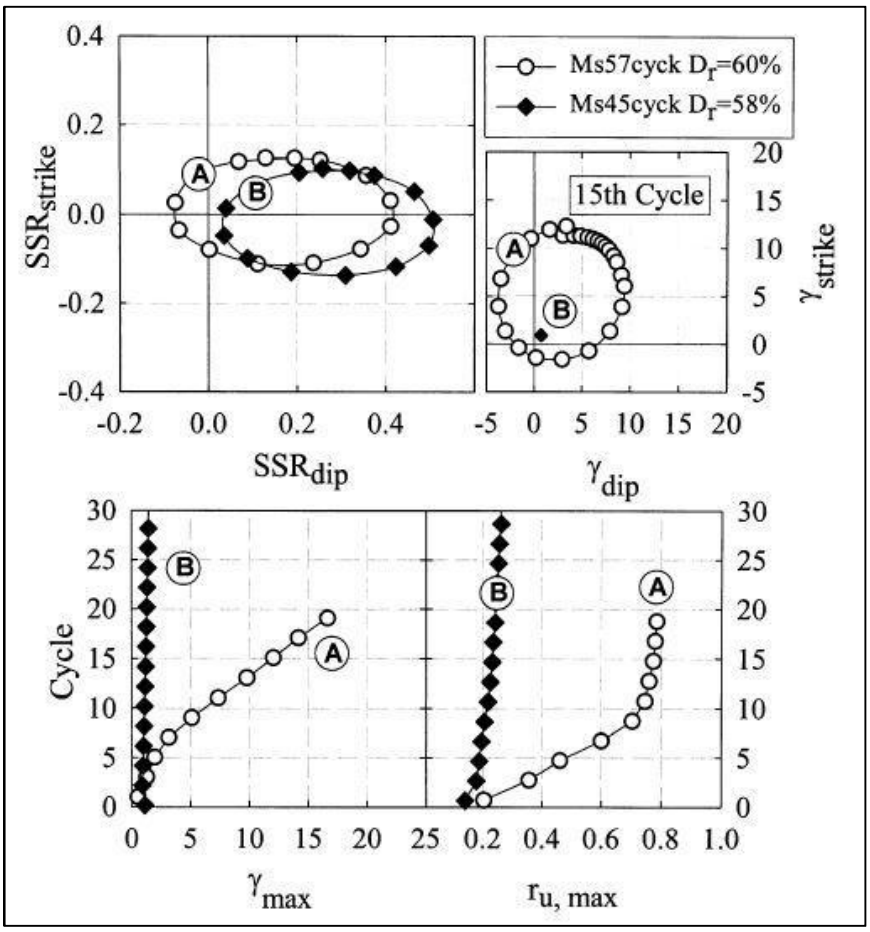

Figure 12: Comparison of oval dip-oriented tests with increasing α-values (from Kammerer et al., 2005)

The use of small-scale simple shear tests has contributed greatly to the knowledge of liquefaction triggering, helping the engineering community to better understand the importance on pore water pressures and static shear stresses in the liquefaction triggering process.

1.4 Field Performance

Performance of a sub-surface investigation before the occurrence of liquefaction is rare and few exist. Difficulties associated with predicting the occurrence and location of

earthquakes along with the corresponding propagation of S-waves in the presence of liquefiable soil and groundwater conditions accounts for the difficulty in acquiring liquefaction resistance data before the occurrence of liquefaction. In some instances, sub-surface investigations have been performed in locations with poor soil conditions that have later experienced liquefaction. This is the case in the San Francisco Bay Area. In other cases, liquefaction has occurred so many times within a distinct geographic location that a sub-surface investigation is performed and a site is instrumented with the anticipation of liquefaction. This is the case in California's Imperial Valley and Treasure Island and Japan's Port Island, among others. The Treasure Island site was instrumented after the 1989 Loma Prieta Earthquake, and has not experience earthquake induced liquefaction, while Port Island and Imperial Valley have experienced significant shaking events since their initial instrumentation. In San Francisco, where limited space, and demand for urbanization has resulted in the expansion of the city's waterfront using hydraulic filling, most of which was placed between 1850 and 1920. In the Yerba Buena Cove area, large ground deformations due to liquefaction were observed in the Great 1906 Earthquake. Cone Penetration Testing was performed in 1979 in the same area as part of a seismic response study (Clough and Chameau, 1979). After the 1989 Loma Prieta Earthquake an additional CPT study was (Chameau et al., 1991) was performed in 1990 in the Yerba Buena Cove area, where observations of ground cracking and lateral displacement indicated liquefaction once again. Comparison of CPT tip resistance at the Yerba Buena Cove location indicated an increase in stiffness due to liquefaction throughout a roughly 20 foot thick layer of soil (Figure 13). Although the 1979 study was performed with a mechanical Delft type cone and the 1990 test was performed with an electric Fugro type cone, the range of tip resistances recorded by the Delft type cone are in the range in which the difference in tip

resistances between the 1979 and 1990 tests would be even greater had they been performed with the same types of cones (Figure 14)

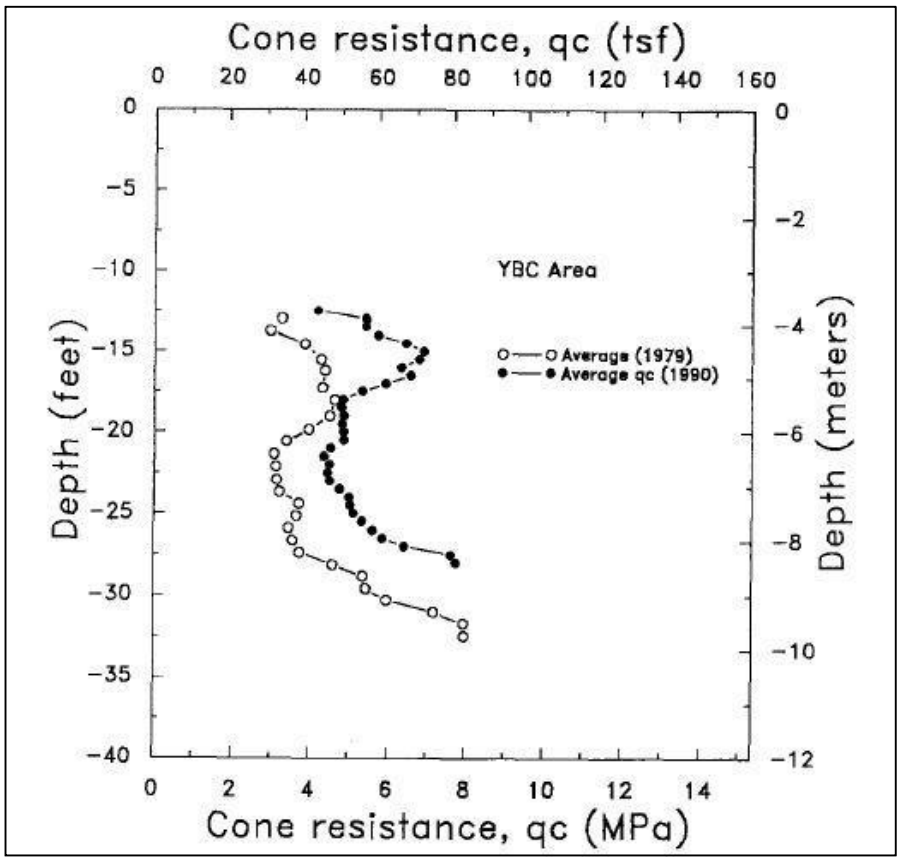

Figure 13: Comparison of CPT tip resistance in the Yerba Buena Cove before and after the Yerba Buena Earthquake (from Chameau et al., 1991)

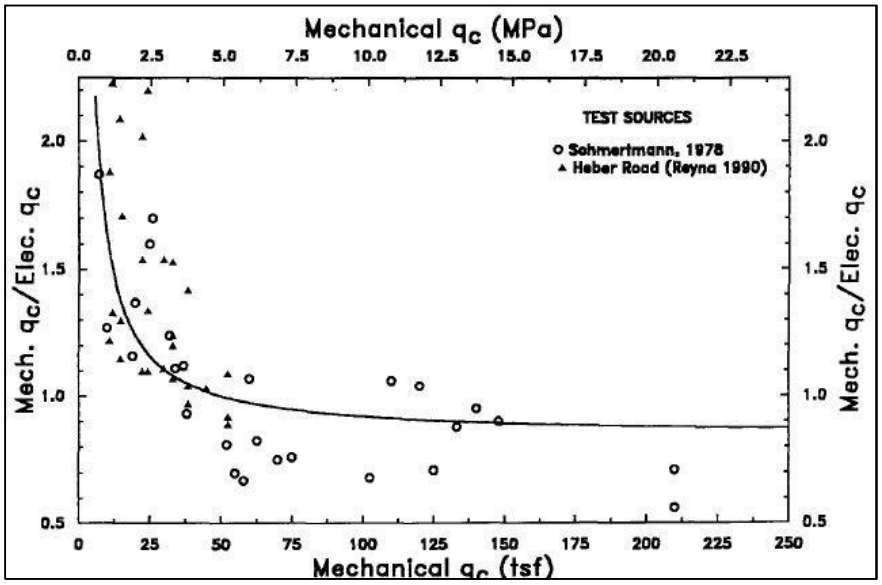

Figure 14: Comparison of Mechanical and Electric CPT tip resistances (from Chameau et al., 1991)

Although it is rare to be able to perform Cone Penetration Testing in the same location before and after liquefaction, the data is very useful as a means of quantifying the densification caused by liquefaction. Unfortunately, this data does not provide much insight into the process of liquefaction as it occurs.

Imperial Valley, California, is another site that has experienced liquefaction over and over again. Proximity to the Colorado River accounts for the abundance of liquefiable material, and The San Andreas, Imperial, San Jacinto, and Elsinore faults are the main contributors to the site's seismic hazard.

The earliest reports that describe the possibility of liquefaction date to November 29, 1852. Since then, 15 earthquakes in 135 years with the possibility of liquefaction have occurred. While it cannot be confirmed that all of these ground failures were the result of soil liquefaction, liquefaction likely occurred because descriptions include lateral spreading, ground cracking, differential settlement and sand ejecta, all of which are indicators of liquefaction.

In 1982 the Wildlife Liquefaction Array (WLA) (Figure 15) was established with the hopes of recording acceleration time histories at and below the ground surface and excess pore water pressures measured by pore pressure transducers within the liquefiable sand layer. CPT recordings before the occurrence of liquefaction show the presence of relatively high tip resistances and negligible friction ratios, indicating the presence of granular material situated from roughly 2.5 to 6.5 meters below the ground surface. Pore pressure transducers are embedded at even increments within the liquefiable layer.

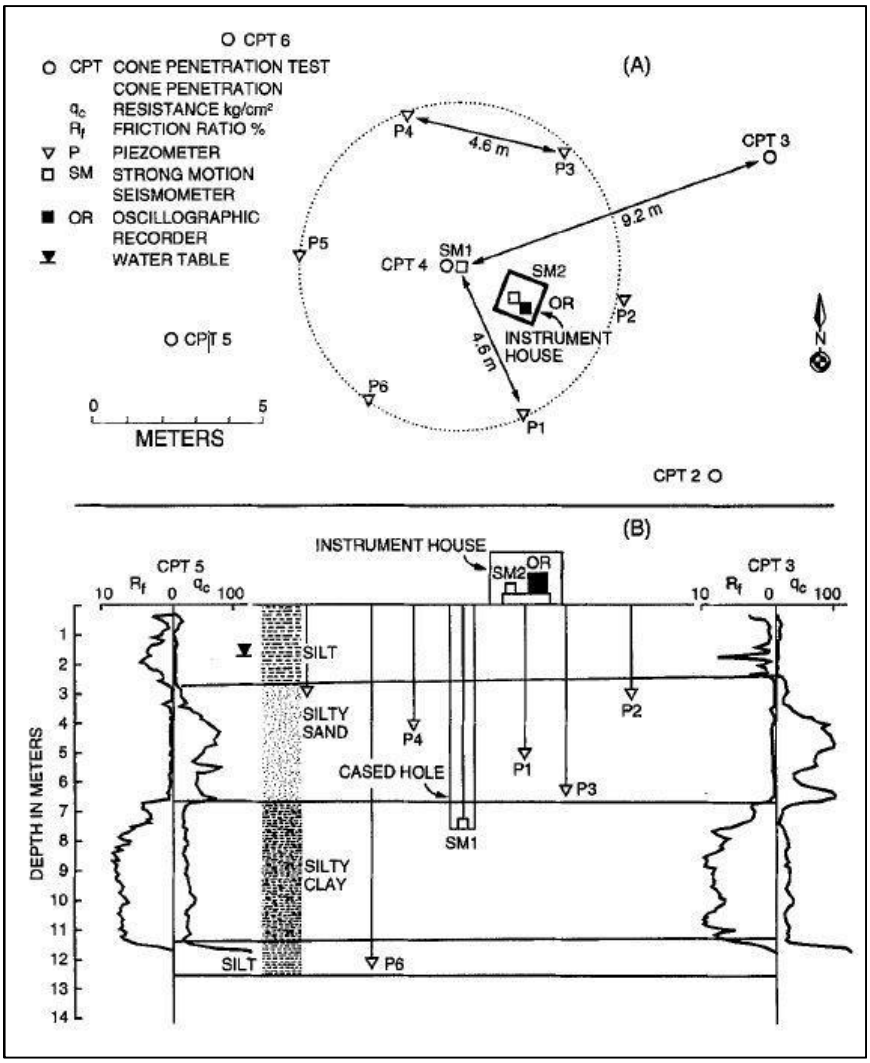

Figure 15: Wildlife Liquefaction array, presented in plan and section view with accompanying CPT tests (from Youd and Holzer, 1994)

Liquefaction occurred at the WLA in 1987 during the Superstition Hills earthquake (Mw=6.6). Excess pore-water pressures were measured near and above unity by the embedded pore-water pressure transducers (Figure 16), and the occurrence of liquefaction was confirmed at the ground surface by the presence of ejecta and ground cracking

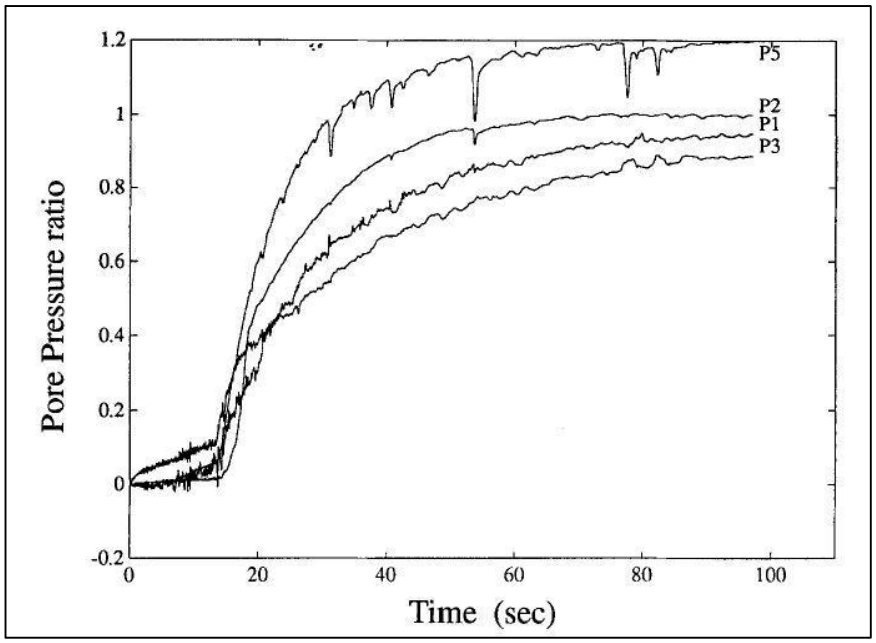

Figure 16: Excess Pore Pressure ratios generated during the Superstition Hills Event at the Wildlife Liquefaction array (from Youd and Holzer, 1994)

Examination of strong ground motion recordings from the Superstition Hills earthquake suggests most shaking had stopped at roughly 20 seconds into the event (Figure 17). Before the 20 second mark, pore-water pressure transducers situated lower in the sample experience higher pore-water pressure ratios than the transducers situated above them. Near the 20 second mark, a crossing over occurs, and increasing pore-water pressure ratios begin to accumulate with increasing height within the liquefiable layer compared to the transducers below. The excess pore-water pressure ratios nearing 1.2 at the top of the liquefied layer are likely due to the formation of a water

film/blister/hydroplane between the liquefied sand layer and the impermeable silt above, which forms an area of localized strain (Figure 18).

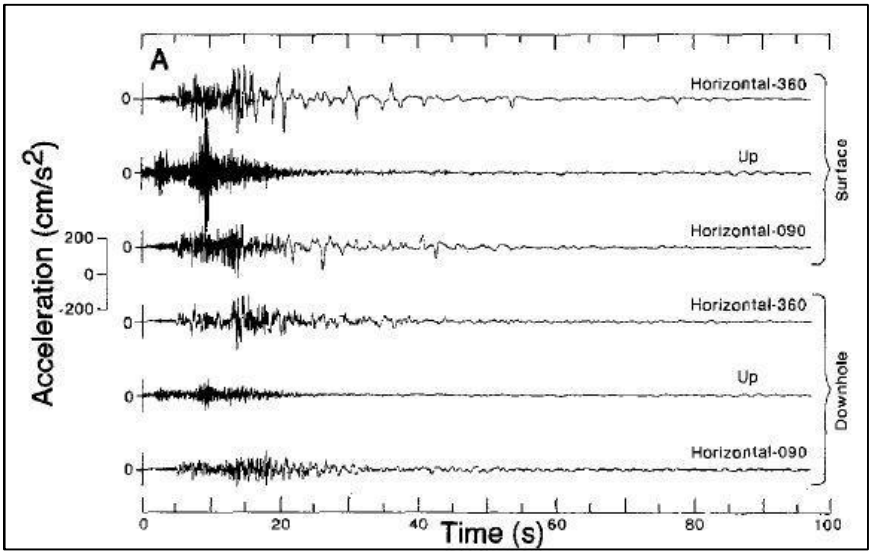

Figure 17: Superstition Hills earthquake surface and downhole strong ground motion recordings (from Youd and Holzer, 1994)

1.5 Large-scale testing

Comparison of the pore water generated throughout the liquefied layer in the Superstition Hills earthquake indicates that the samples and testing used to create Figures 9-12 presented by Wu (2003) and Kammerer et al. (2005) do not provide a complete description of the liquefaction process. Small-scale simple shear tests do not have the ability to capture void re-distribution or the spatial distribution of excess pore-water generation within a sample. Additionally, small-scale simple shear testing is also too small to investigate the effect of layered or sloped geometries and does not allow for full-scale cone penetration index testing. The use of full-scale geotechnical centrifuges and shake-table testing are desirable for their ability to capture phenomena that small-scale simple shear testing cannot.

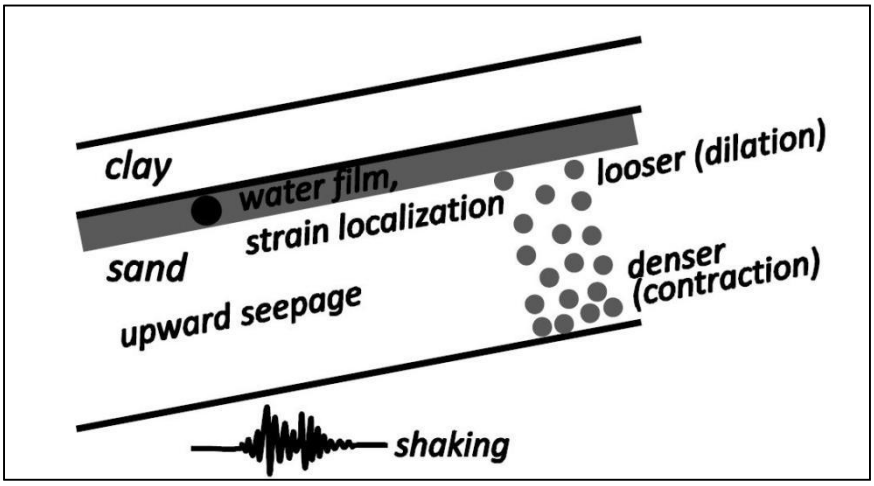

Figure 18: Void re-distribution and the generation of a water film below an impermeable layer within an infinite slope (from Park, 2013)

Laminar boxes and flexible walled buckets are the most common containers used when performing shake table testing. Flexible walled buckets are best at replicating free-field soil conditions (Figure 19), but its flexible walls make sample preparation difficult. Laminar boxes ease the process of sample preparation but it has been shown that they do not replicate free-field soil conditions. Additional complexities that both laminar boxes and flexible walled buckets share are insurance of saturation and instrument placement during deposition.

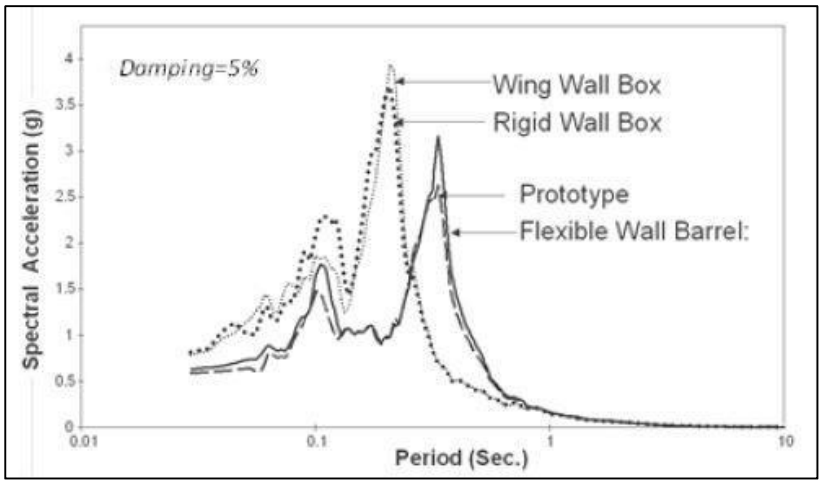

Figure 19: Dynamic response of different model soil containers (from Moss and Crosariol, 2013)

When performing liquefaction testing, saturation of liquefiable soil is required to achieve excess pore-water pressures to induce liquefaction. If soil is inadequately saturated, volume change in the compressible air void-space can have an adverse effect on pore-water pressure response and corresponding measurements. When performing small-scale simple-shear testing, samples can be easily back-saturated using de-aired water, but using de-aired water may not be realistic with the volume of pore-fluid used in large-scale testing and the container must be fabricated specifically to allow for the use of back-saturation. Saturation is generally confirmed by the measurement of p-wave velocity, where values in the range of 1500 m/s are reflective of p-waves moving only through water and solids. More recently, the legitimacy of using p-wave speeds as an indicator of saturation has been called into question by Hatanaka and Masuda (2008). Hatanaka and Masuda varied the degree of saturation in a triaxial cell by applying back-pressure to the soil sample and incrementally measuring p-wave velocity as the degree of saturation was increased. Results (Figure 20) indicated an immediate increase in p-wave velocity with saturation values above 90%, but the high variability suggests that p-wave speeds are not a reliable indicator of sample saturation.

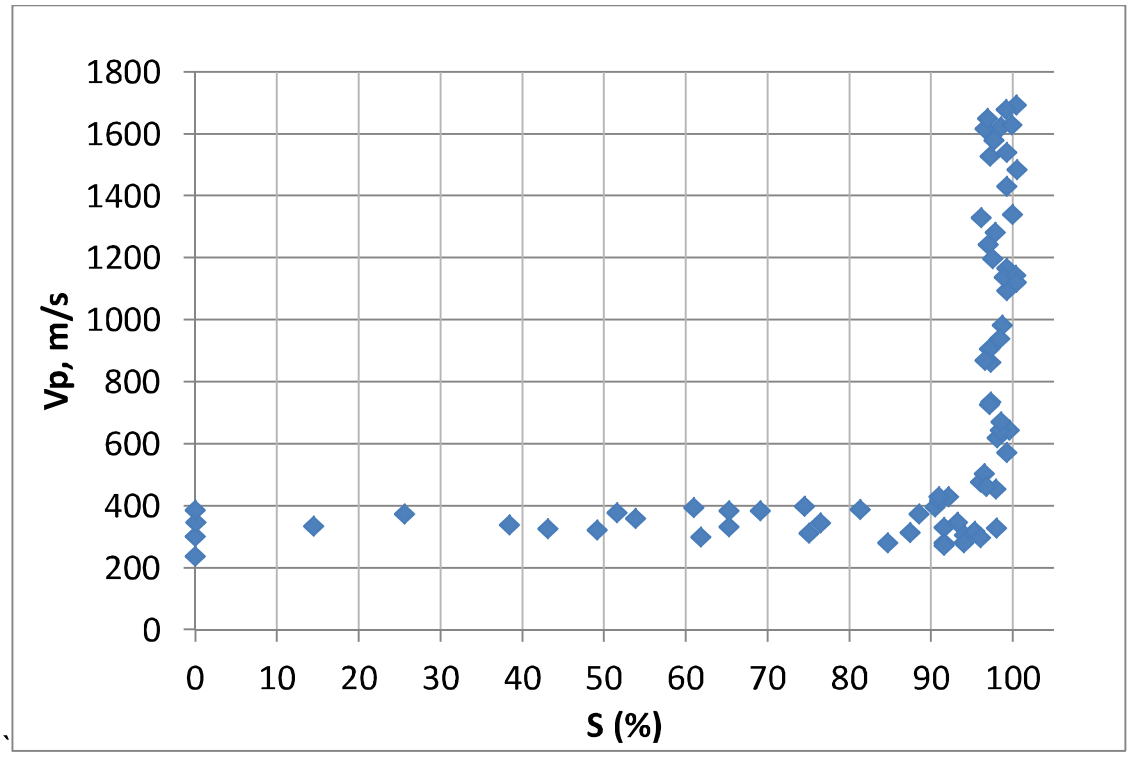

Figure 20: Measured P-Wave Velocity – Degree of Saturation Comparisons (after Hatanaka and Masuda, 2008)

Abdoun et al. (2013) compared the results of full-scale liquefaction tests on sloped and level 6 m high submerged sand deposits in laminar boxes (Figure 21) with scaled centrifuge tests. No additional overburden stress was applied to the laminar box soil samples, which were constructed using a hydraulic filling process at 40% relative density. Centrifuge specimens were constructed using dry pluviation and back saturation with viscous pore fluid at similar densities. Samples were subjected to prototype levels of shaking below 0.02g for 5 seconds resulting in excess pore water pressures insufficient to cause liquefaction, followed by moderately higher shaking at 0.05g which was sufficient to induce liquefaction for both laminar box and centrifuge tests. Slope ground tests were inclined at 2°. Abdoun et al. measured V_{s1} values of 118 m/s in laminar box samples with d_{50} ranging from 0.1 to 0.25 mm.

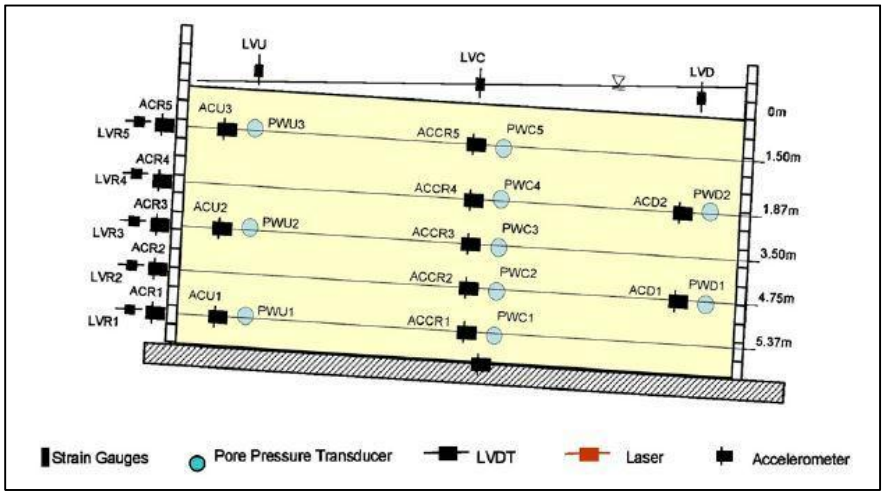

Figure 21: Laminar Box Dimension and Instrumentation Schematic (from Abdoun et al., 2013)

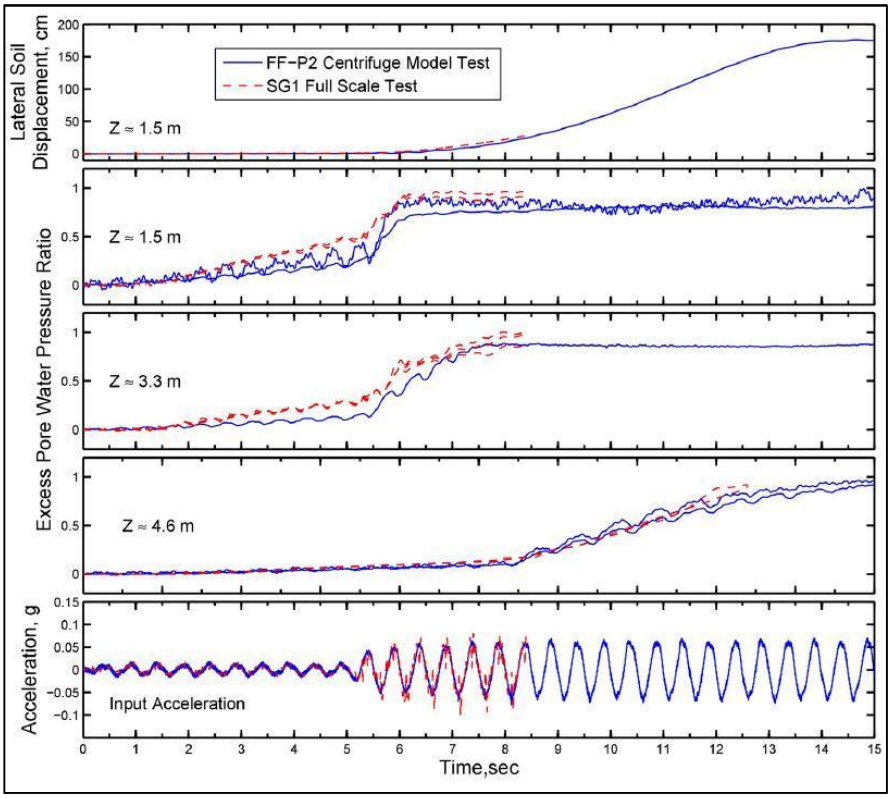

Figure 22: Acceleration, Excess Pore-Water Pressure, and Lateral Displacements for Full-scale and Centrifuge testing (from abdoun et al., 2013)

Figure 22 indicates the difference in excess pore-water pressures generated in centrifuge and full-scale laminar box shake table testing. It is evident that during low-

level shaking, excess pore pressure ratios accumulated faster higher in the sample (z=1.5m) compared to at greater depths (z=4.6m). Once higher levels of shaking began, more significant excess pore-water pressures began to accumulate lower in the sample as the soil reached liquefaction (Figure 23).

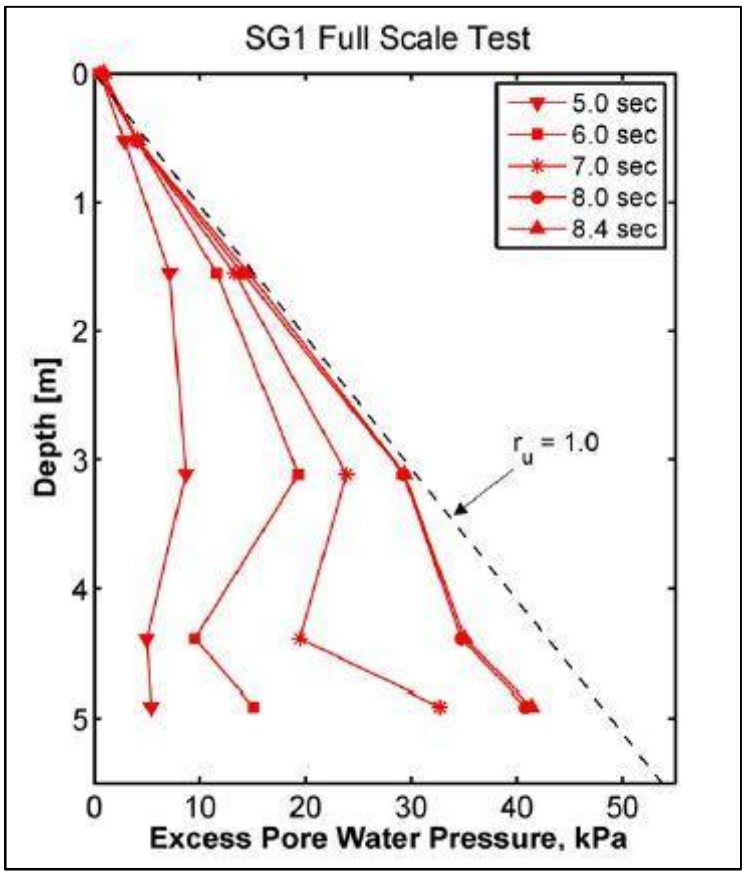

Figure 23: Excess Pore Water Pressure Profiles Measured in Large-Scale Laminar Box Testing (from Abdoun et al., 2003)

Abdoun et al. performed cone penetration testing on centrifuge samples before liquefaction, but not after. Variation in cone penetration tip resistance due to liquefaction was not captured, and no information regarding void re-distribution was collected. No cone penetration testing was performed on the full-scale laminar box soil sample.

Some concerns arise when considering the data produced from the 2013 study by Abdoun et al. The effect of the rigid boundary condition imposed by the laminar box

testing apparatus on the reproduction of free-field soil conditions during liquefaction triggering is a not necessarily addressed. Scalability of cone penetration tip resistance data on small scale centrifuge models due to small cone size and lower tip resistances compared to larger cones used in field testing is also questionable.

CHAPTER 2 MODEL PREPARATION

The experiment detailed herein was designed to perform full-scale cyclic simple-shear testing on liquefiable soil. Experiments performed by Wu (2003) and Abdoun et al. (2013) have set the framework for performing the tests described in this study. Small-scale simple shear tests by Wu (2003) were of insufficient scale to fully describe where liquefaction first occurs within a soil layer and how it propagates through the soil layer. Testing by Abdoun et al. (2013) has introduced added complexities that may not adequately re-create the conditions of Wu's 2003 study at full scale. These complexities include the effects of a rigid boundary condition imposed by a laminar box soil container as well as the presence of a static driving shear stress imposed by the sloped testing apparatus. In addition, neither Wu (2003) nor Abdoun et al. (2013) have used index testing before and after the occurrence of liquefaction as an indication of void re-distribution.

A uniform sample was constructed in a 2.3 meter diameter by 1.5 meter tall flexible-walled testing apparatus. An impermeable layer of clay was first placed at the bottom of the testing apparatus to prevent water from leaking through the bottom of the flexible-walled testing apparatus. Loose sand was then deposited using a dry pluviation method into standing water above the clay layer. The top of the water table was intended to be concurrent with the top of the sand layer upon the completion of sample preparation. The remaining free space above the liquefiable sand layer in the test apparatus was reserved for placement of an overburden apparatus. Figure 24 represents an idealized model of the filled and instrumented flexible walled testing apparatus

The flexible walled testing apparatus was instrumented to allow for changes within the liquefiable soil to be monitored before, during, and after cyclic testing. Cone penetration testing was performed to link field liquefaction performance to laboratory testing and serves as an indication of void re-distribution. Instruments within the liquefiable material were embedded during the soil deposition process with the aid of cables anchored to the bottom of the flexible walled testing apparatus. All information regarding the preparation, placement, and use of instruments for data collection is located in Chapter 3.

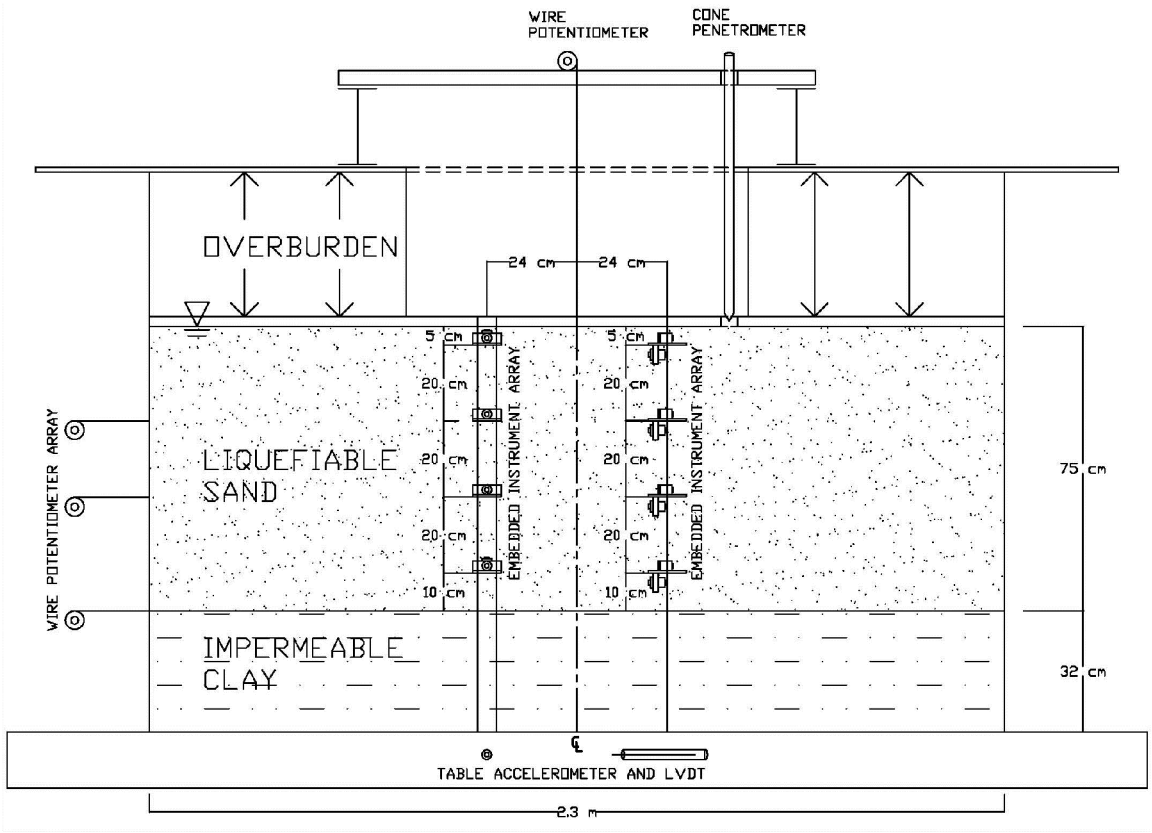

Figure 24: Testing Apparatus, Soil, and Instrumentation Diagram

2.1 Soil Sample Preparation

A layer of clay was placed before the deposition of the loose sand layer above it. The clay mixture consisting of kaolinite, bentonite, class C fly ash, and water mixed in a Chem-Grout soil mixer (Figure 25) was pumped into the bottom of the flexible-walled

testing apparatus. Sand was deposited into a standing head of water above the clay layer using a dry pluviation technique to create a loose liquefiable specimen with consistent unit weight.

2.1.1 Clay Constitution and Placement

A 32 cm thick layer of soft clay was deposited in the bottom of the flexible walled testing apparatus. The clay layer formed an impermeable boundary at the bottom of the flexible walled testing apparatus and filled the apparatus to a desired level considering the amount of loose sand available for testing. The soft clay recipe herein has been vetted in studies by Crosariol (2010), Kuo (2012), Noche (2013), and Stanton (2013). The recipe, consisting of 67.5 % kaolonite, 22.5 % bentonite, and 10% class C fly ash by mass of solids and a water content of 125% was mixed and pumped into the flexible-walled testing apparatus using an industrial grade Chem-Grout soil mixer. A layer of semi-permeable landscaping fabric (Figure 26) was placed at the top of the clay layer before the deposition of the liquefiable sand layer. Placement of the landscaping fabric between the sand and clay layers prevented the introduction of fines into the loose sand layer, insuring the creation of a clean sand sample for liquefaction testing.

Figure 25: Chem-Grout Soil Mixer

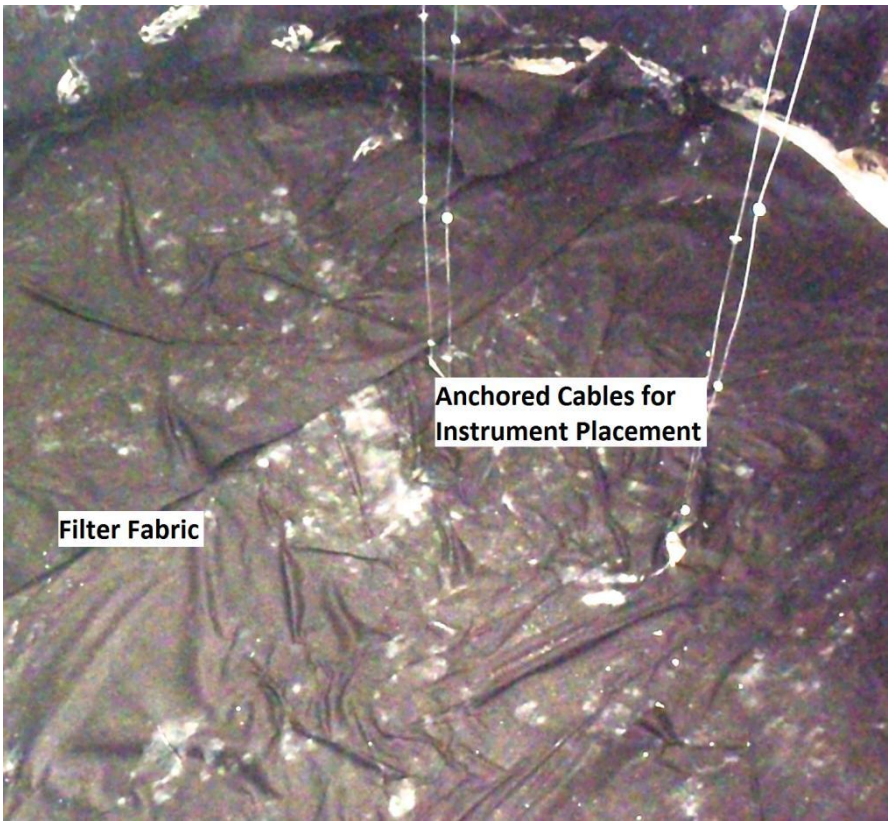

Figure 26: Anchored Cables Extending from Clay Covered with Filter Fabric

2.1.2 Sand Sample Deposition

A #2/16 Monterey sand was used to construct a 75 cm thick layer of liquefiable material above the soft clay. Sand was sourced from the CEMEX Lapis Plant in Marina, California. Figure 27 is a grain size distribution curve characterizing the #2/16 Monterey Sand used during cyclic simple-shear testing.

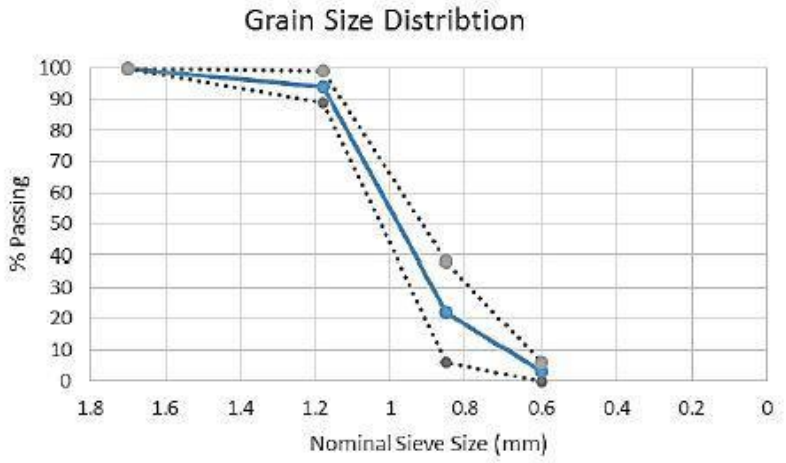

Figure 27: Upper Bound, Lower Bound, and Average Grain Size Distributions for #2/16 Monterey Sand (from Stanton 2013)

The liquefiable sand layer was constructed using dry pluviation into a standing head of water ranging from 5 to 15 cm in depth. A large-scale pluviation device (Figure 28) consisting of a large canvas bag with an opening at the bottom suspended over an expanded metal screen constructed within a timber frame with a 24” square opening was used for sand pluviation. The pluviation device was hung from and moved with the gantry crane in the Parsons Geotechnical and Earthquake Engineering Laboratory during sample construction. The large-scale pluviator was modeled after a No. 8 ASTM E-11 sieve with a 2.36 mm aperture. Small samples were constructed with both the ASTM and expanded metal screens in a large 15 cm diameter by 15 cm height proctor

mold to confirm samples created with each pluviation device were the same. The difference between total unit weights of samples created with each pluviation device was measured to be 0.19%. The total unit weight of a virgin sand sample created in the flexible walled testing apparatus was estimated to be 19 kN/m^3.

In an effort to calculate relative density of the #2/16 Monterey Sand, maximum and minimum index densities were measured using ASTM D4254 – 14 and D4253 – 14 procedures, respectively. The maximum and minimum unit weights were calculated at 17.1 and 14.7 kN/m^3, respectively. These values are in relative agreement with studies by Hazirbaba and Rathje (2009), Boulanger and seed (1995), and Kammerer et al. (2005) where maximum unit weights or Monterey Sand ranged from 16.0-17.1 kN/m^3, and minumum unit weights ranged from 13.1-13.9 kN/m^3. Pluviation of a sand sample into a proctor mold without the presence of a standing head of water produced a dry unit weight of 16.75 kN/m^3 resulting in a relative density (D_r) of 87%. The rigid boundary condition imposed by the proctor mold, difference in sample size, and lack of standing water indicate that the estimated relative density and total unit weight is non-representative of the sample produced in the flexible walled testing container.

During pluviation, the large pluviation device and a smaller No. 8 ASTM sieve were used in conjunction to produce a uniform soil sample. The large pluviation device was used to deposit large volumes of sand around the center of the flexible walled apparatus. The smaller No. 8 ASTM sieve was used to deposit smaller amounts of sand near the walls of the flexible walled bucket where it was not possible to deposit material with the large pluviation device. The drop height from the bottom of the pluviation device to the water surface ranged between 5-30 cm. As pluviation progressed, additional water was added to the container to maintain a consistent head of water to pluviate into and to prevent pluviated sand from accumulating above the water surface. Instrument packages were

embedded incrementally during the pluviation process. After the completion of deposition, the overburden application assembly was constructed above the liquefiable sand at the top of the flexible walled testing apparatus.

Figure 28: Large Pluviator and Reservoir Sack

2.2 Soil Container Modification and Overburden Assembly

Modifications to the flexible-walled testing apparatus were required in order to perform liquefaction testing. The flexible-walled bucket was originally constructed for soil-structure interaction testing with clay-based materials. The bucket was modified to incorporate an overburden application assembly at the top of the bucket. Holes were drilled in the bucket top to allow for the attachment of wide flange beams at the top of the apparatus. The beams were used as a reaction for the overburden assembly placed below them and above the liquefiable sand layer (Figure 29). The remaining components

of the overburden application assembly include a large inner-tube, upper and lower plywood confining plates, and a large pipe to confine the center of the inner-tube.

2.2.1 Container Top Modification

Holes were drilled in the upper rim of the flexible walled testing container with a portable magnetic drill press in order to attach two W8x13 grade A992 rolled steel beams as part of the vertical overburden assembly.

Figure 29: Assembled Flexible-Walled Testing Apparatus

2.2.2 Overburden Assembly

Confinement of the soil within the flexible walled testing apparatus was applied by inflating an 18.4/20.8R-42 inner tube (originally intended for tractor tire use) within a confined area in the overburden application assembly. The inner-tube was confined on all sides to inflate the inner-tube to a desired pressure (Figure 30). Nominal dimensions

of the inner-tube include a width of 18.4 inches (47 cm), a 20.8% width/height aspect ratio, and a 42 inch (107 cm) rim diameter. The inner tube was situated between upper and lower plywood confinement plates cut to fit the circular shape of the flexible walled bucket with a computer numerically controlled (CNC) router. Holes were drilled in the bottom plate of the overburden application assembly to allow for CPT soundings, instrument cable access, and the placement of a shear wave generation device. An additional 91 cm inner diameter high density polyethylene corrugated drain pipe was placed in the annular space of the inner tube as a means of confinement to allow pressure to accumulate in the inner-tube while preventing the tube from expanding into the space reserved for cone penetration testing, instrument cable access and shear wave generation. The beams fastened to the top of the flexible walled bucket provided a reaction for the upper plywood plates to confine the inflated inner tube, in turn applying an overburden pressure to the soil below. Beams were placed spanning the bucket top with adequate spacing for instrument access and the performance of CPT soundings but close enough to minimize bending in the upper plywood confinement plates. The rubber walls of the flexible-walled testing apparatus were thought to be sufficient to confine the outer walls of the inner-tube.

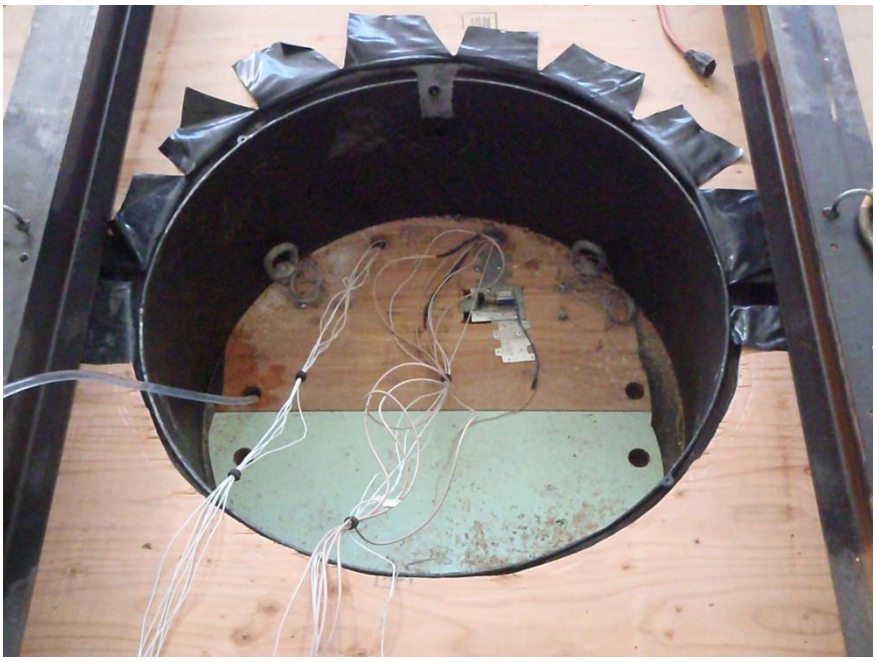

Figure 30: Overburden Assembly with shear wave generator and instrument cables

2.2.3 Overburden Estimation

The overburden pressure applied to the soil skeleton was estimated to be 11 kPa. A flat scale was inserted between the inner-tube and the top plywood overburden plate. The inner-tube was inflated to the desired pressure and the corresponding force measured on the scale was recorded. The area of contact between the scale and the inner-tube was measured to determine the stress applied to the overburden plate by the inflated inner-tube. A ratio of the plan area of the inflated inner-tube to the total area of the bucket top was multiplied by the pressure applied by the inner-tube to estimate the overburden applied by the overburden assembly on the soil below. This method required the assumption that the bottom overburden plate was stiff enough to distribute the applied load evenly on the soil skeleton below.

CHAPTER 3 INSTRUMENTATION

The flexible-walled testing apparatus was instrumented to perform a wide variety of measurements. Information of interest included P- and shear-wave (S-wave) velocity, cyclic stress, hydrostatic and excess pore water pressures, lateral and vertical deformations, and void re-distribution. Waterproofed instrument packages were embedded within the sand layer during deposition and additional instruments were placed around the perimeter of the testing apparatus.

Instrumentation used for full-scale liquefaction testing included accelerometers, pore-pressure transducers (PPT's), wire potentiometers, a linear variable displacement transducer (LVDT), a shear-wave generation device, and a cone penetrometer. Water-proofed accelerometers were embedded within the sand during deposition in a variety of orientations to measure s-wave velocity, p-wave velocity, and horizontal accelerations with time. Water-proofed PPT's were embedded in the loose sand layer to measure hydro-static and excess pore-water pressures. Wire potentiometers were used to measure lateral displacements on the perimeter of the flexible-walled testing apparatus and vertical displacements of the bucket top during cyclic testing. An additional accelerometer and LVDT, part of the shake table's electronic control system were used to measure the accelerations and displacements of the shake table's input motion during cyclic testing. A shear-wave generation device was designed and constructed to induce S-waves in the soil sample so that accelerometers embedded within the soil sample could be used to measure S-wave velocity. A cone penetrometer was used to measure changes in soil penetration resistance within the soil sample and to correlate the sample with field measurements

3.1 Instrument Embedment

Two vertical arrays of instruments were embedded in the soil sample and exposed to submerged conditions. Each array contained 4 instrument packages, each package mounted on an acrylic plate spaced equidistant within the sample. The placement of each instrument package used anchored cables with crimped cable stoppers to rest against. The acrylic plate for each instrument package was cut with a notch on each side and placed between the two anchored cables on the crimped stoppers when the sand reached the pre-determined level for instrument package placement (Figure 32).

Two 1.6 mm diameter cables were attached to eyelets epoxy-bonded to the bottom of the flexible-walled testing container for each vertical instrument array (Figure 33). Aluminum stoppers were crimped to each cable at the pre-determined instrument locations (Figure 34). Cable stoppers for instrument placement were spaced equidistant at a 20 cm spacing and the bottom cable stop for instrument placement was located 10 cm above the clay-sand interface.

One array contained accelerometers oriented in the direction of shaking and included vertically oriented accelerometers paired with the top and bottom accelerometers. The second array contained accelerometers and pore pressure transducers (PPT's), both of which were oriented perpendicular to the direction of shaking (Figure 32). In plan-view, both vertical arrays were spaced 24 cm forward of the center of the bucket. One array was placed 24 cm to the left of the center of the bucket, the other was placed 24 cm to the right of the bucket. Intended location of CPT soundings was taken into account when placing instrument arrays to avoid instrument strike during CPT soundings (Figure 31).

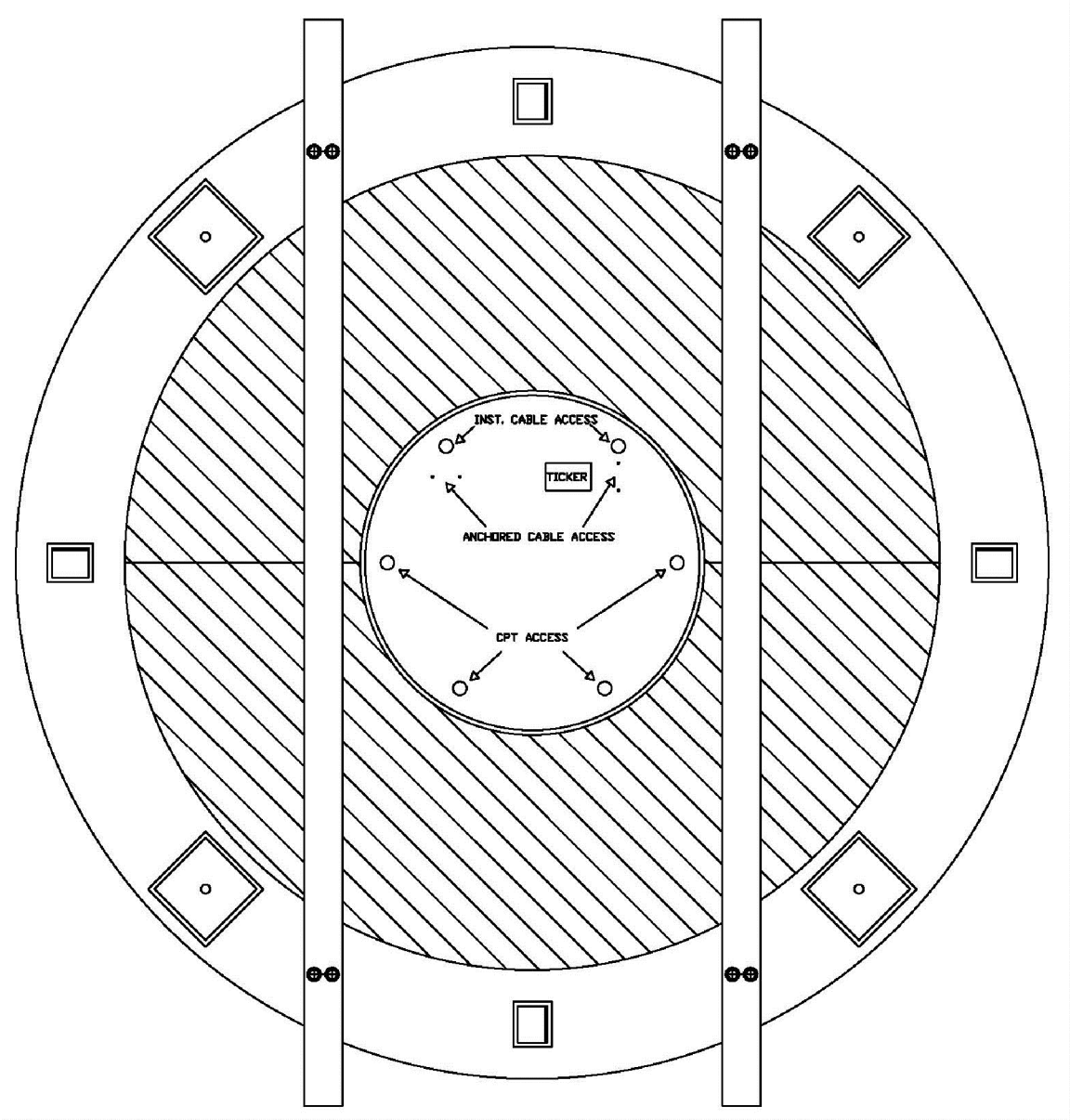

Figure 31: Flexible-Walled Testing apparatus Plan-View Diagram

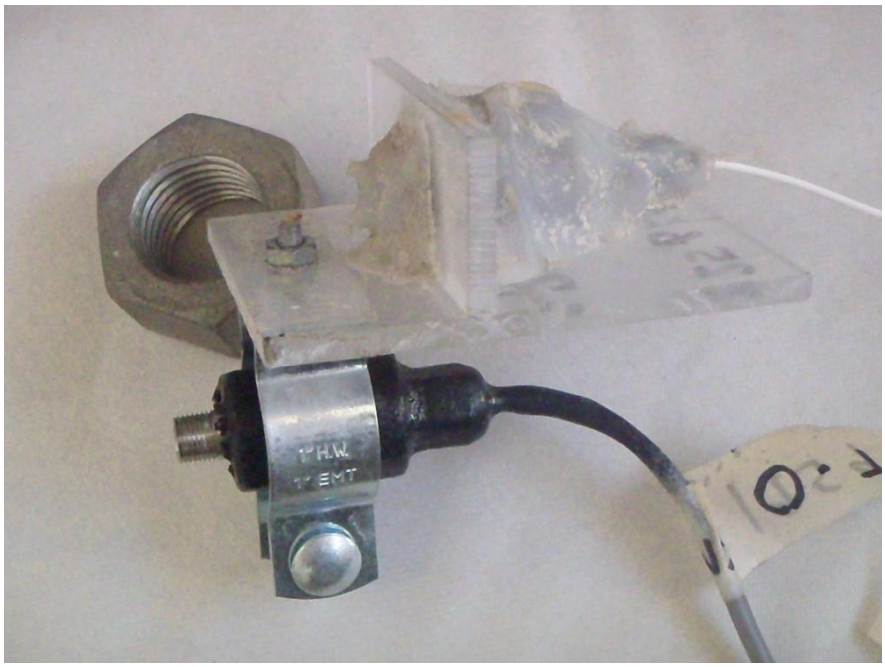

Figure 32: Accelerometer and Pore-Pressure Transducer Instrument Package

Figure 33: Cable Anchors at Bottom of Flexible Walled Bucket

Figure 34: Crimps and Washers for Instrument Package Placement

3.2 Instrument Waterproofing

PPT's were water-proofed by sealing the instrument-cable interface with multiple layers of liquid-rubber sealant spray. PPT's were spliced to longer cables in order to reach the data acquisition (DAQ) device. PPT cable splices were also water-proofed by first applying heat-shrink tubing and second sealing with multiple layers of liquid electrical tape. Water-proofed transducers were submerged for 48 hours while measuring hydrostatic pressures intermittently to ensure adequacy of water-proofing before embedment in the loose sand layer. Accelerometers were water-proofed with silicone caulking by previous researchers for embedment in soil as part of a prior study and were not modified before embedment.

3.3 Instrument Calibration

Calibration values were assigned for all accelerometers, pressure transducers, and displacement transducers connected to a data acquisition system utilizing LabVIEW software. Calibration data supplied by the manufacturer was utilized for all accelerometers. Pressure and displacement transducers were individually calibrated as part of this study.

3.3.1 Accelerometer Calibration Values

PCB 393B04 integrated circuit piezoemeter (ICP) accelerometers capable of measuring accelerations ranging from 0 to 5 g's with calibration values provided by the manufacturer were embedded within the soil sample. An additional PCB 353B52 ICP accelerometer, with a calibration value of 502 mV/g, also provided by the manufacturer was used to measure the shake table (input) accelerations. Accelerometers were connected to the DAQ system via a National Instruments SCXI 1531 accelerometer amplifier. Accelerometers were named as follows: the name "acct" corresponds to instrument orientation transverse to the direction of shaking while the name "acci" corresponds to orientation in the direction of shaking and the name "accv" corresponds to a vertical orientation. The number following the instrument name refers to the instrument's location within the soil sample, where an increasing number refers to a higher elevation within the sample. An 0 refers to an instrument located at the bottom of the sand layer, 3 refers to an instrument located at the top of the layer. Instruments with the number 1 and 2 following the instrument name are located intermediately within the soil sample. Accelerometer calibration values are presented in Table 1.

Accelerometer	Calibration Value mV/g
acct0	1000
acct1	1000
acct2	988
acct3	1028
acci0	982
acci1	1020
acci2	1000
acci3	1028
accv0	1000
accv3	1000

Table 1: Accelerometer Calibration Values

3.3.2 Pore Pressure Transducer Calibration

Omega PX481A-015G5V stainless steel industrial pressure transducers were chosen for embedment within the liquefiable sand to measure excess pore-water pressures during cyclic testing. The nominal pressure range for the Omega PX481A-015G5V is 0 to 103 kPa gage, with corresponding output voltages ranging between 0 and 5 volts D.C.. PPT's were calibrated simultaneously by attaching all transducers to a manifold (figure 35) which was subjected to applied pressures. An Omega DPG4000 high accuracy pressure gage connected to the manifold was used to record pressures applied to the pressure transducers during the calibration process. The DAQ system was used to record voltages produced by the pore pressure transducer as a response to applied pressure.

Figure 35: Manifold, Pressure Gage, and Pore-Pressure Transducers

Two methods of PPT calibration were performed. During the first calibration sequence, pressures were applied to the manifold using a hydrostatic water column with varying water height. During the second phase, pressures were applied using an air compressor attached to the pressure manifold in series with a pressure regulator to control the pressure applied to the manifold, gage, and each pressure transducer. During calibration and subsequent data collection, an excitation voltage of 10 Volts D.C. was applied to power each instrument. PPT's were wired to National Instrument's SCXI 1520 Universal strain gage input modules which interface with the LabVIEW environment. Applied pressures for calibration were recorded using the DPG4000 pressure gage and transducer voltages were recorded using the DAQ system and LabVIEW. The method of pressure application was determined to be inconsequential. PPT's behaved linearly within the 0-103 kPa range, 5 calibration points were sufficient to characterize the instrument's response to applied pressure (Figure 36). Calibration values for each pressure transducer are presented in Table 2.

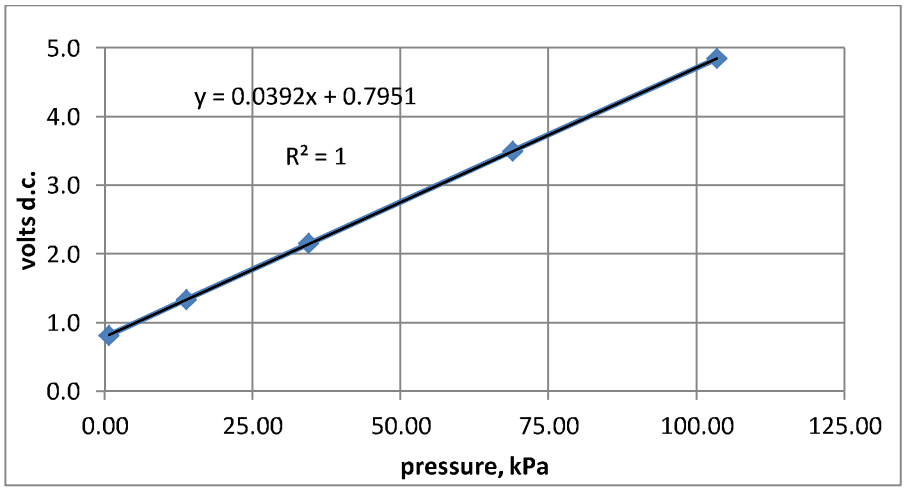

Figure 36: PPT0 Calibration Line

ppt	0	1	2	3
kPag	Volts D.C.			
0.7	0.82	0.79	0.81	0.81
13.8	1.34	1.31	1.33	1.33
34.5	2.15	2.13	2.15	2.14
68.9	3.50	3.47	3.49	3.49
103.4	4.85	4.82	4.84	4.84

Table 2: Pore Pressure Transducer Calibration Values

3.3.3 Displacement Transducer Calibration and Placement

A vertical array of three wire potentiometers (Figure 37) was attached to beams separated from the shake table in an effort to measure lateral displacements of the flexible walled testing apparatus along its height. The lowermost wire potentiometer (wp0) was placed to measure displacements of the clay/sand interface, the next two wire potentiometers (wp1 and wp2) were placed to measure displacements in the sand at the elevations of the two instrument packages embedded intermediately within the loose sand. Similar to the naming convention of embedded accelerometers and PPT's, the number following the wire potentiometer's name increases with increasing height above the bottom of the loose sand layer. An additional potentiometer was fixed to the top of the overburden application beams with its wire connected to the bottom plate of the soil

overburden assembly in order to measure equivalent footing settlement above the liquefied soil. Although volumetric strains could not be measured due to the ejecta flowing through the overburden apparatus' bottom plate, a measure of the volumetric strains minus the volume of ejecta was possible. These displacements can be considered similar to structural settlements in the presence of liquefaction where ejecta has migrated to the ground surface.

Figure 37: Wire potentiometer

Displacement transducers were connected to a National Instruments SCXI 1540 LVDT Amplifier to interface with the DAQ environment. The calibration process for each wire potentiometer involved fixing a potentiometer to the top of a laboratory work bench, extending the potentiometer's wire, measuring the displacement with a tape measure, and committing the measured value using the LabVIEW instrument calibration tool. The

LabVIEW calibration tool associates a measured displacement with a voltage produced by the potentiometer when a value is committed so that measurements are presented in the preferred units during data acquisition.

3.4 Shear Wave Generation Device

A shear-wave generator named 'The Ticker' (Figure 38) was constructed to automatically induce S-waves into the flexible walled testing apparatus that it was mounted atop of. The frequency of ticker operation was calibrated to 2 Hz. A steel flange extending from the bottom of the plate that the ticker was mounted to was embedded into the liquefiable sand below. A high-current power source, an Arduino micro-controller, and a circuit-board consisting of bipolar junction transistor (BJT) and MOSFET transistors and a resistor were designed to control the Ticker. The Ticker's control system was placed off-board from the shake table and flexible-walled testing apparatus. Accelerometers embedded within the sand sample in the same orientation as the ticker (transverse to the direction of shake table movement) were used to record shear waves induced by the ticker. Shear-wave velocity was calculated by comparing time histories recorded in the vertical array during post-processing.

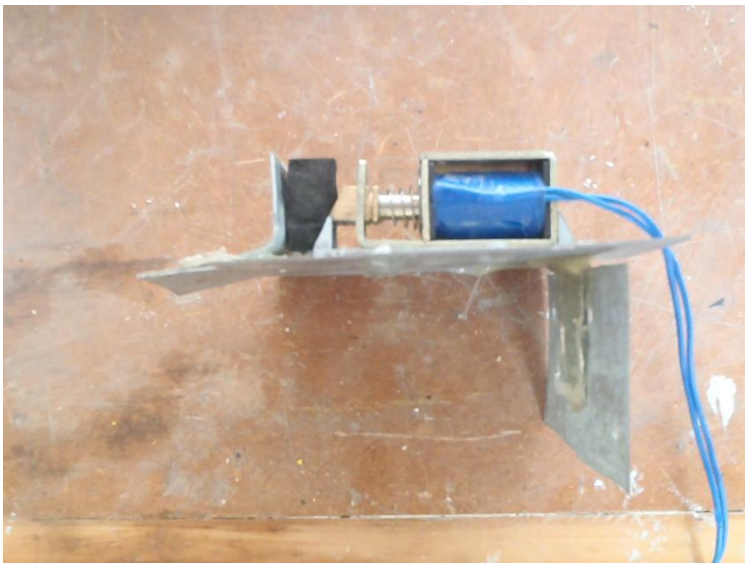

Figure 38: Side View of Shear-Wave Generator

3.4.1 Device Construction and Operation

The Ticker contains a solenoid electro-magnet with a loose steel rod inside a cylinder surrounded by the magnet's coil. The electro-magnet was mounted on a steel plate with a flange extending into the soil sample on which the Ticker was mounted. When the magnet is engaged the steel rod is pulled into a locked position against a rigid boundary at the end of the electro-magnet. Release of the electro-magnet allows a compressed spring to pull the opposing end of the rod into its resting position where a clip-washer attached to the rod contacts another boundary preventing it from falling out of the Ticker assembly. Both the electro-magnet and spring induced actions produce a signal that can be recorded by the accelerometer's embedded in the soil below. An additional boundary padded with a piece of high density neopreme foam was added to the ticker assembly, serving the same function as the clip washer in preventing the steel rod from falling out of the ticker assembly. The foam-backed boundary allowed for the removal of the clip washer and eliminated the noise produced by the clip washer rattling against its rigid boundary.

The Ticker control system contains a power source, Arduino micro-controller, and a wiring configuration of BJT and MOSFET transistors and a resistor (Figures 39 and 40). The Arduino micro-controller was programmed to output a square wave oscillating between 0 and 5 volts D.C. at a 50% duty cycle and a calibrated frequency. The power source used is a Tehma Laboratory D.C. Power Supply 72-420 set to 20 V D.C. with a current of 1.2 amps. The high current of the Tehma power source was required to operate the high-resistance solenoid electro-magnet. When combined, the transistors and resistor function to oscillate the power supply at the corresponding frequency and duty cycle as the micro controller signal to operate the Ticker.

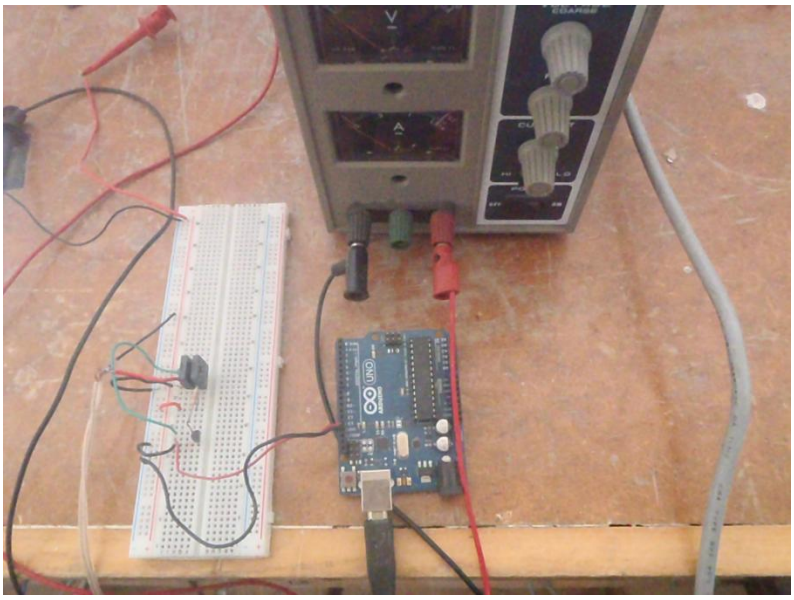

Figure 39: Ticker Control Assembly

Each transistor contains three prongs. The MOSFET contains gate, drain, and source prongs, and the BJT contains collector, base, and emitter prongs. The BJT emitter is connected to ground, the base is connected to the positive pin on the micro-controller, and the collector is connected to the power source as well as the MOSFET gate. The resistor is positioned between the power source and the BJT to prevent it from burning out. When the micro-controller supplies sufficient voltage (position high), the BJT

engages allowing the power to flow to ground, otherwise power flows directly to the MOSFET (micro-controller position low). This process effectively amplifies micro-controller signal so that it can operate the MOSFET switch. When the signal on the micro-controller is high, the signal on the wire between the BJT collector and the MOSFET gate is low and vice versa.

As previously mentioned the MOSFET gate and BJT collector are connected, the remaining MOSFET pins are allocated as follows: the drain is connected in series to the mechanical ticker mechanism followed by power and the source is connected to ground. When the gate is closed by the BJT (position high), current is allowed to flow from the power source through the Ticker and the MOSFET to ground, engaging the ticker. When the gate is open (gate position low), no current flows causing the Ticker to release. Multiple MOSFETs and BJTs are used in parallel to add redundancy to the system. In the case that one of each transistor fails, the system will still maintain functionality although each transistor will be under a higher load.

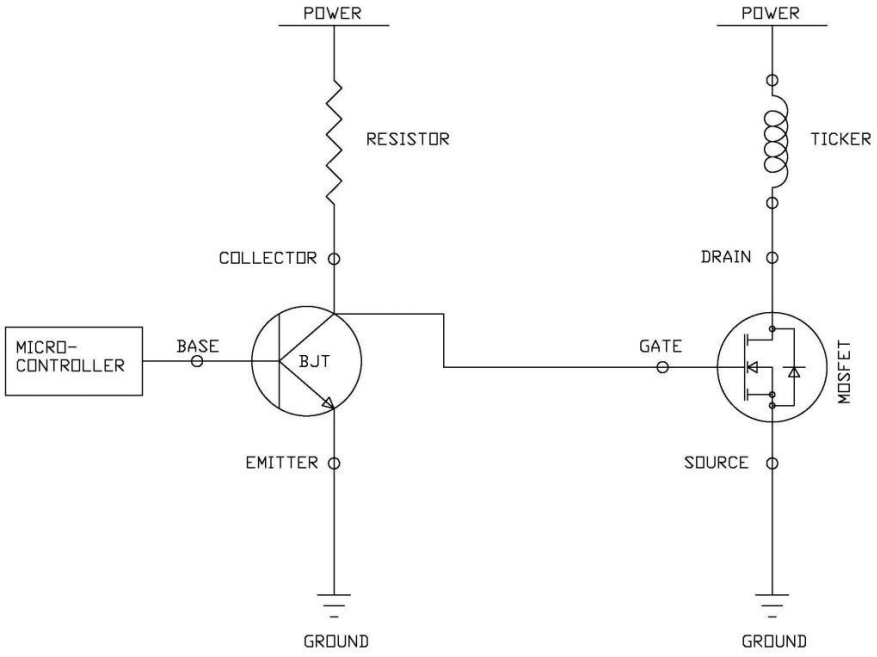

Figure 40: Ticker Electronic Wiring Diagram

The Ticker was calibrated to operate at 2 Hz for optimal S-wave measurement. Operating the Ticker with increasing frequency decreases the time between S-wave measurements, increasing the fidelity of S-wave measurements throughout the soil column. A maximum frequency of 20 Hz was set because the Ticker began to function in a non-cyclic manner. A much lower, 2Hz operation frequency was set to allow for full wave-train passage to ease the task of determining S-wave velocity, eliminating the possibility of confusing an early arrival with a trailing peak of an S-wave train. Although both the electro-magnet and spring based signals induce S-waves into the soil column, the spring based signal is considerably weaker than the electro-magnet induced one, and is therefore not recommended for determination of S-wave speed.

3.4.2 Determination of Shear-Wave Speed

The procedure of estimating shear wave velocity is outlined in *Seismic Cone Downhole Procedure to Measure Shear Wave Velocity* (Butcher et al. 2005). While some authors advocate for picking the first arrival as part of the shear wave velocity measurement procedure, Butcher et al. suggest that the first major cross-over of oppositely polarized (butterflied) shear waves can be taken as a "reference" arrival or an arrival pick can be made by an experienced operator. Suggesting that an arrival pick can be made by an experienced operator indicates that the determination of S-wave velocity is a partially subjective process. Butcher et al. vaguely state that like points can be compared to calculate S-wave speed if they are sufficiently close to the first arrival.

A number of tools including wave stacking, opposite polarization, and filtering may be used in an effort to ease the S-wave speed determination process. Wave stacking and opposite polarization can be employed during static field testing, but may not be possible during dynamic testing. Filtering is possible to reduce the effect of noise on the accelerometer time history, however epistemic uncertainty is induced during the process

and may reduce precision in determining s-wave speed. Comparing relative arrival times of like peaks and troughs towards the beginning of an individual wave train is the preferred method to determine wave speed because multiple values allow for the determination of an average and the removal of outliers.

3.5 Cone Penetration Testing

Cone Penetration testing was performed to correlate lab measurements with field measurements and to monitor void re-distribution by measuring changes in soil stiffness before and after liquefaction. Cone Penetration Testing was performed with the aid of MAR Incorporated and the Naval Facilities Engineering Command (NAVFAC).

A 2.54 cm diameter instrumented piezometric cone penetrometer was used to perform cone penetration testing. A smaller, 1.5 cm diameter cone was available for testing, but the larger cone was chosen because it would develop larger forces resulting in more accurate measurements than the smaller cone. Additionally, the considerably stiffer 2.54 cm cone was expected to stay plumb compared to the 1.5 cm cone that could be expected to drift laterally during CPT soundings. For stress calculation purposes, the nominal conical tip area of the 2.54 cm diameter cone is equal to $10 cm^2$.

The gantry crane in the Parsons Geotechnical and Earthquake Engineering Laboratory was used to suspend and lower the cone and rod assembly into the flexible-walled testing apparatus to perform CPT soundings. A cross-bar was included in the cone assembly to attach the cone penetrometer to the gantry crane (Figure 41) and hang a 205 kg mass (Figure 42) required to drive the cone through the soil specimen. CPT soundings were performed at a descent rate of 1.3 cm/s, the default crane descent rate. 1.3 cm/s is slower than the 2 cm/s suggested by the ASTM D 5778 specification, but was not expected to result in appreciable differences in cone tip resistance compared to

the 2 cm push rate. Centralizers were attached to the overburden reaction beams at the top of the flexible-walled soil testing apparatus to help keep the cone plumb during testing. An additional wire potentiometer was attached to the fixed centralizer guides with its cable extended and attached to the cone penetrometer crossbar to monitor the cone tip position during CPT soundings (Figure 43). Instrumentation and calibration for the performance of CPT soundings was provided by MAR Incorporated.

Figure 41: Cone Penetrometer Assembly

Figure 42: Cone Penetration Reaction Mass

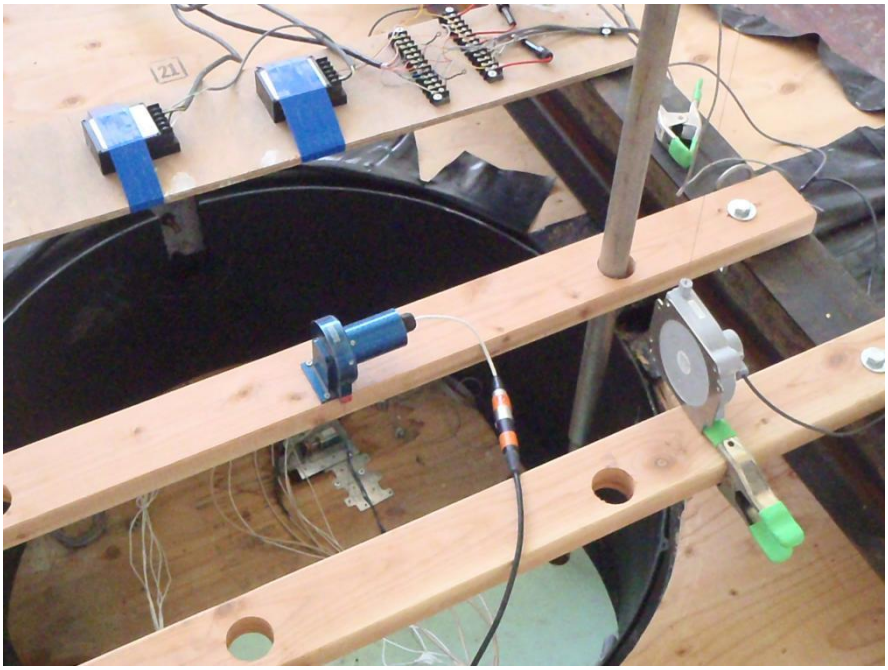

Figure 43: Cone Penetration Centralizing Guides and wire potentiometer

CHAPTER 4 TESTING

Testing in the flexible-walled testing apparatus consisted of a series of static and dynamic tests. A series of small-scale pilot tests was performed to assess the feasibility of testing at full scale. A sine-sweep was performed to determine the first natural frequency of the testing apparatus with soil. A P-wave velocity test was performed before the occurrence of liquefaction in an effort to estimate the soil's degree of saturation. The amplitude of cyclic loading was estimated using a simplified triggering analysis. A series of cyclic tests was performed near the natural frequency of the container and virgin sand to induce and observe the liquefaction process. CPT soundings and S-wave testing was performed before and after cyclic testing.

4.1 Wave Speed Calculations

P- and S-wave velocity measurements provided valuable information in both pilot and full-scale testing for their ability to provide indications of both degree of saturation and soil stiffness, respectively. P- and S-wave Velocity was estimated using accelerometers embedded within the sand sample. Both procedures required the relative locations of embedded accelerometers in order to estimate wave speed.

4.2 Pilot Testing

Prior to the performance of full-scale cyclic testing in the flexible-walled testing apparatus, a smaller scale series of pilot tests was performed in a plastic 55 gallon barrel. Goals of the pilot program were to develop soil deposition methods, optimize the Ticker mechanism, and take index P- and S-wave velocity measurements of the soil. Instrument locations used to estimate P- and S-wave velocity during index testing was determined when the instruments were embedded in the sample. P-wave velocity estimates during pilot testing ranged from 234-381 m/s. Comparison of P-wave velocity data from pilot testing with data from Hatanaka and Masuda (2008) (figure 44) is

inconclusive regarding the degree of saturation of soil deposited during pilot testing. S-wave velocity estimates ranged from 190-227 m/s after the soil was deposited. A hammer was used to strike the side of the 55 gallon barrel to induce impulse liquefaction in the embedded soil. S-wave velocity estimates after impulse liquefaction ranged from 243-261 m/s. Measurements taken during pilot testing within the relatively stiff boundary of the 55 gallon barrel were expected to result in higher P- and S-wave velocities compared to those measured in the flexible walled testing apparatus for a similar deposition technique. The larger sample size and more flexible boundary condition imposed by the flexible-walled testing apparatus was hoped to have less of an effect on measurements taken during full-scale testing. Results from pilot testing suggested that the soil deposited in the 55 gallon drum may not have been fully saturated, but that liquefaction was still possible. The same deposition technique was employed for full-scale testing in the flexible-walled testing apparatus.

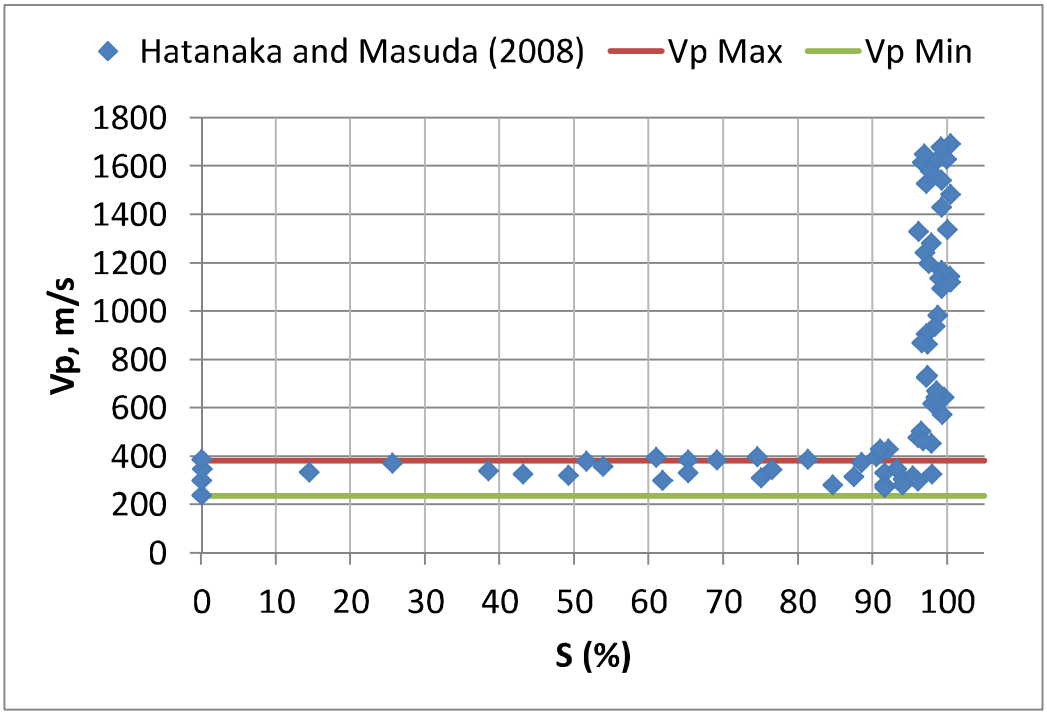

Figure 44: Range of P-Wave Velocity During Pilot Testing Compared to P-Wave Velocity and Degree of Saturation Data (after Hatanaka and Masuda, 2008)

4.3 Sine-Sweep Testing

A preliminary sine-sweep on the flexible-walled testing apparatus filled with virgin soil. The magnitude of acceleration during the sine sweep was set to 0.01 g and the sweep was performed between the frequencies of 1 and 20 Hz. A fast-fourier transformation performed in Matlab using accelerometer time-histories of the sine-sweep from the time to the frequency domain indicated that the first mode of the flexible walled testing apparatus filled with virgin loose sand was 8.371 Hz (Figure 45). All four accelerometers embedded in the sample oriented in the direction of shake table movement were in agreement with the frequency of the first mode of the flexible-walled soil testing container's vibration.

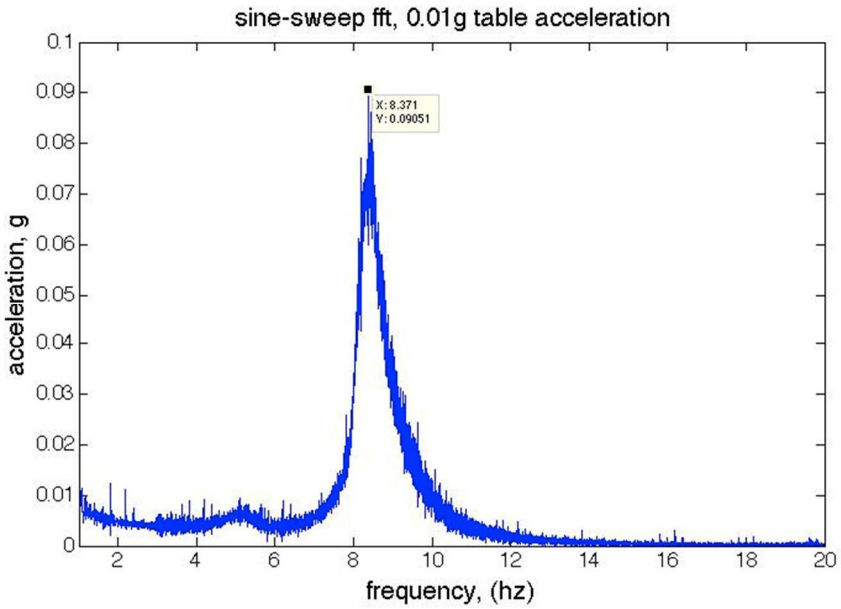

Figure 45: Sine Sweep Fast Fourier Transformation of the Uppermost Accelerometer Embedded in the Virgin Liquefiable Sand Oriented in the Direction of Shake Table Movement

Pore-water pressures were monitored during sine-sweep testing. At the magnitude 0.01g, the cyclic stress was low enough to prevent excess pore pressures from being

generated during the sine sweep, indicating that liquefaction was not induced during the sine-sweep.

4.4 Initial Cone Penetration Test Soundings

Two CPT soundings were performed within the flexible-walled testing apparatus (Figure 46) before cyclic testing. Each CPT sounding was performed through a CPT access hole in the overburden apparatus where no CPT sounding had been performed before. CPT tip resistance measurements for the loose sand were used for comparison against CPT soundings performed after cyclic testing. Maximum CPT tip resistances were recorded at depths ranging from 40 to 50 cm below the sand surface, with a maximum tip resistance of approximately 400 kPa. At depths greater than 50 cm below the sand surface, CPT tip resistance began to decrease as the proximity to the soft clay layer below had an increasing influence on recorded values. CPT tip resistance values increased momentarily when the cone tip reached the sand-clay interface where the landscaping fabric intended to separate the clay and sand during sample preparation was located. The cone penetrometer measured relatively uniform tip resistances through the soft clay layer after the tip pierced the landscaping fabric until the termination of testing.

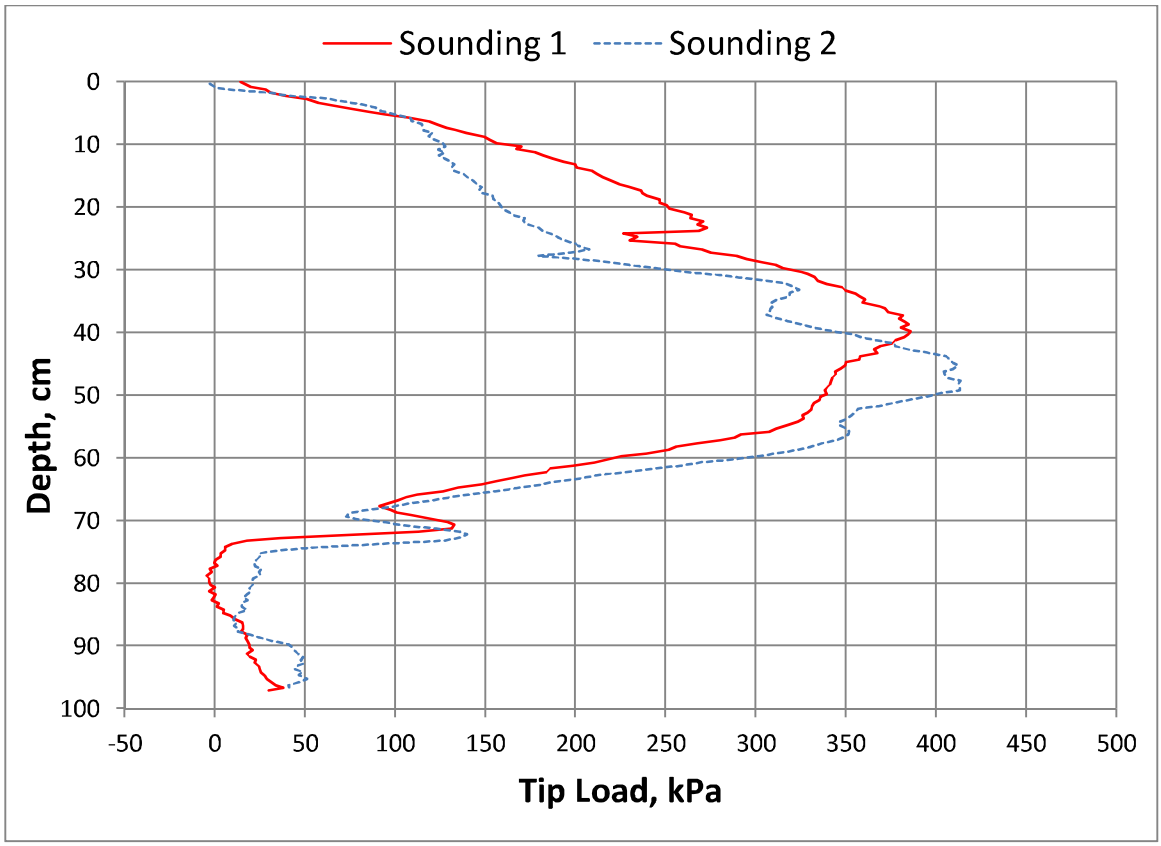

Figure 46: Initial CPT Soundings Performed on Virgin Loose Sand

4.5 Full-scale P- and S-Wave Velocity Testing

P- and S-wave speeds were used to confirm similarity of the sample deposited in the flexible-walled testing apparatus to that deposited in the 55-gallon drum. In addition, s-wave velocity was used to monitor the soil's change in stiffness as an effect of cyclic shaking.

4.5.1 Instrument Locations

Instrument locations were estimated by converting measurements of hydro-static water pressure to instrument depth below the water surface. The piezometric surface was observed to be concurrent with the top of the sand layer. The depth of instruments not attached to PPT's was assumed to be located at the same depth as the PPT's it was embedded at the same depth as. Hydro-static measurements were in agreement with

the intended embedment depths associated with locations of crimped cable stoppers placed on anchored instrument placement cables in the flexible-walled testing container.

4.5.2 P-Wave Velocity

A P-wave velocity test was performed before the occurrence of cyclic testing. A hammer was used to repeatedly strike the bottom plate of the overburden application apparatus directly above the vertically oriented accelerometers embedded within the loose sand sample. P-wave velocity was calculated by comparing the relative first arrival times of the hammer induced P-wave and divided by the distance between the vertically oriented accelerometers. P-wave velocity estimates ranged from 324-531 m/s for the virgin un-liquefied sand deposit. Comparison of P-wave velocity to data reproduced after Hatanaka and Masuda (2008) (figure 47) is similarly inconclusive regarding degree of saturation compared to pilot testing, but indicates that the samples created during pilot testing and full-scale testing differ slightly. Differences in P-wave velocity measured before pilot testing and full-scale testing is attributed to variation in the sample deposition technique and difficulties in creating a similarly uniform sample as sample size increases. Estimation of the P-wave velocity of the sample brought the liquefiability of the sand and the ability for embedded instruments to capture the liquefaction process in both pilot and full-scale testing into question.

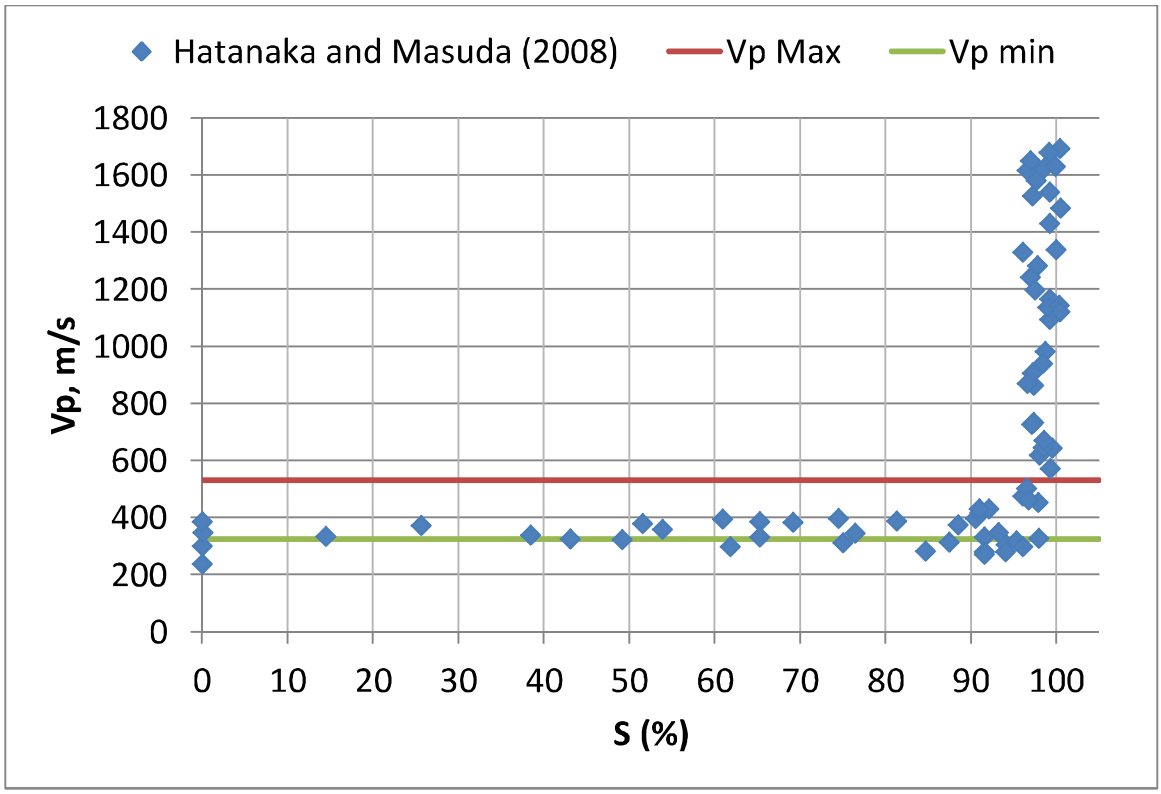

Figure 47: Range of P-Wave Velocity Recorded Before Full-Scale Testing Compared to P-Wave Velocity and Degree of Saturation Data (after Hatanaka and Masuda, 2008)

4.5.3 S-wave Velocity

S-wave velocity was measured in the loose sand before cyclic testing using the Ticker (Figure 48). Measurement methods discussed in 3.4.2 were utilized for S-wave velocity estimation. S-wave velocity data was used for comparison against S-wave velocity measurements taken after cyclic testing to observe the change in S-wave velocity due to cyclic testing.

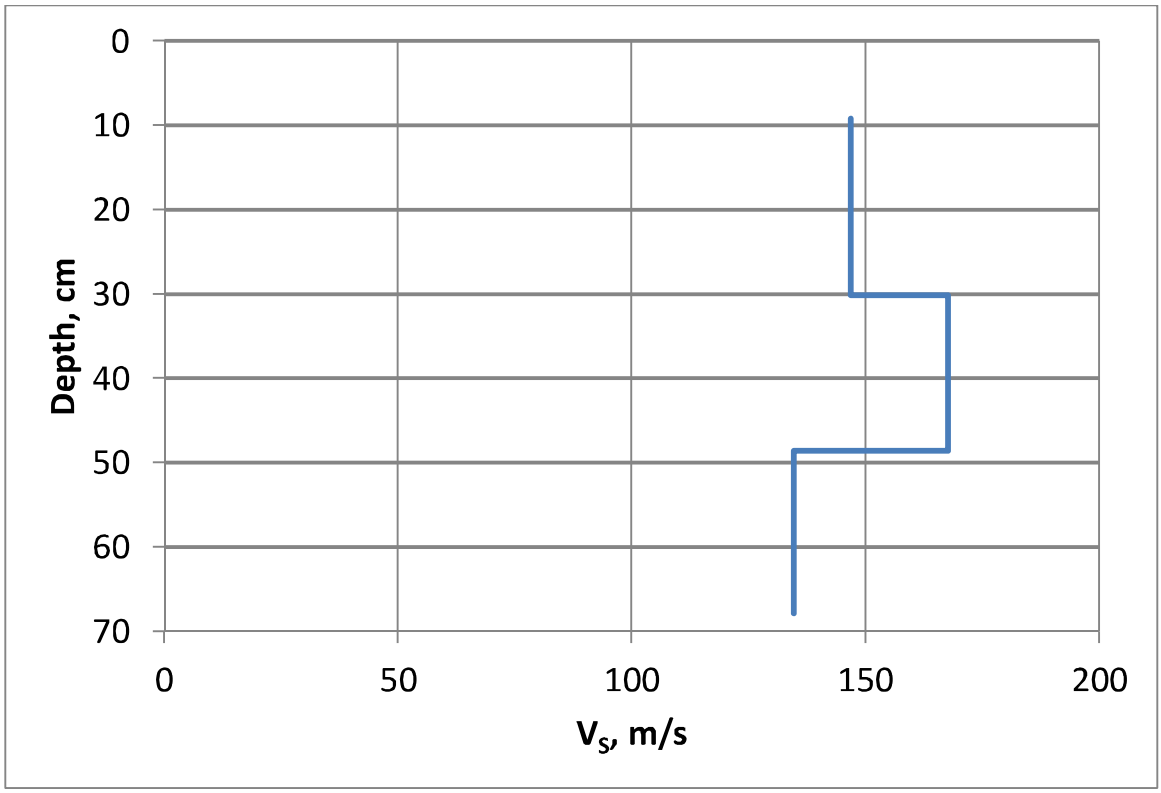

Figure 48: S-Wave Velocity Profile Before Cyclic Testing

4.6 Cyclic Testing Parameters

A testing frequency of 8 Hz was chosen for all cyclic simple-shear testing. Normalized S-wave velocity (V_s) and CPT tip resistance techniques were used to determine the liquefaction resistance of the liquefiable sand deposited in the flexible-walled testing apparatus. A testing duration of 40 cycles was chosen to enable observation of the entire liquefaction process.

Although the first natural frequency of vibration was calculated to be 8.371 Hz, a testing frequency of 8 Hz was chosen as a means of practicality for cyclic testing. The container and soil's natural frequency was expected to drift during testing and from test to test due to changes in stiffness and volume of the liquefied soil. The testing frequency did not change from test to test.

A target CSR of 0.2 was chosen to induce liquefaction in the virgin loose sand. Lateral cyclic accelerations of 15% of Gravity were determined using equation (3) corresponding to the target CSR of 0.2 at the depths where CPT and V_s measurements were greatest during their initial soundings. A CSR of 0.2 was considered to be sufficient to liquefy the loose sand sample as it is a region on liquefaction triggering curves highly populated with liquefaction case histories.

$$\frac{a}{g} = \frac{csr * \sigma'_{v0}}{\sigma_{v0}} \quad \text{.....(3)}$$

A reference 15 cycles associated with the M_w 7.5 earthquake triggering curves was assumed to be too short to observe the complete liquefaction process. A testing duration of 40 cycles was chosen to ensure that the full development of liquefaction triggering, shear-strain accumulation, and drainage of excess pore-water pressures would be observed during cyclic testing

4.7 Cyclic Testing

A series of cyclic simple-shear testing was performed with increasing cyclic stress from test to test. Unfortunately, a data acquisition error prevented the collection of any data during the first round of cyclic testing. As a result, the first two tests were performed with the same cyclic stress. Additional tests were performed with an emphasis on observing performance of the testing apparatus under extreme loading.

4.7.1 Cyclic Test 1

During the first phase of cyclic testing a data acquisition timeout error occurred that prevented the collection of data for the duration of the test. The timeout time is the time the computer must wait after measurements made by the data acquisition instruments before the data becomes available to be committed to memory. The timeout was modified from 10 seconds to a significantly lower value of 1 second. The lower timeout

value was successful in allowing the data acquisition program to record for the entirety of future tests without error.

Evidence of liquefaction was observed during test 1, consisting of 1.69 inches of settlement of the lower overburden apparatus plate and the observance of ejecta around the perimeter and within the interstitial space of the overburden apparatus. Ejecta also submerged the Ticker mechanism, causing it to become inundated at which point it stopped functioning. The ticker was not available for testing during Cyclic test 2, but was later fixed so that it could be used for subsequent testing.

4.7.2 Cyclic Test 2

Although the Ticker was not functional during Cyclic Test 2, lateral accelerations, lateral displacements, bottom overburden apparatus plate vertical displacement, and excess pore-water pressures within the sample were successfully recorded for the entirety of the test. Measured vertical displacement of the bottom overburden apparatus plate during Test was 0.43 inches. All time-history figures of Cyclic Test 2 were plotted from the beginning to the end of cyclic shaking. The number of cycles represented in accelerometer and PPT time histories is not an integer, but is the elapsed time from the start of excess pore-water pressure generation multiplied by the test frequency (8 Hz). This format is consistent to the cyclic testing figures produced by Wu and Kammerer (Figures 9-12). Figure 49 shows the shake table input acceleration time history during cyclic test 2. Figure 50 shows the time histories recorded during cyclic test 2 of accelerometers embedded in the soil oriented in the direction of cyclic loading. Figure 51 shows the time histories recorded by pore pressure transducers during cyclic test 2. Plots of acceleration time-histories are paired with excess-pore water pressure time histories recorded by PPT's embedded at the same depth as the accelerometer it is

paired with in figures 52-55. Lateral displacement time-histories of the flexible-walled testing apparatus during Cyclic Test 2 are plotted in Figure 56.

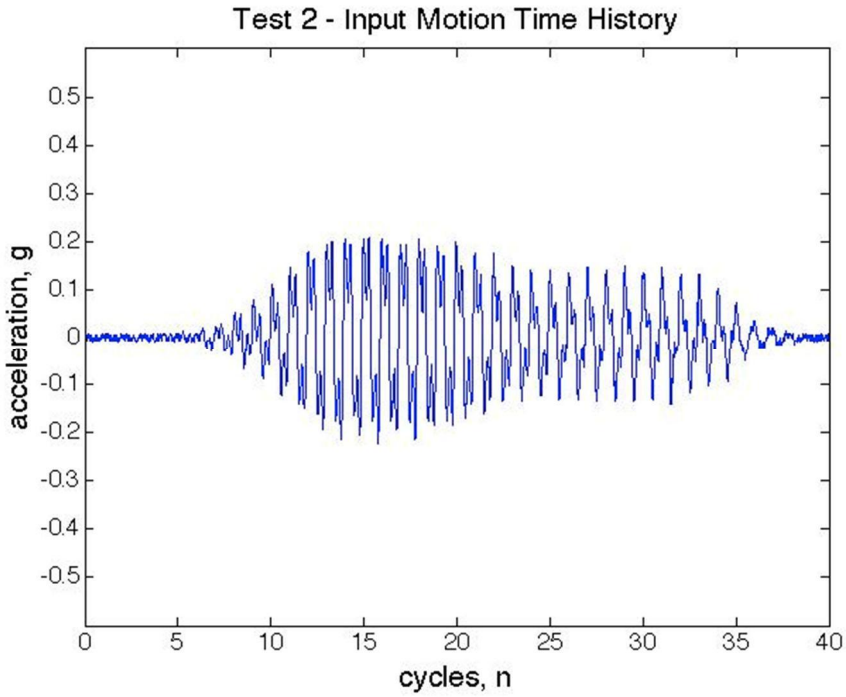

Figure 49: Cyclic Test 2 Shake Table Input Motion Acceleration Time History

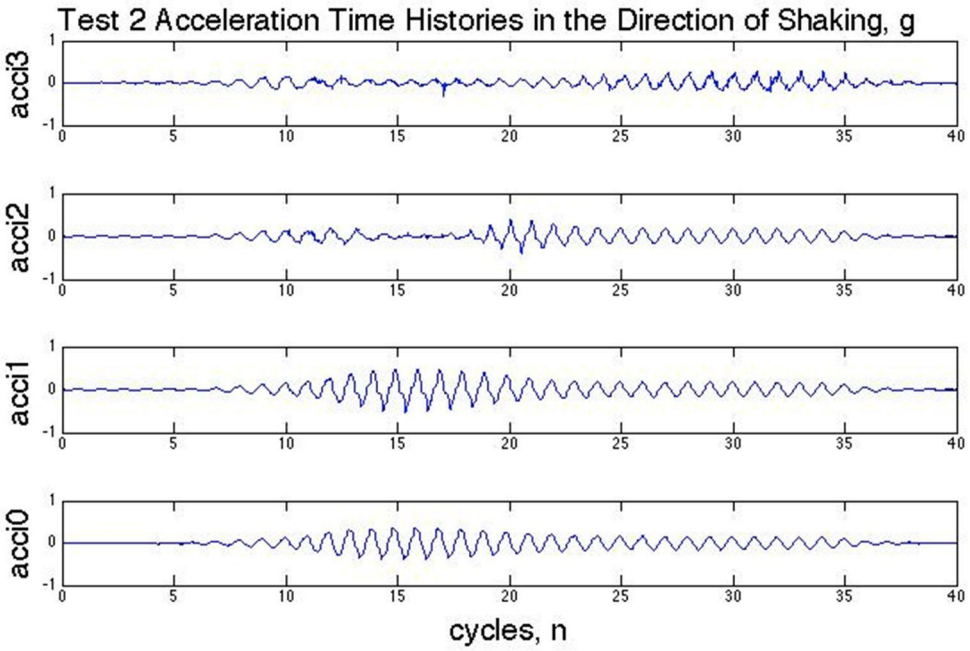

Figure 50: Cyclic Test 2 Acceleration time histories recorded by accelerometers oriented in the direction of shaking

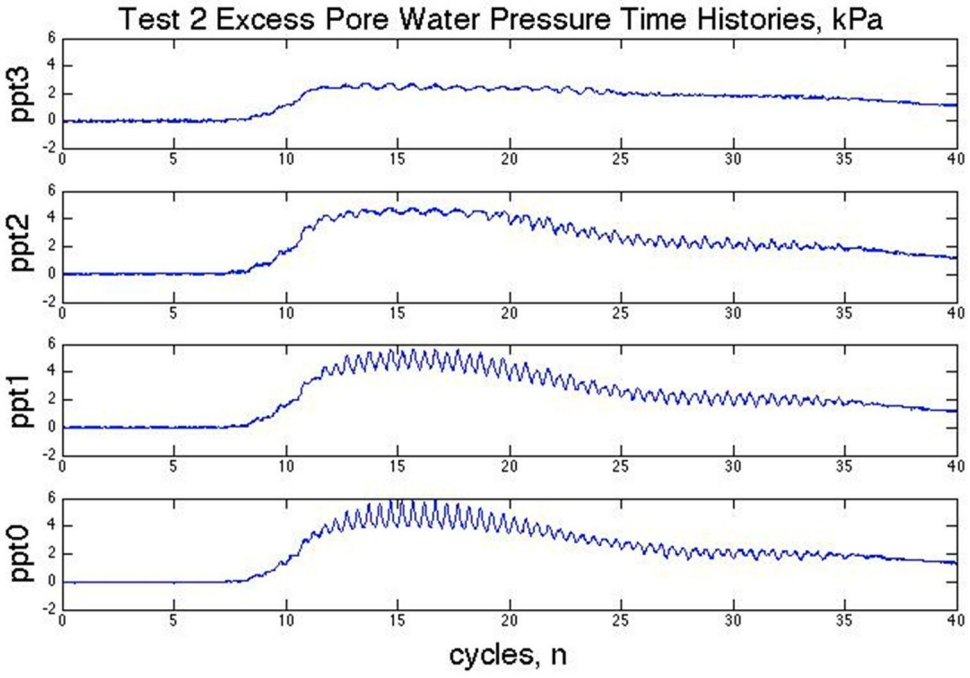

Figure 51: Cyclic Test 2 Excess Pore Water Pressure Time Histories

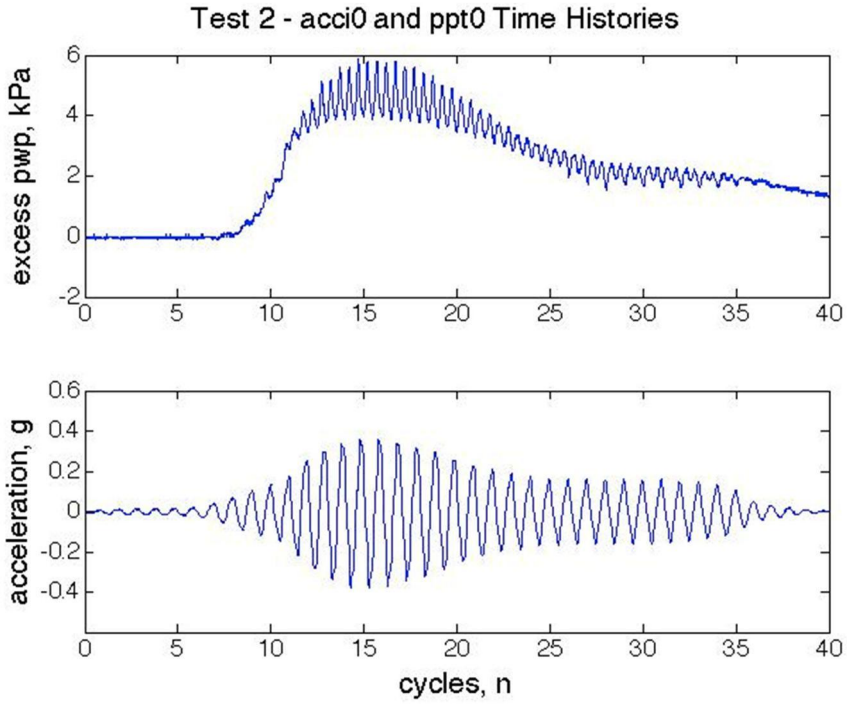

Figure 52: Cyclic Test 2 acci0 and ppt0 acceleration and excess pore-water pressure time histories, respectively

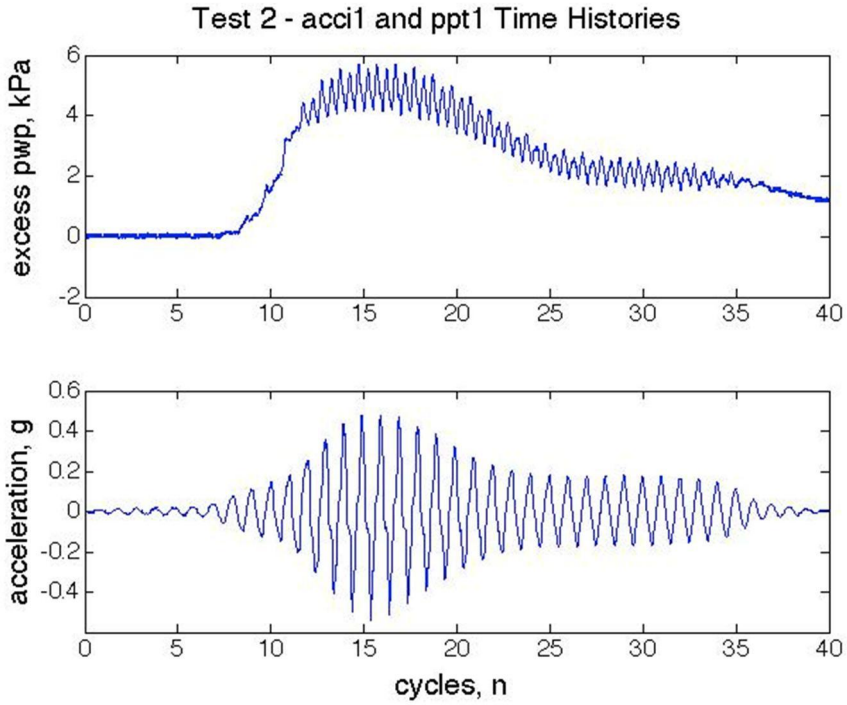

Figure 53: Cyclic Test 2 acci1 and ppt1 acceleration and excess pore-water pressure time histories, respectively

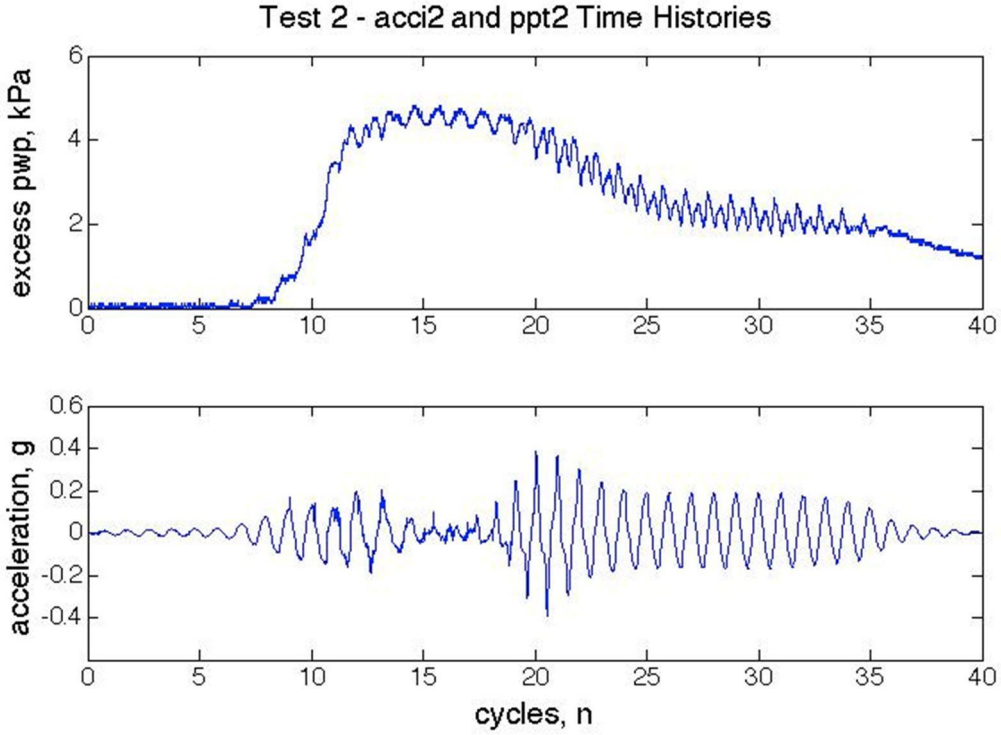

Figure 54: Cyclic Test 2 acci2 and ppt2 acceleration and excess pore-water pressure time histories, respectively

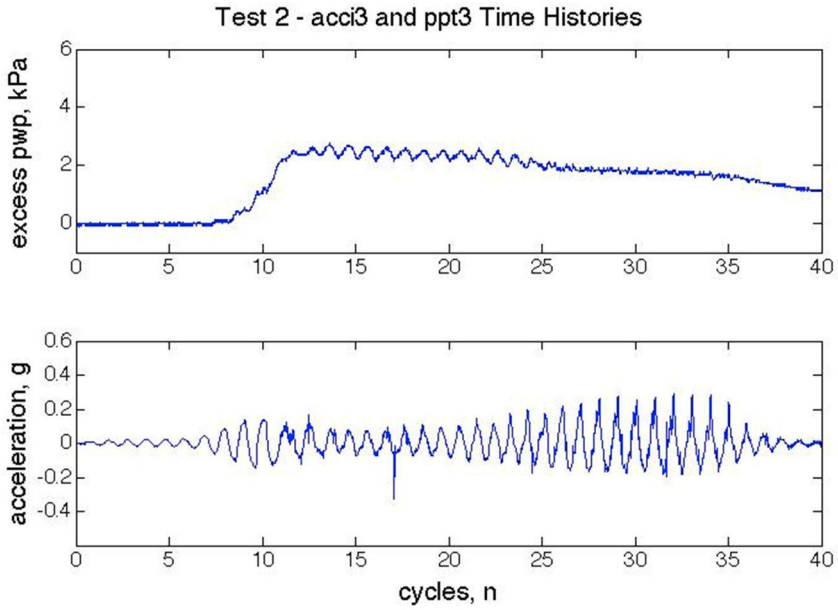

Figure 55: Cyclic Test 2 acci3 and ppt3 acceleration and excess pore-water pressure time histories, respectively

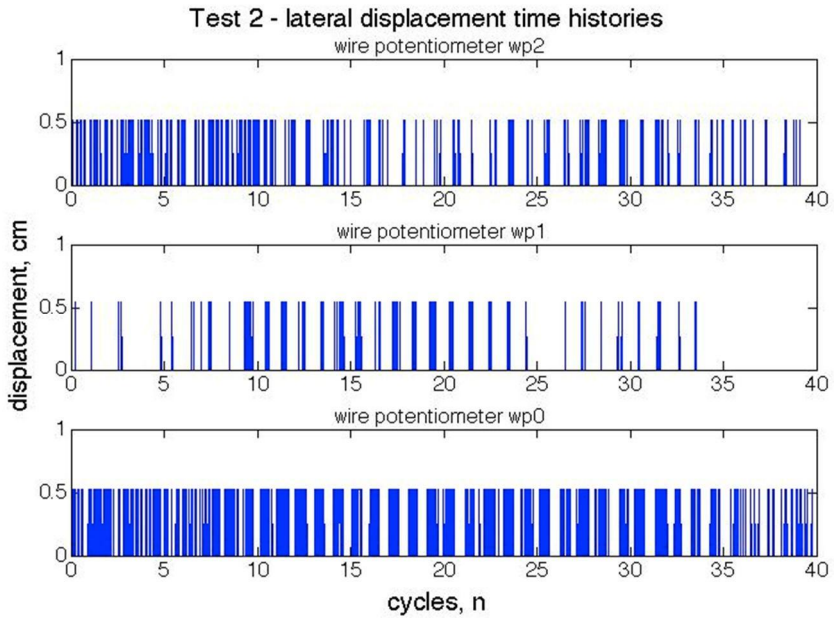

Figure 56: Test 2 lateral Displacement Time Histories

4.8 Additional Index Testing

An additional round of CPT and S-wave velocity tests was performed after Cyclic Test 2. The Ticker was repaired before S-wave velocity measurements after Cyclic Test 2 (Figure 57). Additional CPT soundings (Figure 58) were performed through access holes that had not been previously used so that the effect of cyclic testing alone could be observed through CPT tip resistance. Comparison of CPT soundings and S-wave velocity index testing before and after cyclic tests is presented and discussed in Chapter 5.

The maximum CPT tip resistances of approximately 1400 kPa for Soundings 3 and 4 was measured at a depth of approximately 45 cm below the sand surface. During Sounding 3 the cone tip experienced refusal at a depth of approximately 55 cm below the sand surface and the test was ended. During test 4 the cone experienced refusal a

second time and an additional approximately 70 kg mass (roughly the weight of a lean Civil Engineering graduate student) was added to the existing 205 kg driving mass to push the cone penetrometer to the bottom of the clay layer. The influence of the clay layer on the CPT tip resistance at the bottom of the sand layer as well as the effect of the landscaping fabric can be seen in Sounding 4.

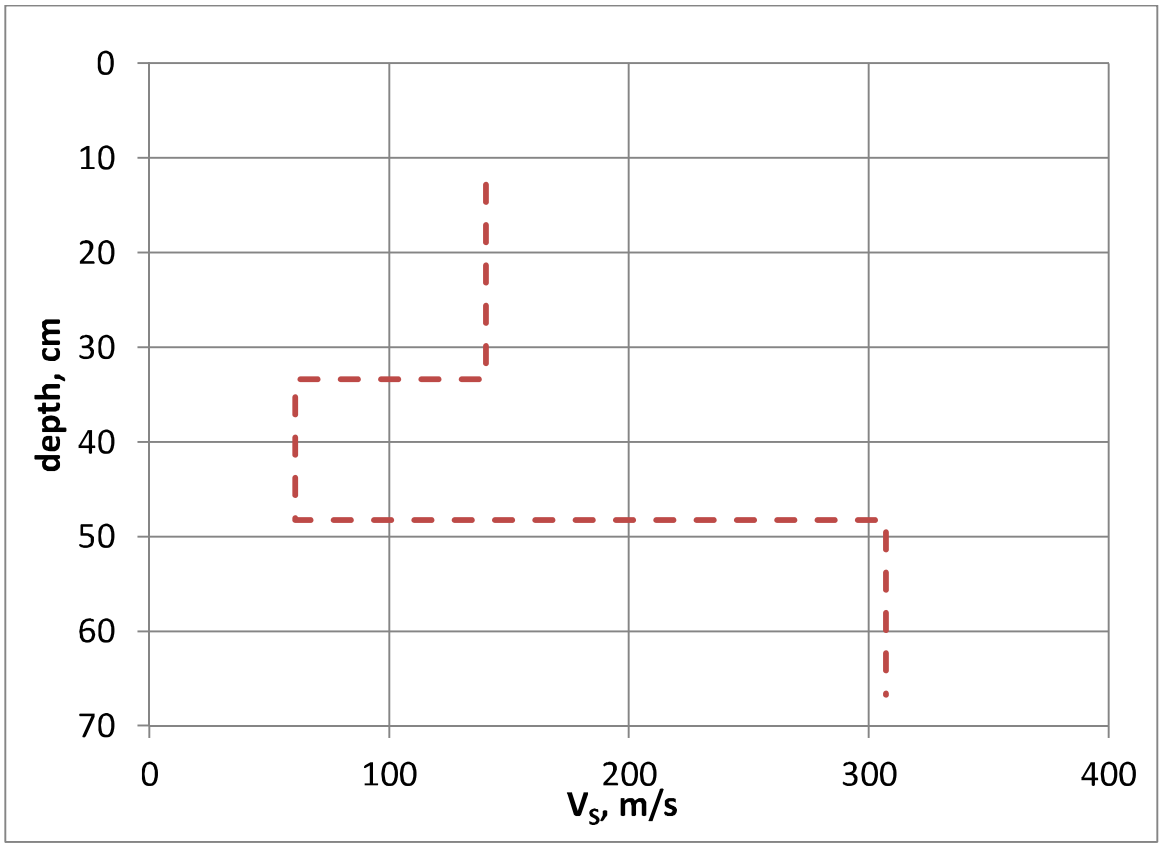

Figure 57: S-Wave Velocity Measurements Performed after Cyclic Test 2

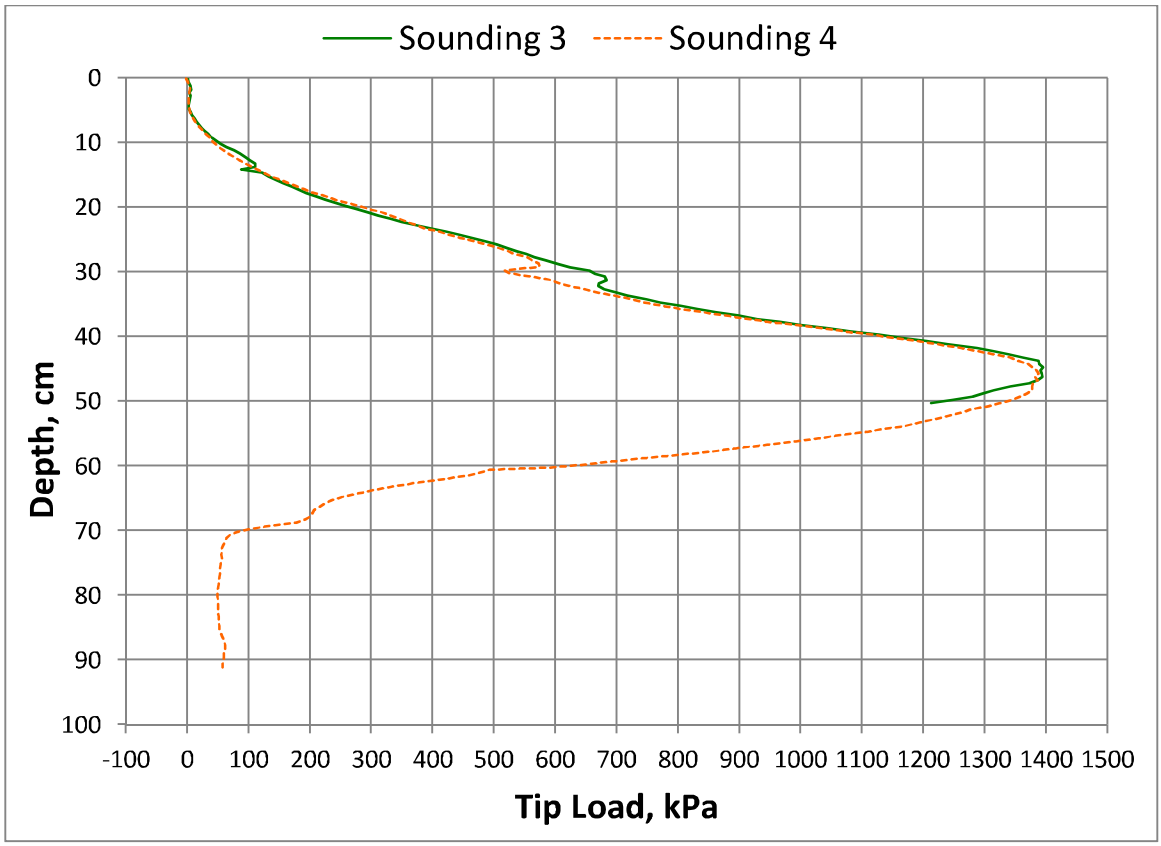

Figure 58: Additional CPT Soundings Performed After Cyclic Test 2

CHAPTER 5 DATA ANALYSIS AND RESULTS

This chapter presents analysis of the data presented in chapter 4 and results drawn form that analysis. Excess pore-water pressure and accelerometer time histories were used to estimate cyclic stress ratio to trigger liquefaction, generation of excess pore-water pressures, and excess pore-water pressure ratios throughout the sample during cyclic testing. Quality of data recorded during testing is discussed. Rationalization of assumptions required to estimate these values is provided. Observation of excess pore-water pressure ratio contours gives insight into the effectiveness of the overburden assembly and estimation of effective vertical stresses within the soil sample. A correction was made to the elevation of CPT soundings and S-wave velocity measurements during the second phase of soundings to allow for superposition of CPT and S-wave velocity data and observance of changes in soil stiffness due to cyclic testing.

5.1 Cyclic Stress Estimation

The Cyclic Stress Ratio (CSR) required to trigger liquefaction was estimated to better understand the conditions experienced by soil embedded within the flexible-walled testing apparatus during cyclic testing. Table 3 represents the range of CSR values and the parameters required to calculate CSR.

Total and effective vertical stresses and lateral accelerations were required to assess the cyclic stress experienced by soil during cyclic testing. Determination of vertical stress required the estimation of the applied overburden. The lateral acceleration used to calculate cyclic stress was estimated by the average magnitude of acceleration of each cycle from the cycle in which excess pore-water generation began until the cycle in which changes in pore water pressure as an effect of fluctuation in void space

(corresponding with the onset of liquefaction) were experienced. The period used to calculate cyclic stress was chosen because the context in which CSR is discussed in this experiment is primarily focused on liquefaction triggering. In the case of Cyclic Test 2, the duration was 5 cycles from the beginning of excess pore-water pressure generation.

Reasonable pore-water pressure ratio (R_u) values from tabletop testing were used to back-calculate the applied overburden. Although an R_u of 1.0 is traditionally considered to mark the onset of liquefaction, small-scale simple shear testing by Wu (2003) and Kammerer et al (2005) indicate that liquefaction can be induced at R_u as low as 0.6, and that R_u values well above unity can be generated during liquefaction. A maximum R_u value of 2.0 corresponding to the upper limit of values experienced during small-scale cyclic testing was used for cyclic stress calculation purposes. The minimum excess pore-water pressure experienced to induce liquefaction of 2.12 kPa by ppt3 (Figure 55) and the maximum excess pore water pressure of 4.7 kPa experienced by ppt0 (figure 52) indicated that the overburden pressure ranged from 0.36 to 2.83 kPa. Table 3 represents minimum and maximum CSR values corresponding to the range of overburden pressures provided herein. Equations (4) - (6) were utilized to determine total vertical stress, effective vertical stress, and average shear stresses presented in Table 3.

$$\sigma_v = \gamma_{total} * d + overburden \quad (4)$$

$$\sigma'_v = (\gamma_{total} - \gamma_{h_2o}) * d + overburden \quad (5)$$

$$\tau_{ave} = \frac{a_{ave}}{g} * \sigma_v \quad (6)$$

Estimation of cyclic stress also required the determination of the initial effective overburden stress, and subsequently soil unit weight and instrument depth below the sand surface. Instrument location was estimated using the same methods outlined in section 4.5.1 using hydrostatic water pressure to estimate instrument depth. The unit weight used for initial stress estimation was 19 kN/m^3 as discussed in 2.1.2. CPT soundings were not performed between cyclic tests 1 and 2, and therefore relative density correlations were not available to estimate unit weight for CSR estimation.

A correction to account for shifts in instrument location between test 1 and 2 and standing water atop the soil surface was performed to better estimate the location of instruments before test 2. This correction was performed with the aid of the observed instrument locations during sample de-construction.

After testing and the removal of the overburden apparatus, instrument packages were visible at the soil surface having migrated slightly upwards with respect to the overburden apparatus while the bottom of the overburden apparatus moved downwards during cyclic testing. The depth below the sand surface to the center of PPT3 was measured to be 7.6 cm, and it was assumed that the vertical migration to that position occurred during Cyclic Test 1 and experienced no further migration during additional tests. Presence of ejected water above the sand surface after cyclic test 1 required an adjustment to the hydro-static depths measured by embedded PPT's to estimate all instrument's depth below the sand surface. Similar to the procedure for wave speed estimation, the depth of instruments not attached to PPT's was assumed to be located at the same depth as the PPT's it was embedded at the same depth as. Each instrument was expected to experience similar conditions during cyclic testing as other instruments embedded at the same depth, and would therefore experience similar migration during cyclic testing.

Instrument	Average Acceleration a/g	Depth, cm	Minimum Initial Effective Vertical Stress, kPa (σ'_{vo})	maximum Initial Effective Vertical Stress, kPa (σ'_{vo})
ppt3/acci3	0.12	7.6	1.06	3.53
ppt2/acci2	0.14	24.5	2.61	5.08
ppt1/acci1	0.16	40.7	4.10	6.57
ppt0/acci0	0.15	60.6	5.93	8.40
Instrument	Minimum Average Shear Stress, kPa (τ)	Maximum average Shear Stress, kPa (τ)	CSR_{max} = τ_{ave}/σ'_{vo}	CSR_{min} = τ_{ave}/σ'_{vo}
ppt3/acci3	0.22	0.53	0.21	0.15
ppt2/acci2	0.72	1.07	0.28	0.21
ppt1/acci1	1.26	1.64	0.31	0.25
ppt0/acci0	1.74	2.11	0.29	0.25

Table 3: Cyclic Stress Ratio Estimations for Cyclic Test 2

5.2 Relative Density Estimation

CPT tip resistance correlations by Mayne Et al. (2002) were used to estimate the soil's relative density and to understand the soil's behavior with respect to critical state during cyclic testing. The maximum CPT tip resistance before cyclic testing (400 kPa at a depth of 40-50 cm below the soil surface) was chosen as the reference tip resistance and depth as the soil sample was deposited in a uniform manner, and CPT tip resistance was fully developed. The range of estimated initial effective vertical stress values estimated in Table 3 are used to normalize CPT tip resistance to estimate the normalized tip stress per equation (7). Mayne Et al. (2002) established the correlation between normalized tip stress, over-consolidation ratio (OCR), and relative density by equation (8). In this scenario, the soil deposited in the flexible walled testing container is assumed to be normally consolidated (OCR = 1). Utilizing the correlation by Mayne Et al.

(2002) suggests the relative density of the soil as deposited in the flexible-walled testing container ranges between 23-26%.

$$q_{T1} = \frac{q_t}{(\sigma_{atm} * \sigma_{v0}')\text{^}0.5} \quad \text{.....(7)}$$

$$D_R = 100\sqrt{\frac{q_{T1}}{300 * OCR\text{^}0.2}} \quad \text{.....(8)}$$

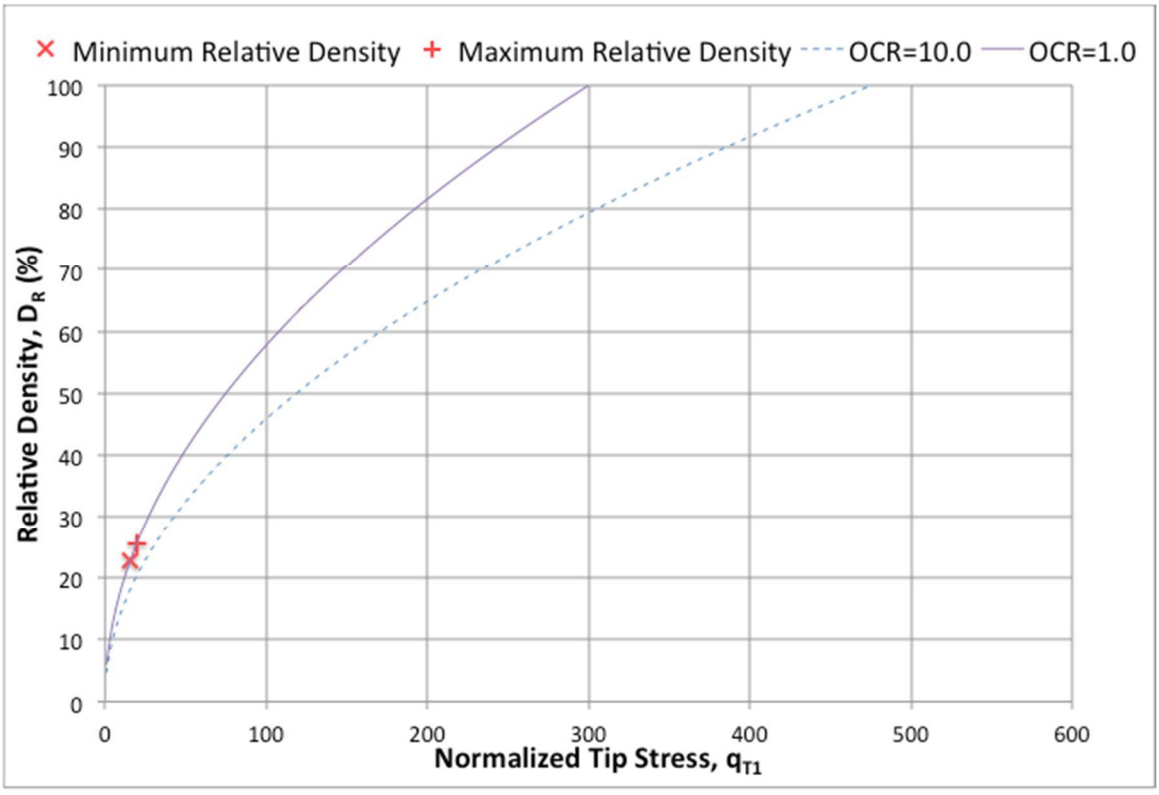

Figure 59: Relative Density Evaluation of Sand Deposited in Flexible Walled Testing Container from CPT Data (After Mayne Et al. 2002)

Evaluation of the soil's relative density using the CPT tip resistance measurements recorded after Cyclic Test 2 indicate that the soil's relative density increased, ranging from roughly 41-46%. This Estimation uses a maximum CPT tip resistance of roughly 1400 kPa at 50 cm below the sand surface after Cyclic Test 2.

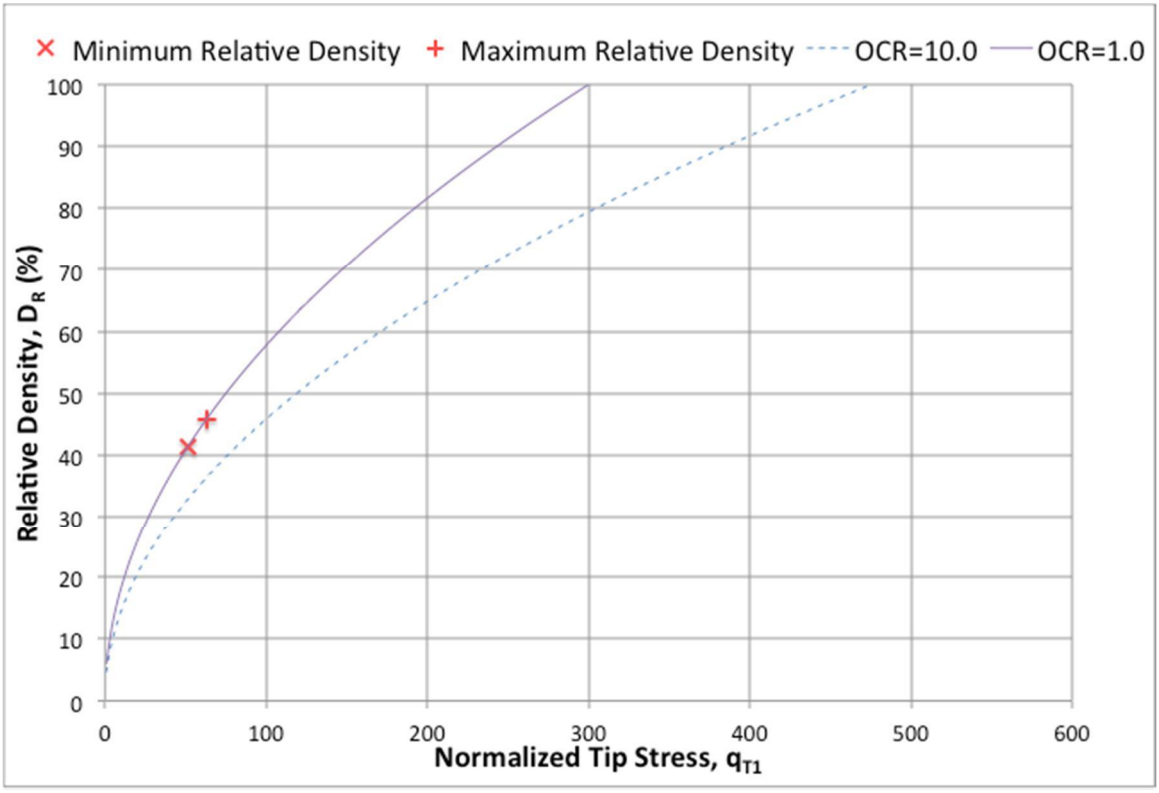

Figure 60: Relative Density Evaluation of Sand After Cyclic Test 2 from CPT Data (After Mayne Et al. 2002)

5.3 Excess Pore-Water Pressure Contours

Excess pore-water pressure contours (Figure 59) were produced by determining the maximum excess pore-water pressure within the time range defined for each contour. Estimation of instrument depth required to create excess pore-water pressure contours utilizes the same procedure required to estimate instrument locations for CSR estimation.

Excess pore-water pressure contours indicate that as cyclic testing progresses, excess pore-water pressures originate in the region of ppt2, and propagate downwards. Due to the ability for drainage through the overburden apparatus and lower CSR, excess pore-water pressures generated at the top of the sample are much lower towards the bottom of the sample. Low excess pore-water pressures at the top of the soil sample are an indication that the overburden apparatus was successful in not creating the water blister effect. Lastly, excess pore water pressure contours confirms the assumption of 5 cycles used to calculate liquefaction triggering during cyclic test 2 due to the observation of fluctuation in pore water pressures due to the change in void space at the onset of liquefaction. After 5 cycles of cyclic loading have been completed fluctuation in excess pore-water pressure is relatively uniform until pore pressure drainage occurs as can be seen in figures 52-55.

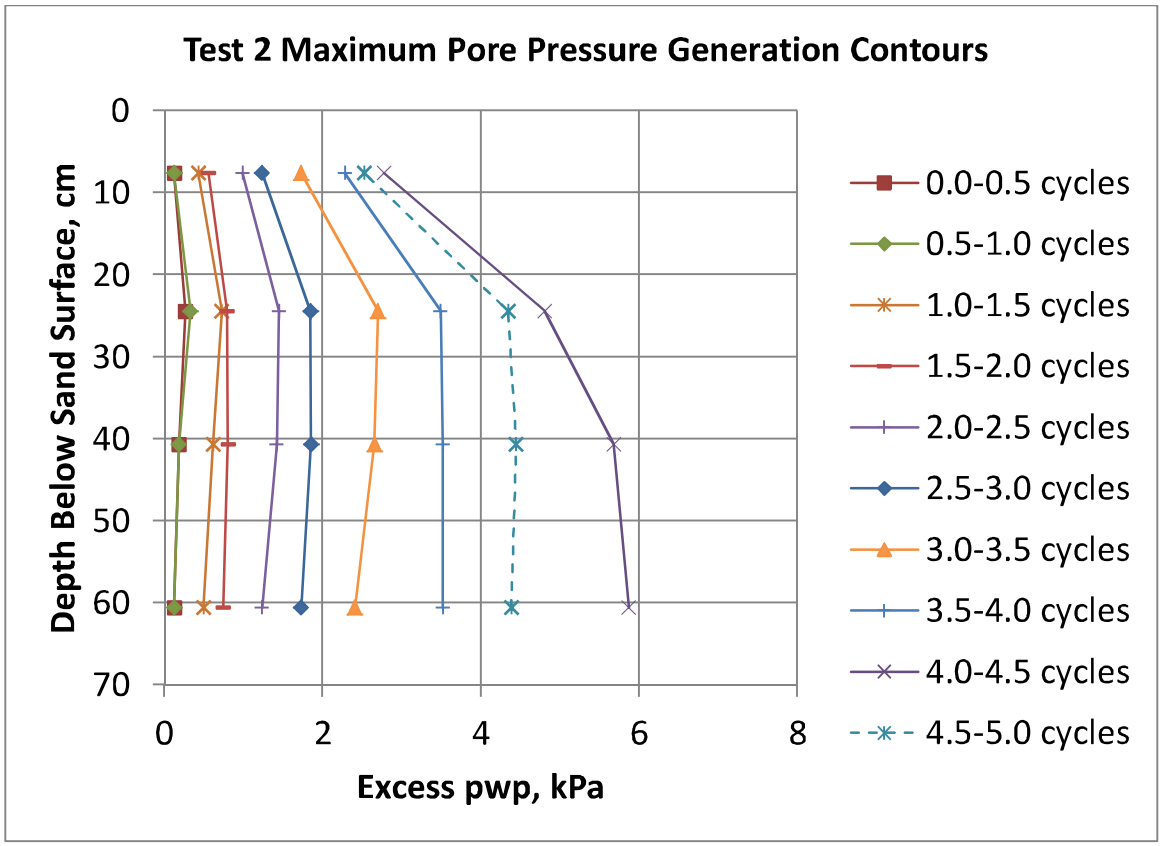

Figure 61: Test 2 Maximum Pore Pressure Generation Contours

5.4 CPT Soundings

Each CPT sounding began at the bottom plate of the overburden apparatus, but the location of the bottom plate was not the same during each sounding. Volumetric strains and the production of ejecta during cyclic testing caused settlement of the bottom overburden apparatus plate. A correction was made to the elevation of the top of the sand surface to account for this settlement, normalizing the depths recorded for CPT tip resistance during soundings 3 and 4. CPT tip resistances recorded during soundings 1-4 are presented in Figure 60.

Observance of superimposed tip resistances from CPT soundings 1-4 indicates that the maximum tip resistance is recorded at similar depths for all tests. After the maximum tip resistance is recorded, all tests experience a decrease in tip resistance at depths below

the elevation of maximum tip resistance due to influence of the clay layer below. The effect of the landscaping fabric is also apparent for all tests that reached the depth of the sand-clay interface.

Performance of CPT soundings on a laboratory tested sample is in effect performing a field-scale test in a laboratory environment. Controlling testing conditions for CPT soundings in the laboratory environment allows for the calibration of Cone Penetration Testing for field liquefaction investigations. In general, the vast majority of liquefaction investigations utilizing Cone Penetration Testing is performed after the observance of evidence that liquefaction has occurred. In this study, liquefaction is confirmed by monitoring the measurements recorded by PPT's embedded within the sample.

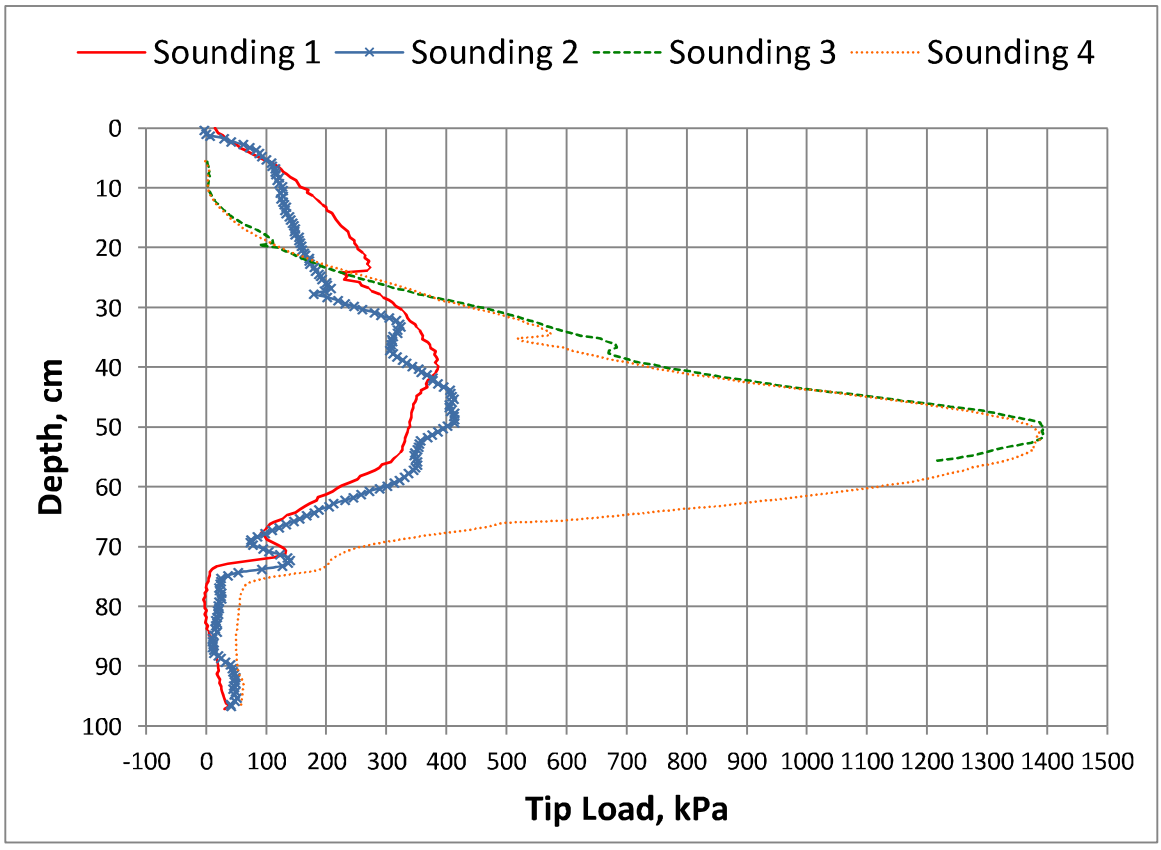

Figure 62: Depth Normalized CPT Soundings 1-4

5.5 S-Wave Velocity

S-wave measurements performed after Cyclic Test 2 were also corrected for changes in instrument depth due to migration during cyclic testing to allow for superposition of S-wave velocity data (Figure 61). Comparison of S-wave data from before and after cyclic testing indicates a change in S-wave velocity as an effect of cyclic testing. A dramatic increase in S-wave velocity at the bottom of the sample as well as decrease in S-wave velocity at higher elevations is in agreement with the results of CPT soundings before and after cyclic testing. Consideration of the fact that CPT tip resistances are effected by the stiffness of soil below the cone tip indicates that in order to compare S-wave velocity and soil stiffness measured by the cone penetrometer, the CPT soundings should be displaced downwards 20-25 cm in this case. Uniformity of S-wave velocity measurements at the top of the sample may be an effect of the soil's interaction with the stiff boundary condition induced by the overburden apparatus.

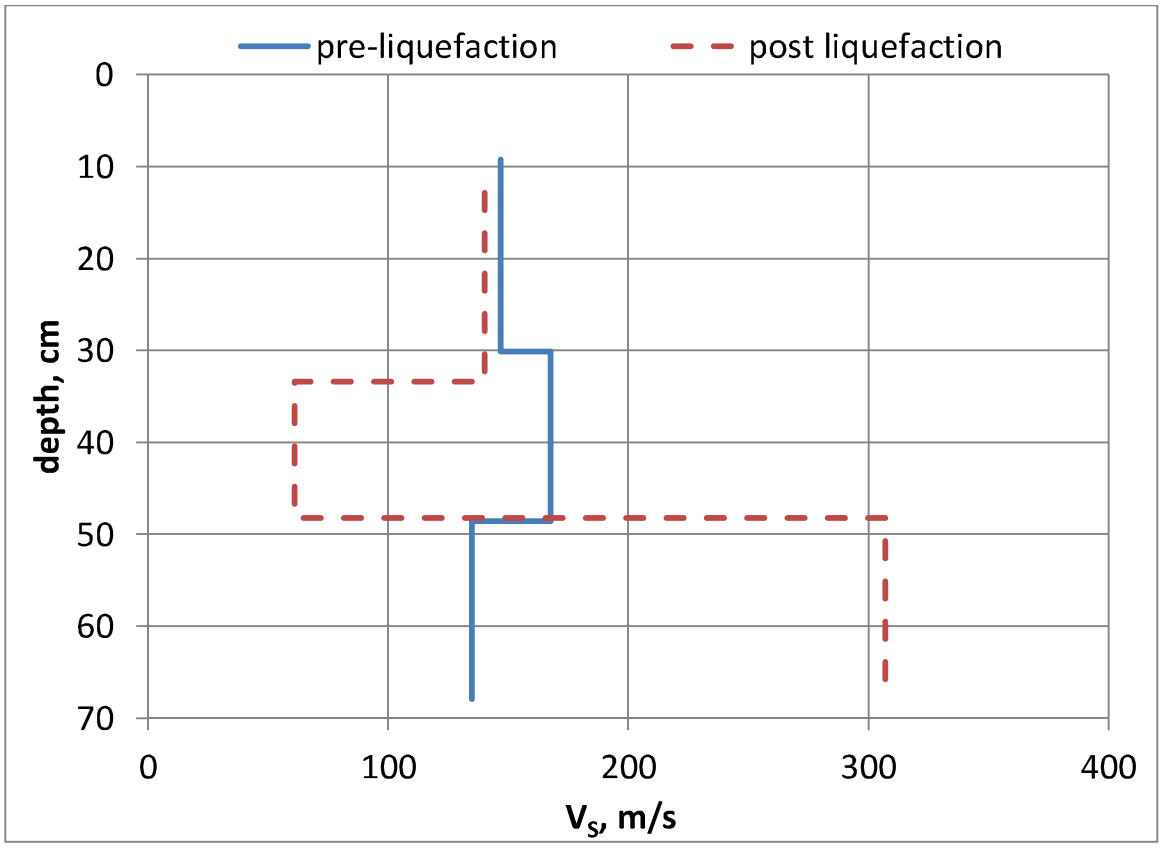

Figure 63: S-Wave Velocity Before and After Testing

5.6 Lateral Displacement Measurements

Lateral displacement measurements captured by the array of wire potentiometers (Figure 56) offer very limited information of value. Displacements measured are relatively uniform throughout the flexible-walled testing apparatus, which does not indicative of the expected first mode shape. No accumulation of strain was captured by the wire potentiometer array. Evidence of oscilation of the flexible-walled testing container is apparent, but quality is considered to be relatively low.

CHAPTER 6 CONCLUSIONS AND RECOMMENDATIONS FOR FUTURE RESEARCH

The full-scale cyclic simple shear tests and accompanying index testing performed in this study are a valuable progression in both laboratory and field liquefaction testing. Pore-water pressure recordings were used to directly observe the occurrence of liquefaction and produce pore-water pressure time-contours showing the propagation of liquefaction throughout the soil sample at full-scale. Accelerometer time-histories were used with pore-water pressure recordings to calculate CSR to evaluate liquefaction triggering. S-wave velocity and CPT tip resistance soundings performed before and after cyclic simple-shear testing indicate the changes that would be measured using relatively common in-situ field testing before and after liquefaction. The S-wave velocity and CPT tip resistance measurements recorded as part of this laboratory experiment form a very valuable link between laboratory and field liquefaction testing.

Certain issues were not foreseen before testing and not realized soon enough to be rectified before testing. Other issues are inherent to the experimental design and also cannot be avoided. Experimental testing serves as a learning experience, so it is expected that issues are uncovered during testing. Before further testing is performed, overburden confinement, overburden measurement, relative density, testing apparatus water-proofing, displacement measurement, shear wave velocity measurement, instrument placement and shaking control methods should be modified to improve the testing process and eventual results.

6.1 Overburden Confinement

The inner-tube used to apply confinement around the perimeter and on top of the overburden apparatus needs better confinement to allow higher overburden pressures to be safely applied to the soil within the bucket. Additional beams attached to the top rim on the flexible-walled testing apparatus or an upper confinement plate made of a more stiff material will help confine the top of the inner-tube. Additional Kevlar bands should are needed to better confine the outer diameter of the inner-tube and to help preserve the flexible-walled bucket's membrane.

6.2 Overburden Measurement

Development of a more accurate overburden measurement method is needed. A reliable flat-plate pressure transducer that can be connected to the data acquisition system, reliably calibrated, and embedded within the overburden application apparatus will improve the overburden pressure measurement process.

6.3 Relative Density Estimation

The results of relative density estimates varied widely between the values produced when calibrating the pluviation device indicating dilative behavior and the values obtained using CPT tip resistance correlations, which indicated contractive behavior. The results of CPT tip resistance correlations are most similar to the minimum attainable relative densities for wet pluviation discussed by Wu (2003), which is reasonable considering the great caution exercised to produce a uniform, loose sample. It is expected that a relative density estimation which is performed at an appropriate scale to replicate the conditions the soil was deposited in at full scale will produce a soil unit weight which is in agreement with the minimum relative density for wet pluviation and the CPT tip resistance correlations by Mayne (2002).

6.4 Testing Apparatus Water-proofing

A comprehensive water-proofing plan is needed for future cyclic simple-shear testing using liquefiable sand. Water-proofing was not an issue during previous studies when the flexible-walled testing apparatus was filled with soft clay. Hydrated clay retains the water it is constituted with; however, water freely drains from the space it occupies within a sand skeleton. Use of the impermeable clay layer to prevent migration of free water within the sand skeleton to the bottom of the flexible-walled testing apparatus was unsuccessful. Placement of additional dry bentonite between the soft clay layer and the membrane of the flexible-walled testing apparatus was intended to capture any water migrating from sand layer to the bottom of the flexible-walled testing apparatus was also unsuccessful. Water was able to drain from a few places in the bottom of the flexible-walled testing apparatus. Attempts were made to water-proof the bottom of the flexible-walled testing apparatus using silicon caulking where leakage was anticipated prior to sample construction. Water leaked from the bottom of the flexible-walled testing apparatus where it was bolted to the shake table, where the bottom plate of the testing apparatus was welded to the rim used for membrane attachment, and holes in the rim used to bolt the membrane to the bottom of the flexible-walled testing apparatus. Consequences of leaks in the flexible-walled testing apparatus include the need to constantly add water to the testing apparatus to maintain the desired water level within the loose sand, and the accumulation of surface rust on the shake table. Re-surfacing was necessary to preserve the table surface after the completion of cyclic simple-shear testing. Additionally, changes in the water surface elevation due to leakage introduced unnecessary uncertainty when estimating pore-water pressure transducer location by converting hydrostatic pressure to instrument depth. Taking extra precautions during assembly of the flexible-walled apparatus will save a large amount of time and prevent leaks in the bucket after the sample has been constructed in the testing apparatus.

6.5 Displacement Measurement

The process of displacement measurement during cyclic testing needs to be improved. Wire potentiometers were considered to be unsuccessful at measuring high fidelity strain data during cyclic testing. Wire potentiometers are generally thought to be very successful at measuring displacements during pushover testing, but are not generally used for high frequency cyclic testing. Inability for the potentiometer mechanism to respond at the rate of shake table movement account for the potential latency between cyclic displacement and potentiometer measurement. Higher fidelity laser displacement transducers are recommended because they are not limited by the response of a physical mechanism to measure displacements, especially when testing is performed at a high frequency.

6.6 Shear-Wave Velocity Measurement

Measurement of S-wave velocity was not possible to perform reliably with the Ticker mechanism during cyclic testing. Part of the difficulty of designing and constructing the ticker mechanism was the desire to use only easily sourced parts in the case that a component needed to be replaced. The best solenoid electro-magnet that could be found for the Ticker was not as strong as desired, as a result the quality of S-wave measurement was wanting, especially in loose sand. Accelerometers embedded transverse to the direction of shake table acceleration still captured table accelerations, preventing S-waves induced from the ticker from being adequately measured. In addition, the ticker was not adequately water-proofed. The Ticker was submerged by liquefied ejecta during cyclic testing, preventing S-waves from propagating into the sample. Water-proofing is necessary to induce S-waves into the sample during cyclic testing.

6.7 Instrument Package Placement

Proximity of the uppermost instrument packages to the overburden apparatus may have affected the measurements recorded by those instrument packages. The upper most instrument package of each array was placed near the top of the sand layer, in close proximity to the bottom overburden apparatus plate. The stiffness of the bottom overburden apparatus plate may have adversely affected the accelerometer's ability to record free-field soil accelerations as well as the measurement of S-wave velocity. Additionally, the possibility that the bottom plate of the overburden apparatus may have unintentionally introduced a low-permeable boundary at the top of the soil layer was a concern during testing. Observation of the pore-water pressure contours indicates that excess pore-water pressures induced by the presence of a low permeability upper boundary inducing a water blister was a non-issue in this round of cyclic simple-shear testing. For future testing, it is recommended to place the upper most instrument packages lower within the soil sample in an attempt to avoid the effects of the overburden apparatus on wave speed measurements.

6.8 Testing Control

Non-linear material behavior during cyclic testing introduced difficulties in performing cyclic testing at an consistent amplitude. While it is also possible that this issue is inherent to performing cyclic testing on liquefiable soils further investigation of the feedback loop used to control the test is necessary before additional cyclic simple-shear testing. The only accelerometer used for control feedback was situated on the shake table. It is possible that for addition of control accelerometers situated on/within the soil bucket can be used to monitor the soil's non-linear behavior and improve test control.

REFERENCES

Abdoun , T., Gonzalez, M. A., Thevanayagam, S., Dobry, R., Elgamal, A., Zeghal, M., et al. (2013). Centrifuge and Large-Scale Modeling of Seismic Pore Pressures in Sands: Cyclic Strain Interpretation. *Journal of Geotechnical and Geoenvironmental Engineering* , 1216-1234.

Andrus, R. D., & Stokoe, K. H. (2000). Liquefaction Resistance of Soils From Shear-Wave Velocity. *Journal of Geotechnical and Geo-Environmental Engineering* , 1015-1025.

ASTM D4253 - 14: Standard Test Methods for Maximum Index Density and Unit Weight of Soils Using a Vibratory Table. (2014, December 15). West Conshohocken, Pa: ASTM International.

ASTM D4254 - 14: Standard Test Methods for Minimum Index Density and Unit Weight of Soils and Calculation of Relative Density. (2014, December 15). West Conshohocken, Pa: ASTM International.

ASTM D5778 - 12: Standard Test Method for Electronic Friction Cone and Piezocone Penetration Testing of Soils. (2012, January 1). West Conshohocken, PA: ASTM International.

Boulanger, R. W., & Seed, R. B. (1995). Liquefaction of Sand under Bidirectional Monotonic and Cyclic Loading. *Journal of Geotechnical Engineering* , 870-878.

Butcher, A. P., Campanella, R. G., Kaynia , A. M., & Massarsch, K. R. (2005). *Seismic Cone Downhole Procedure to Measure Shear Wave Velocity - A Guide Prepared*

by ISSMGE TC10: Geophysical Testing in Geotechnical Engineering. London: International Society for Soil Mechanics and Geotechnical Engineering.

Chameau, J. L., Clough, G. W., Reyna, F., & Frost, J. D. (1991). Liquefaction Response of San Francisco Bayshore Fills. *Bulletin of the Seismological Society of America* , 1998-2018.

Clough, G. W., & Chameau, J. L. (1983). Seismic Response of San Francisco Waterfront Fills. *Journal of Geotechnical Engineering* , 491-506.

Crosariol, V. (2010). *Scale Model Shake Table Testing of Underground Structures in Soft Clay.* San Luis Obispo, Ca: Cal Poly Digital Commons.

Faris, J. R., & de Alba, P. (2000). National Geotechnical Experimentation Site at Treasure Island, California. *National Geotechnical Experimentation Sites* , 52-71.

Hatanaka, M., & Masuda, T. (2008). Experimental Study on the Relationship Between Degree of Saturation and P-Wave Velocity in Sandy Soils. *Geotechnical Engineering for Disaster Mitigation and Remediation* (pp. 347-351). Beijing: Science Press and Springer-Verlag.

Hazirbaba , K., & Rathje, E. M. (2009). Pore Pressure Generation of Silty Sands due to Induced Cyclic Shear Strains. *Journal of Geotechnical and Geoenvironmental Engineeering* , 1892-1905.

Kammerer, A. M., Pestana, J. M., & Seed, R. B. (2005). Behavior of Monterey 0/30 Sand Under Multidirectional Loading Conditions. *Geomechanics* , 154-173.

Kuo, S. (2012). *Scale Model Shake Table Testing of Shallow Embedded Foundations in Soft Clay.* San Luis Obispo, Ca: Cal Poly Digital Commons.

L.F., H. (n.d.). *http://research.engineering.ucdavis.edu/gpa/wp-content/uploads/sites/43/2015/02/Aerial-of-collapsed-crane.jpg*. Retrieved July 29, 2015

Luna, R., & Frost, J. D. (2000). Treasure Island's Spatial Liquefaction Evaluation. *National Geotechnical Experimentation Sites* , 306-320.

Mayne, P. W., Christopher, B. R., & DeJong, J. (2002). *Subsurface Investigations - Geotechnical Site Investigations.* Washington, D.C.: National Highway Institute.

Moss, R. E., & Crosariol, V. A. (2013). Scale Model Shake Table Testing of an Underground Tunnel Cross Section in Soft Clay. *Earthquake Spectra* .

Moss, R. E., Seed, R. B., Kayen, R. E., Stewart, J. P., Der Kiureghian, A., & Cetin, K. O. (2006). CPT-Based Probabilistic and Deterministic Assessment of In Situ Seismic Soil Liquefaction Potential. *Journal of Geotechnical and Geoenvironmental Engineering* , 1032-1051.

Noche, R. (2013). *Scale Model Shake Table Testing of Seismic Earth Pressures in Soft Clay.* San Luis Obispo, Ca: Cal Poly Digital Commons.

Robertsion, P. K., & Wride, C. E. (1998). Evaluating Cyclic Liquefaction Potential Using the Cone Penetration Test. *Canadian Geotechnical Journal* , 442-459.

Robertson, P. K., & Cabal (Robertson), K. L. (2014). *Guide to Cone Penetration Testing for Geotechnical Engineering.* Signal Hill, California: Greg Drilling.

Robertson, P. K., & Campanella, R. G. (1985). Liquefaction Potential of Sands Using the CPT. *Journal of Geotechnical Engineering* , 384-403.

Seed, H. B., & Idriss, I. M. (1971). Simplified Procedures for Evaluating Soil Liquefaction Potential. *ASCE Journal of Soil Mechanics and Foundations* , 1249-1273.

Seed, H. B., Tokimatsu, K., Harder, L. F., & Ching, R. M. (1985). Influence of SPT Procedures in Soil Liquefaction Resistance Evaluations. *Journal of Geotechnical Engineering* , 1425-1445.

Seed, R. B., Cetin, K. O., Moss, R. E., Kammerer, A. M., Wu, J., Pestana, J. M., et al. (2003). *Recent Advances in Soil Liquefaction Engineering: a Unified and Consistent Framework.* University of California, Berkeley: Earthquake Engineering Research Center.

Shibata T., T. W. (1988). Evaluation of Liquefaction Potentials of Soils Using Cone Penetration Tests. *Soils and Foundations* , 49-60.

Stanton, K. (2013). *Envestigation of Parameters Influencing Reverse Fault Rupture Propogation to the Ground Surface.* San Luis Obispo, Ca: Cal Poly Digital Commons.

Wu, J. (2003). Liquefaction Triggering and Post Liquefaction Deformations of Monterey 0/30 Sand Under Uni-Directional Cyclic simple Shear Loading. *Dissertation in Partial Fulfillment for the Degree of Doctor of Philosophy, University of California, Berkeley* .

Youd T.L., I. I. (2001). Liquefactrion Resitance of Soils: Summary Report from the 1996 NCEER and 1998 NCEER/NSF Workshops on Evaluation of Liquefaction Resistance of Soils. *Journal of Geotechnical and Geoenvironmental Engineeering* , 297-313.

APPENDIX A

Discussion of “Problems with Liquefaction Criteria and their Applications in Australia”

Discussion of "Problems with Liquefaction Criteria and their Applications in Australia" by R. Semple. Australian Geomechanics, 48(3) September 2013.

Robb Eric S. Moss[1] and Jasper S. Jacobs[2]

[1]Associate Professor, California Polytechnic State University, San Luis Obispo, CA
[2]Graduate Researcher, California Polytechnic State University, San Luis Obispo, CA

R. Semple (2013) has written a thorough, extremely well referenced, erudite discussion of the current state-of-practice of liquefaction triggering analysis as it pertains to Australia. This critique points out many questions, deficiencies, contradictions, and disagreements that confront researchers and practitioners that grapple with the problem of seismic soil liquefaction. These come about due to the complexity of the problem, highly variable nature of seismic loading interacting with inherently variable soil resistance, and the uncertainty that is introduced through measurement, lack of data, binning, modeling, trending, equation-fitting, and generalizing. The latter uncertainty is often termed epistemic, and the former termed aleatory to differentiate the uncertainty that we introduce to the problem and that uncertainty that exists as part of the phenomenon itself.

The total uncertainty in any given liquefaction engineering project may be large and can often lead to a conservative design that includes liquefaction mitigation and/or increased structural reinforcement. This is a logical approach to limited information and lack of certainty. But there is a rational means of dealing with this uncertainty that the author did not address, that of using risk analysis to quantify the uncertainty and find the most cost effective path forward given an acceptable level of risk. This requires performing a probabilistic analysis that includes not only the likelihood of liquefaction triggering but also the consequences of liquefaction, which examines the effect any subsequent deformations will have on the engineered structure. The benefits of this approach:

1. Multiple methods of assessing triggering can be used to minimize the epistemic uncertainty, thereby addressing the deficiencies of any one method,
2. In presenting the analysis in a probabilistic manner the liability of the project lies with the client, where it should be, and not with the engineer,
3. Different solutions and the cost of these solutions can be evaluated with respect to each other knowing that the level of risk has been evenly quantified.

Risk by its engineering definition is the product of the probability of failure and the consequences (Moss, 2003; Chistian and Baecher, 2003; Ang and Tang, 1984).

$$Risk = (probabiity\ of\ failure)(consequences\ of\ failure)$$

Probability of failure in this context could be the probability of liquefaction triggering, the probability of the post-liquefaction strength being less than the static driving shear stresses, the probability of a certain level of volumetric or shear deformations, or the probability of flow failure. The consequences could be the cost or extent of structural damage, the cost of remediation, the potential for life loss, or some other metric.

A deterministic approach to liquefaction analysis has been the traditional way to assess a project. The typical client request takes a black-and-white view of the problem, "will the foundation soil liquefy or not?". If that is the level of answer required for a particular project then Figure 1 shows the authors' recommended approach of taking many existing methods, here for CPT penetration resistance, drawing a thick threshold line that captures some of the differences of the methods, and clearly defining the "Liquefaction" or "No Liquefaction" regions. This Figure shows graphically the same conclusions that Youd (2011) presents in an assessment of the discrepancies and disagreements in liquefaction triggering. This approach however is not nuanced engineering so much as it is applying engineering tools in the manner of a technician. And by providing a "Yes" or "No" the engineer has now assumed liability of the project by making a certain and definitive statement about an uncertain process.

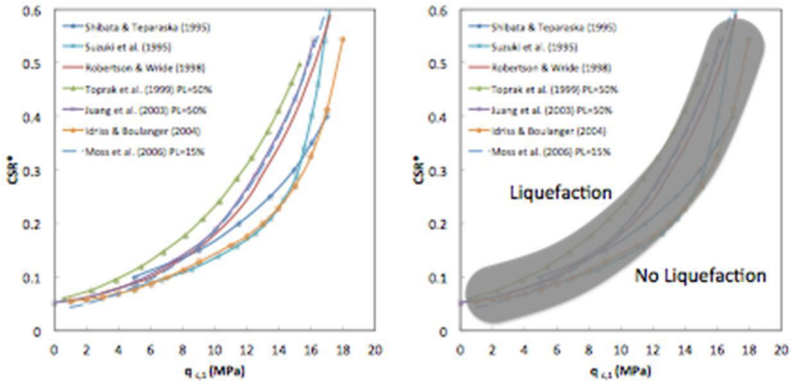

Figure 1. Deterministic liquefaction triggering considering different methods.

A better approach is to determine the probability of liquefaction triggering and let the client decide if the risk is acceptable. This was the intent of the liquefaction triggering methods found in Cetin et al., 2004; Moss et al., 2006; and Kayen et al., 2013, and other probabilistic presentations of the triggering phenomenon. The load and resistance from many past occurrences were defined as joint probability distributions, capturing the respective uncertainty in each case history, thereby

weighting the importance of any one case history by its magnitude of uncertainty. The answer to the clients question is then "there is a annual probability of liquefaction of X % that could cause peak shear and volumetric deformations on the order of X meters." This information could then be fed back to the structural engineering for a performance evaluation and to the client's insurance company for assessing the risk of seismic foundation damage with respect to other risks such as seismic structural response, wind loading, fire, etc.

If an engineer is uncomfortable using a single probabilistic method to assess triggering then multiple methods can be used to come up with a composite probabilistic liquefaction triggering curve thereby minimizing the epistemic uncertainty that each method brings to the analysis. This is shown in Figure 2 which weights all the methods shown equally to come up with a mean and plus/minus one standard deviation curves. This process of weighting different methods to come up with a robust median and composite standard deviation is typically called a logic tree. Note that the spread on the standard deviation curves is very similar to the spread found in Moss et al. (2006), showing some consistency in the uncertainty of the problem whether assessed by one study or multiple studies.

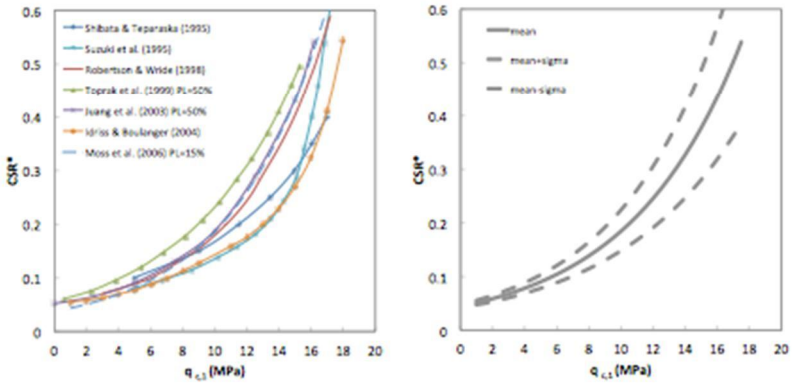

Figure 2. Composite probabilistic liquefaction trigging relationship calculated from different methods.

A similar logic tree can be used to defeat the epistemic uncertainty that is well laid out by Semple (2013) on the topics of; soil age influencing the cyclic resistance, soil fabric impact on the soil column's liquefaction response, loading mechanism in Australia versus continental margin boundaries, the loading intensity described by a single peak value or through more comprehensive energy measures, and other effects.

Often, for any engineering project it is not the likelihood of liquefaction but the likelihood of adverse deformations that could compromise the structural integrity of the project. Whether the project is a building, a bridge, a tunnel, a pipeline, a canal, or some other feature, the performance during and after an extreme loading event is the critical concern and deformations are the controlling parameter in foundation-structure performance. As laid out in Seed et al. (2003), liquefaction engineering is a multi-step process as shown in the flowchart below where the likelihood of triggering is only the first step. Towards the end of the flowchart are the consequences of liquefaction induced deformations. Mitigation is warranted only when the consequences threaten the engineering project, not when triggering is determined to be likely.

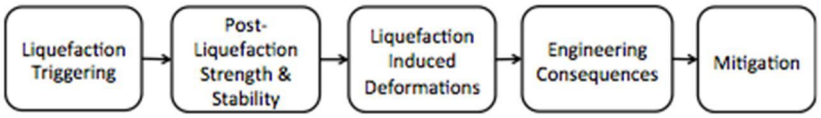

Figure 3. Liquefaction Engineering Flowchart (after Seed et al., 2003).

Current research is moving towards developing a comprehensive performance-based liquefaction framework that can accommodate the uncertainty in every step of the liquefaction flowchart to produce bounded estimates of the likelihood of adverse deformations. However liquefaction engineering, from the authors' perspective, is not a realm that is amenable to a code-based procedure. Unlike manmade materials used in structural engineering, the natural variability of soil in time and space and the measurement uncertainty (which includes measurement error, data disparity, poor model fitting, etc.) are always going to be large in liquefaction engineering and each liquefaction project should be examined on a case by case basis. There is no substitute for observing the native soil and engineering to the specific soil, site, and project conditions.

In summarizing the above discussion the authors propose that:

1. Probabilistic methods help defeat epistemic uncertainty in liquefaction triggering analyses (and other related analyses), which is the same epistemic uncertainty that R. Semple so clearly described,

2. Deformations should be the goal for a risk-based approach to liquefaction projects to determine the potential engineering consequences of liquefaction, and

3. Liquefaction engineering is not amenable or well served by a code-based approach due to the inherent uncertainty in the phenomenon of liquefaction and the process of liquefaction engineering.

Although this may not be appealing to practicing engineers, it provides a means of dealing with the uncertainty that exists in liquefaction engineering and leads to a better design against liquefaction.

References:

Ang, A. H-S., and Tang, W. H. (1984). **Probability Concepts in Engineering Planning and Design: Volume II-Decision, Risk, and Reliability**. Published by the authors.

Baecher, G.B. and Christian, J.T. (2003). **Reliability and Statistics in Geotechnical Engineering.** Wiley & Sons. New Jersey. ISBN#0471498335.

Cetin, K. O., Seed, R. B., Der Kiureghian, A., Tokimatsu, K., Harder, L. F. Jr, Kayen, R. E., and Moss, R. E. S. (2004). "SPT-Based Probabilistic and Deterministic Assessment of Seismic Soil Liquefaction Potential." Journal of Geotechnical and Environmental Engineering, 130(12). Middlebrooks Award Recipient.

Idriss, I. M. and Boulanger, R. W. (2004). "Semi-empirical Procedures for Evaluating Liquefaction Potential During Earthquakes." Proc. 11th Int. Conf. Soil Dynamics and Earthquake Engineering and 3rd Int. Conf. Earthquake Geotechnical Engineering, Berkeley, January, Vol. 1, 32-56.

Juang, C. H., Yuan, H., Lee, D. H., and Lin, P. S. (2003). "Simplified Cone Penetration Test-based Method for Evaluating Liquefaction Resistance of Soils." Journal of Geotechnical and Geoenvironmental Engineering, 129(1), 66-80.

Kayen, R. E., Moss, R. E. S., Thompson, E. R., Seed, R. B., Cetin, K. O., Der Kiureghian, A., Tanaka, Y., and Tokimatsu, K. (2013). "Shear Wave Velocity-Based Probabilistic and Deterministic Assessment of Seismic Soil Liquefaction Potential." Journal of Geotechnical and Geoenvironmental Engineering, March, Vol. 139, No. 3, pp. 407-419.

Moss, R. E. S. (2013) **Applied Civil Engineering Risk Analysis**. Shedwick Press. ISBN#0989889602. https://www.createspace.com/4412096.

Moss, R. E. S., Seed, R. B., Kayen, R. E., Stewart, J. P., and Der Kiureghian, A. (2006) "Probabilistic Seismic Soil Liquefaction Triggering using the CPT." Journal of Geotechnical and Geoenvironmental Engineering, 132(8).

Robertson, P. K. and Wride, C. E. (1998). "Evaluating Cyclic Liquefaction Potential Using the Cone Penetration Test." Canadian Geotechnical Journal, 35(3), 442-459.

Seed, R. B., Cetin, K. O., Moss, R. E. S., Kammerer, A., Wu, J., Pestana, J. and Riemer, M., Sancio, R. B., Bray, J.D., Kayen, R. E., and Faris, A. (2003) "Recent Advances in Soil

Liquefaction Engineering: A Unified and Consistent Framework." Earthquake Engineering Research Center Report No. EERC 2003-06.

Semple, R. (2013) "Problems with liquefaction criteria and their applications in Australia." Australian Geomechanics, 48(3), September.

Shibata, T. and Teparaska, W. (1988). "Evaluation of Liquefaction Potential of Soils Using Cone Penetration Testing." Soils and Foundations, Journal of the Japanese Society of Soil Mechanics and Foundation Engineering, 28(2), 49-60.

Suzuki, Y., Koyamada, K., Tokimatsu, K., Taya, Y., and Kubota, Y. (1995). "Empirical Correlation of Soil Liquefaction Based on Cone Penetration Test." First International Conference on Geotechnical Earthquake Engineering Ishihara, K. A. A. Balkema, Rotterdam, 369-374.

Toprak, S., Holzer, T. L., Bennett, M. J., and Tinsley, J. C. I. (1999). "CPT- and SPT-based Probabilistic Assessment of Liquefaction." Proc., 7th U.S.-Japan Workshop on Earthquake Resistant Design of Lifeline Facilities and Countermeasures Against Liquefaction MCEER, Seattle, WA, 69-86.

Youd, T.L. (2011). "A look inside the debate over EERI Monograph MNO12." Brigham Young University, 65p., http://www.cgea.org/downloads/calgeo-ac-2011.pdf.